Master Thesis

Design of a Motion Monitoring System for Unmanned Offshore Topside Installation based on real-time Visual Object Tracking using drones and fixed cameras on an SSCV

V.E. (Vincent) Mullenders

Supervised by:
Dr. ir. J. F. J. Pruyn
Ir. A. Jongbloed
Ir. J. Velema

SDPO.19.003.m

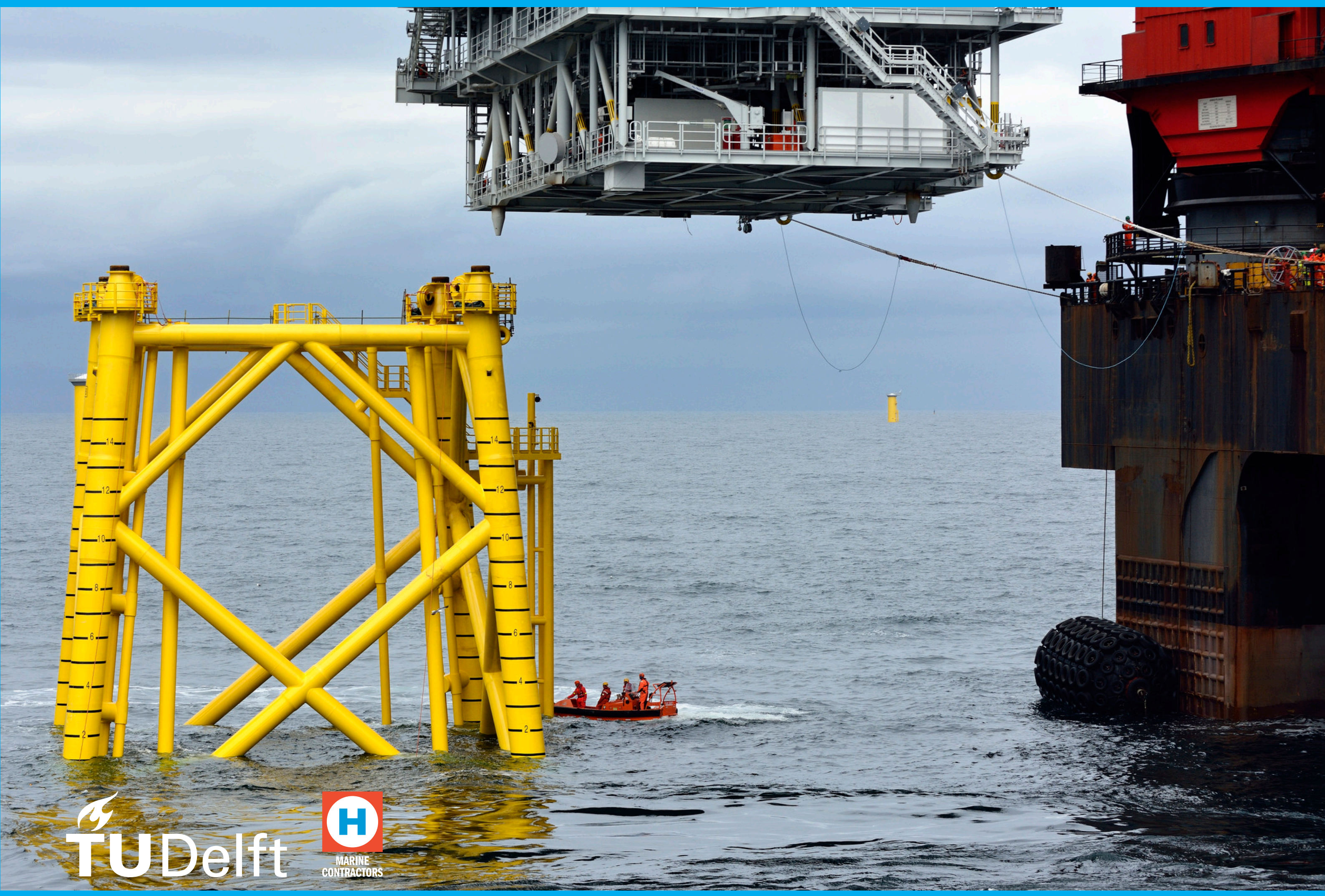

Master Thesis

Design of a Motion Monitoring System for Unmanned Offshore Topside Installation based on real-time Visual Object Tracking using drones and fixed cameras on an SSCV

by

V.E. (Vincent) Mullenders

to obtain the degree of MSc in Marine Technology
at the Delft University of Technology,
to be defended publicly on Tuesday February 26, 2019 at 10:00 AM.

Report number:	SDPO.19.003.m	
Student number:	4221419	
Project duration:	May 14, 2018 – February 26, 2019	
Thesis committee:	Prof. ir. J. J. Hopman,	TU Delft, chairman
	Dr. Ir. J. F. J. Pruyn,	TU Delft, supervisor
	Dr. W. W. A. Beelaerts van Blokland,	TU Delft
	Ir. A. Jongbloed,	Heerema Marine Contractors
	Ir. J. Velema,	Heerema Marine Contractors

An electronic version of this thesis is available at `http://repository.tudelft.nl/`.

TU Delft

Abstract

Imagine standing under a load with a weight equivalent to more than 5,000 Tesla's model X. Panicking is not an option and you need to be fully focused on completing a crucial task. There is no option to leave this precarious situation and your contribution is vital to the success of a multi-million dollar project. Sounds frightening, right? Oddly enough, it's a common event during offshore topside installations at Heerema Marine Contractors. During these kind of operations a rigger foremen and an assistant superintendent take place on the jacket. With the role to communicate topside positioning information to the superintendent, on the crane vessel. They have to provide clear instructions until the installation is completed. Although the installation of offshore topsides have always been carried out with people on the jacket, without any major incident to date, having people operating under suspended loads of up to 10,000 tonnes is considered unwanted. Therefore, HMC is looking for a robust system to replace the presence of people on a jacket during topside installations. Existing techniques developed by HMC consist of robotic total stations and the use of augmented reality. However, these techniques are limited by the view from the stern of an SSCV.

In this thesis, a novel motion tracking algorithm is developed based on drones, fixed cameras and visual object tracking. Drones are already starting to change how businesses operate – and this is happening today. Companies across industries are using them for inspection, monitoring, repair work and onsite security. They are also being used for real-time data collection. Drones are able to take any position with respect to the topside or jacket and can mimic the view from people on the jacket. They are therefore not limited by the view from the SSCV. The developed algorithm is able to localise a pair of Aruco markers in an image captured by the vision system. Aruco was only recently introduced which makes this solution unique in the offshore sector. If a marker pair is recognized successfully, relative distance calculations can be made. By conveniently placing these markers on the topside stabbing cones and jacket legs, the topside relative motions can be estimated. A minimum of two locations need to be monitored in order to perform a successful estimation.

Two configurations have been proposed to test the algorithm. In the first configuration use is made of four fixed cameras on the stern of the SSCV. The four fixed cameras will need to track the marker pairs. Also one drone is available to provide visual confirmation from every desired position. In this configuration, the stabbing cones which are closest to the SSCV are monitored. In the second configuration three drones and one fixed camera on the stern of the SSCV are used. In this configuration the drones are used to track the marker pairs. Unlike configuration 1, the stabbing cones diagonally opposite to each other are monitored. Both configurations are able to provide relative positioning information during a topside installation. The first configuration is limited by the view from the SSCV while the latter configuration is not - since drones are used.

The motion tracking algorithm was tested in a virtual simulation experiment. Experimental 3-DOF results demonstrate the accuracy of the proposed method compared with the simulation log of the virtual environment. For configuration 1 the mean absolute error was found to be 0.048m with a standard deviation of 0.040m. For configuration 2 the mean absolute error was found to be 0.034m with a standard deviation of 0.020m. Both configurations are therefore within the 0.15m acceptable error margin. It can be concluded that the configuration using drones seems to perform better than fixed cameras from the stern of the SSCV. An obstacle of using drones for this purpose is the need of certified operators and the limited power supply. Autonomous drones can be a solution for the first obstacle. The second obstacle might be tackled in the future with the continuous battery improvements fostered by the automotive and electronic consumer goods industry. Nevertheless, the motion tracking algorithm using Aruco markers looks very promising. Taking into account the steep developments of drones over the past year, the future use of drones during offshore topside installations looks promising.

A long time ago, the ancient Chinese already found out that one can generate thrust with rotation to fly. The principle that is nowadays also used by drones. At that time there was a toy called bamboo-copter. This consisted of bamboo sheets that were tied to a stick. Then you had to rub it quickly between your hands and let go. This bamboo copter has had an important influence on aviation pioneers. George Cayley, also known as the 'father of British aviation', made an airplane in 1809 inspired by the bamboo copter. After he had adjusted the rotor of the first prototype, he could fly 30 meters high with it. In 1853, George Cayley drew down his helicopter rotors. It was one of the key elements in the birth of modern aeronautics in the West.

Contents

List of Figures ix

List of Tables xiii

1 Introduction 1
1.1 Background . . . 1
1.2 Problem Description . . . 3
1.3 Research Objectives . . . 4
1.4 Thesis Outline . . . 5

2 Concept Exploration 9
2.1 System Requirements . . . 9
2.2 Concepts . . . 11
2.3 Selecting a computer vision technique . . . 14
2.4 Marker tracking . . . 16
2.5 Summary . . . 21

3 Real-time motion tracking 27
3.1 Object tracking with ArUco markers . . . 27
3.2 Kinematic model . . . 31
3.3 Motion Tracking Algorithm . . . 36
3.4 Summary . . . 37

4 Unmanned Topside Installation 43
4.1 Positioning and orienting . . . 43
4.2 Marker Location . . . 44
4.3 Camera Configuration . . . 45
4.4 Fixed camera . . . 46
4.5 Use of Drones . . . 46
4.6 Electronics and software . . . 53
4.7 A look into the future: autonomous drones . . . 55
4.8 Risk assessment . . . 58
4.9 Summary . . . 63

5 Experiment 67
5.1 Heerema Simulation Center . . . 68
5.2 Experiment 0: Calibration . . . 69
5.3 Experiment 1: Algorithm Accuracy and Precision . . . 71
5.4 Experiment 2: Proof of Principle . . . 79
5.5 Summary . . . 81

6 Conclusion 85
6.1 Discussion . . . 85
6.2 Conclusion . . . 86
6.3 System comparison . . . 88
6.4 Recommendations . . . 89

Bibliography 95

A Predecessor systems 101
A.1 Concept 1: Total Station system . . . 101
A.2 Concept 2: Augmented reality system . . . 104
A.3 System Comparison . . . 105

B Total Station System lay-out and accuracies **109**

C Drone Specifications **111**
C.1 Aerial system requirements 111
C.2 Selecting an aerial platform 112

D Rodrigues' rotation formula **119**

E Experiment results **123**
E.1 Experiment 1: Configuration 1, Procedure 1: limit check. 123
E.2 Experiment 1: Configuration 1, Procedure 1 124
E.3 Experiment 1: Configuration 1, Procedure 2 125
E.4 Experiment 1: Configuration 1, Procedure 3 126
E.5 Experiment 1: Configuration 1, Procedure 4 127
E.6 Experiment 1: Configuration 2, Procedure 5 128
E.7 Experiment 1: Configuration 2, Procedure 6 129
E.8 Experiment 1: Configuration 2, Procedure 7 130

F Visual object tracking: a multidisciplinary system **131**
F.1 Free-decay test of a jacket scale model. 131
F.2 Crane suspended jacket transport. 132

List of Figures

1.1 Rigger foremen and assistant-superintendent are transported to the jacket during an Offshore Topside Installation. Picture by: Jan Berghuis . . . 1
1.2 Position of people on the jacket . . . 2
1.3 Examples of topside installations: (left) relatively small and square topside, (middle) topside located low above the water surface, (right) relatively big topside with overhanging parts on two sides . . . 2
1.4 Application of drones in inspecting (maritime) assets [56], [26], [53] . . . 3
1.5 Key components . . . 4

2.1 Safe margin of stabbing cone . . . 11
2.2 General system requirements . . . 11
2.3 Robotic Total Stations . . . 12
2.4 Man in basket during topside installation . . . 13
2.5 Augmented reality system . . . 13
2.6 Drone as an installation aid during offshore topside installations . . . 14
2.7 Examples of fiducial marker systems [28] . . . 15
2.8 Multiple-camera tracking [57] . . . 15
2.9 Edge detection [62] . . . 16
2.10 Example of markers of different sizes; n=5, n=6 and n=8 [28] . . . 17
2.11 Obtain relative position between a topside and a jacket by using ArUco markers . . . 18
2.12 Drone experiment setup . . . 18
2.13 Drone experiment results translations . . . 19
2.14 Drone experiment results rotations . . . 20
2.15 Two markers pairs with a perpendicular orientation . . . 21
2.16 Experiment setup . . . 22
2.17 User Interface . . . 22

3.1 Example of ArUco marker: ARUCO-MIP-36h12 dictionary . . . 28
3.2 Images of a chessboard being held at various orientations (left) provide enough information to completely solve for the locations of those images in global coordinates (relative to the camera) and the camera intrinsics [12] . . . 29
3.3 Process of marker detection and identification . . . 29
3.4 Bit assignment for each cell . . . 30
3.5 Pinhole camera model [11] . . . 31
3.6 Kinematic model . . . 32
3.7 Kinematic model, $\Delta x-$, $\Delta z-$offset . . . 33
3.8 Verification, expected values . . . 34
3.9 Verification, expected values . . . 35
3.10 Camera and drone configurations . . . 38

4.1 Translations and orientations, axis definition . . . 43
4.2 Marker locations to be placed on the jacket and topside . . . 44
4.3 Camera configurations . . . 45
4.4 Camera lens focal length . . . 46
4.5 Blackmagic Studio Camera and lenses . . . 47
4.6 Camera Control Panel . . . 47
4.7 Types of drones . . . 47
4.8 Selction of five currently existing professional drones . . . 49
4.9 DJI M210 RTK and the Zenmuse X4S 1-inch aerial camera . . . 50

4.10 DJI M210 RTK used for offshore inspection purposes during the Ocean Cleanup 50
4.11 Concept of alternating drones 51
4.12 Flight plan for continuous drone flights 51
4.13 Landing zones. Left SSCV Sleipnir, middle SSCV Thialf, right Kolga 53
4.14 System lay-out for configuration 1 54
4.15 System lay-out for configuration 2 54
4.16 Concept of operations 55
4.17 Autonomous take-off and landing 56
4.18 Automatic docking and recharging. From left to right: DroneBox [38], SkySense [9], UPS's truck launch [20] and Amazon's patent [54] 57
4.19 Communications 57
4.20 Marker area during different stages 63

5.1 Simulation setup 67
5.2 Heerema Simulation Center layout 68
5.3 Calibration checkerboard 69
5.4 'Camera' Calibration process in K-SIM 70
5.5 Axis definition 70
5.6 Configuration 1 71
5.7 Configuration 1 moves 72
5.8 Configuration 2 73
5.9 Configuration 2 moves 74
5.10 Motion Tracking Algorithm - Real Time 74
5.11 Axis rotation 76
5.12 Translational Error Analysis 77
5.13 Translational Error Analysis: Experiment 1 - Configuration 2 78
5.14 Laptop with Motion Tracker provided to the assistant superintendent 79
5.15 Updated motion tracker design 80

6.1 Spider diagram 88
6.2 Tele-operation versus on-board computation 90

A.1 Positioning information from the total station system displayed live in both 2D and 3D . 101
A.2 Total Station and 360° prism 102
A.3 Topside Prism Location Diagram 102
A.4 Jacket Prism Location Diagram 103
A.5 Sketch illustrating how an EM beam reflects on a mirror and on a prism 104
A.6 Recognition of structure 105
A.7 User Interface 106

B.1 Total Station system configuration 109
B.2 Total Station Topside Installation Error Budget [24] 110

C.1 Selction of five currently existing professional drones 113
C.2 RTK Explained 117
C.3 DJI Lightbridge 2 117

D.1 Point V rotated with angle α around axis $\vec{n}$ 119
D.2 Introducing vector projection 120
D.3 2D rotation of vector $\vec{v_r}$ 120
D.4 Vector $\vec{u}$ from plane in origin to point U 121

E.1 Topside moving 20m astern towards jacket. Accurate within 0-12 meters 123
E.2 Topside moving 10 meters to port side. Accurate within 0-8 meters. 123
E.3 X-, Y-, and Z-Translations 124
E.4 Error Analysis 124
E.5 X-, Y-, and Z-Translations 125

E.6 Error Analysis 125
E.7 X-, Y-, and Z-Translations 126
E.8 Error Analysis 126
E.9 X-, Y-, and Z-Translations 127
E.10 Error Analysis 127
E.11 X-, Y-, and Z-Translations 128
E.12 Error Analysis 128
E.13 X-, Y-, and Z-Translations 129
E.14 Error Analysis 129
E.15 X-, Y-, and Z-Translations 130
E.16 Error Analysis 130

F.1 Experiment setup: tripod with Logitech C920 HD Pro, ArUco markers 0.38x0.38m . . . 131
F.2 Screenshot from Motion Tracking Algorithm. Red line represents historical track. 132
F.3 Jacket monitoring 133

List of Tables

2.1 Information to be provided by the system [18] . . . 10
2.2 Comparison between three tracking techniques . . . 17
2.3 Drone experiment results translations. e_{MAE} = mean absolute error, $|e|_{MAX}$ = absolute maximum error, σ_e = standard deviation, μ_e = mean error . . . 19
2.4 Drone experiment results rotations. e_{MAE} = mean absolute error, $|e|_{MAX}$ = absolute maximum error, σ_e = standard deviation, μ_e = mean error . . . 20

4.1 My caption . . . 46
4.2 Comparisons of three types of small aircraft (More “+” implies better) . . . 48
4.3 Comparison of different specifications . . . 49
4.4 Number of flights (battery swaps) per drone position for given installation time . . . 52
4.5 Required drone operators . . . 52
4.6 Hazard Severity Classification . . . 58
4.7 Hazard Probability Levels . . . 59
4.8 Mishap Risk Assessment Matrix . . . 60
4.9 Mishap Risk Categories . . . 60
4.10 Hazard study of marker, drone and fixed camera subsystem . . . 61
4.11 Risk register . . . 62

5.1 Experiment 1 configuration 1: different moves . . . 72
5.2 Experiment 1 configuration 2: different moves . . . 73
5.3 Results procedure 1 and 2 - Configuration 1. e_{MAE} = mean absolute error, $|e|_{MAX}$ = absolute maximum error, σ_e = standard deviation, μ_e = mean error . . . 76
5.4 Results procedure 3 and 4 - Configuration 1. e_{MAE} = mean absolute error, $|e|_{MAX}$ = absolute maximum error, σ_e = standard deviation, μ_e = mean error . . . 77
5.5 Results procedure 5, 6 and 7 - Configuration 2. e_{MAE} = mean absolute error, $|e|_{MAX}$ = absolute maximum error, σ_e = standard deviation, μ_e = mean error . . . 78
5.6 Results experiment 2 . . . 80

C.1 Comparisons of three types of small aircraft (More “+” implies better) . . . 113
C.2 Max flight time and battery specifications . . . 114
C.3 Camera specifications . . . 115
C.4 Payload specifications . . . 115
C.5 Remote range and frequency specification . . . 115
C.6 IP Classifications . . . 116
C.7 Weather conditions . . . 116
C.8 Comparison of identified drone specifications . . . 118

F.1 Decay test results . . . 132

Preface

This thesis concludes the Master of Science program in Marine Technology at the Faculty of 3mE at the Delft University of Technology. In the past nine months, I have been working on this thesis at Heerema Marine Contractors. Heerema provided me with an open and inspiring working environment, which made it a great place to graduate. I would like to thank all the employees and fellow students that were always willing to help me.

During the last two years of my study, I first encountered drones and drone photography. Given the rapid pace of developments in drone technology, I thought it would be a great opportunity to combine the subject of drones with my graduation. I would like to thank my graduation committee for giving me the opportunity to investigate this interesting topic, and giving me the freedom to formulate my own research objective. Arnold, thank you for your positive attitude and enthusiasm during the meetings, and providing me with heaps of suggestions about related studies that I could look at. Jorick, as my daily supervisor you always made time for me when I encountered difficulties in my project, and provided me with great feedback and inspiration to carry on. Moreover I highly valued your guidance throughout the whole process of graduating, and being available for advice even when you decided to leave Heerema. Thank you Jeroen, for your feedback on every version of this report, and giving me thoughtful suggestions on bringing my writing to a higher level and introducing me to the 'Systems Engineering' approach. Lastly, Jenny thank you for your guidance during the first period of my project.

Furthermore, I want to thank my fellow students at Heerema, which made the experience of graduating a great one. Especially the ones that survived one of the hottest summers with me, and even though we pitied ourselves for being stuck inside, we had a great time complaining and laughing about it! I'm guessing that 'bakkie op 2' is the most common phrase in my WhatsApp history of the past months.

Finally I would like to thank my family, and all of my friends from Delft, which made the last 6.5 years of studying incredibly fun! Your support, enthusiasm, entertainment and welcome distractions during these times are highly appreciated. I especially want to thank my parents for their unanimous support for all my choices and making possible an absolutely carefree student time. Furthermore I would like to thank my girlfriend Laurien. Thank you for being there and supporting me in this sometimes stressful period. And lastly Thomas †, for your help from above.

Vincent Mullenders
Leiden, February 2019

1
Introduction

1.1. Background

Installation of offshore structures is a core business for Heerema Marine Contractors (HMC). Setting down a topside on a jacket is considered as a critical offshore installation activity. This is illustrated in Figure 1.1. Once the procedure has started and the topside is lifted from its supporting barge there is no way back. A high level of concentration and perfect communication between parties involved is necessary during this operation. A typical jacket (supporting structure) comprises four legs and the topside comprises of stabbing cones, two of which (primary and secondary) are diagonally positioned and inserted one after the other.

As is customary, prior to positioning the topside, the rigger foremen and assistant superintendent take place on the jacket on a scaffolding installed around the top part of the jacket legs. With the role to communicate topside positioning information to the superintendent, on the crane vessel. The superintendent is in charge of the whole operation. The superintendent gives instruction to the captain and crane operators to control the movement and position of the topside. Flawless information on the topside's location and clear communication are therefore essential to carry out this operation successfully.

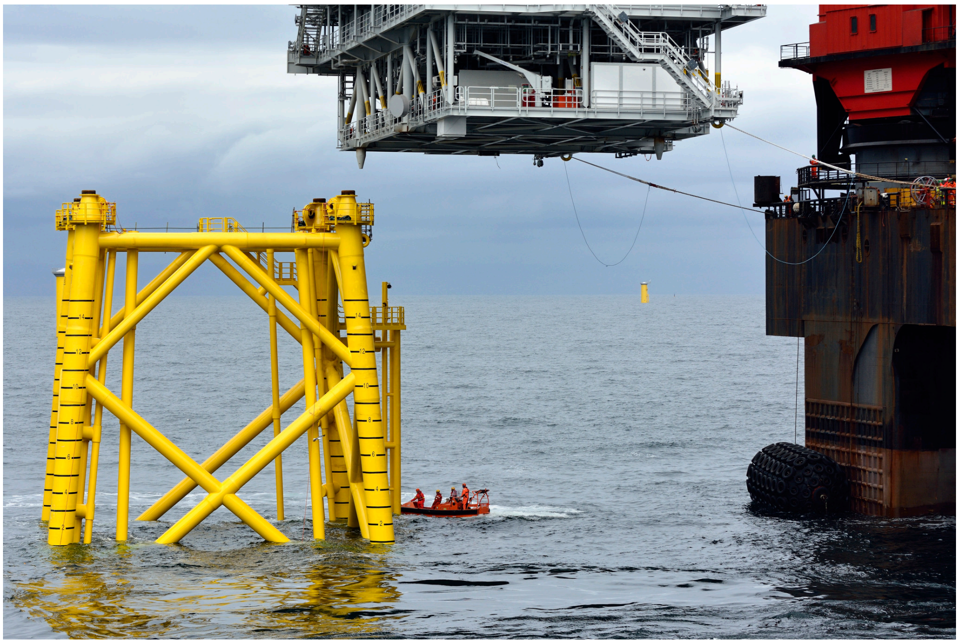

Figure 1.1: Rigger foremen and assistant-superintendent are transported to the jacket during an Offshore Topside Installation. Picture by: Jan Berghuis

The rigger foremen and assistant-superintendent on the jacket need to be experienced to estimate speed and distances. The Dutch proverb for this estimation is 'Timmermansoog' which is in English literally translated to 'Carpenter's eye'. They have to provide clear instructions until the installation is completed. Figure 1.2 illustrates the position of the jacket crew on the installed scaffolding. One can imagine that its a not a job for someone who is suffering from vertigo or claustrophobia.

Figure 1.2: Position of people on the jacket

HMC owns and operates multiple Semi Submersible Crane Vessels (SSCV) to transport and lift offshore structures. For topsides, the dimensions and characteristics of these structures are never the same. For an offshore platform, the topside is high above the sea level and outside the splash zone by design. Depending on the geographic location this can be five meters or up to 20 meters above the water. Figure 1.3 shows three different topside installations. The first figure shows a quite simple and relatively small topside. There is good visibility from the SSCV on the stabbing cones and there is a lot of clearance between the SSCV and the topside. The second figure shows a topside that is located low above the water surface. There is no visibility from the SSCV on the stabbing cones. The last figure shows a relatively big topside with overhanging areas on the side. Of course these are not the only type of topsides but it gives an idea of the size, position above the water and position with respect to the SSCV.

Figure 1.3: Examples of topside installations: (left) relatively small and square topside, (middle) topside located low above the water surface, (right) relatively big topside with overhanging parts on two sides

Although the installation of offshore topsides have always been carried out with people on the jacket, without any major incident to date, having people operating under suspended loads of up to 10,000 tonnes is considered unwanted. House rule number 3 within HMC states: "Do not walk under a suspended load". Working or walking immediately under u suspended load is unsafe as the load can drop and fall on you. Safety requirements in the Oil & Gas industry have become more stringent e.g. Shell's requirements now specify that no one should be standing under a suspended load. Every time a topside is installed for Shell, a waiver form declaring that the approach is safe needs to be signed. Proactive action is needed to increase the safety level in order to still be awarded installation projects.

[18] Therefore, HMC is looking for a robust system to replace the presence of people on a jacket during topside installations.

The main advantage of having people on the jacket is that they can move freely and get in position to obtain the best view. The most obvious idea to replace people on the jacket is to use fixed cameras with a wireless connection. But the disadvantage is that they cannot move freely on the jacket to adjust the viewpoint. It is also extremely difficult to obtain a sense of depth from a 2-D camera image. A way to deliver images from every desired position could be the use of Unmanned Aerial Vehicles (UAVs), also called drones. Drones have become increasingly popular over recent years. The global drone market is estimated to grow from $ 2 billion in 2016 to nearly $ 127 billion in 2020 [30]. The emerging drone technology promises to foster innovations that will disrupt existing industries.

Virtually all kinds of payloads can be attached to drones, the only restrictions are usually the weight and size of payloads. Today, drones can be fitted with several payloads that enable faster and more accurate decisions for organizations across industries. From the use of thermal sensors and cameras to detect tank levels or potential issues to gas detecting sensors, drones are unlocking a new level of information and insight. Besides, most drones are equipped with cameras. This camera can be used as a sensor to monitor the movement and orientation of the topside with respect to the jacket. The process of gaining understanding from digital images or videos is called computer vision. A sub-domain of computer vision is visual object tracking. Object tracking is the process of:

1. Taking an initial set of object detections (such as an artificial squared marker)
2. Creating a unique ID for each of the initial detections
3. And then tracking each of the objects as they move around frames in a video, maintaining the assignment of unique IDs

If a method can be created that uses visual object tracking on determining the relative position and orientation between a topside and a jacket then this could be combined with the use of standard of-the-shelf drones and/or with the use of fixed cameras.

Figure 1.4: Application of drones in inspecting (maritime) assets [56], [26], [53]

Drones have the potential to reduce time, cost and danger of many operations, whilst improving the value of the data captured. Organisations like DNV-GL, Lloyds Register and Maersk have shown their strategic intent to extend their operations by embracing drone technology. Drones are already used in the maritime domain to inspect dangerous and hard-to-reach objects such as ballast tanks, flare tips and cranes. Until now these inspections had to be prepared well in advance and sometimes some systems have to be switched off so that operations cannot continue. This, in turn, reduces costs, reduces downtime, increases efficiency and significantly reduces the risk of human life during essential maintenance. Drones enable operators and experts to get complete, up-close, and real-time visualization into assets from anywhere in the world, for a fraction of the cost of traditional methods, and without the physical constraints or budget constraints. In figure 1.4 some maritime applications of drones are presented.

1.2. Problem Description

The current approach with people on the jacket is not possible anymore. HMC is currently working on new techniques that can replace the physical presence of people on the jacket. Efforts have been made to develop an Unmanned Topside Installation Monitor. For this there are techniques based on laser systems and augmented reality. These techniques have been under development from 2014 onwards. The laser based systems uses robotic 'Total Stations' to simultaneously track 360 degree prisms on the topside and the jacket. These prisms require an accurate setup and initialization by a subcontractor. Good visibility from the SSCV is the prerequisite for the systems to operate as planned. This system is therefore quite complex and expensive to use and is also not applicable for every installation. The system based on augmented reality uses cameras and a predefined 3-D CAD model. A computing device should then be able to match the filmed structures with the 3-D CAD model. The system had difficulties with the limited view on the topside and jacket and was confused by shadow patterns. Unfortunately this system never worked in an offshore environment. So there is still a demand for a relatively simple and affordable system that can be used for any type of topside installation.

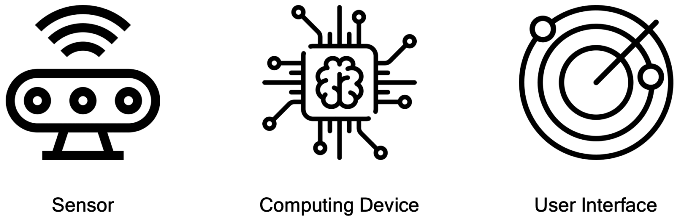

Figure 1.5: Key components

Existing methods use a variety of techniques and equipment, but three key concepts are always present: a sensor, a computing device, and a user interface to display information. The sensor is used to obtain spatial information about the position and orientation of the topside and jacket with respect to an arbitrary reference frame. The computing device is used to calculate the relative position between the topside and jacket based on the sensor measurements. A user interface is then used to deliver this information to the superintendent.

The available space to position sensors is a point of discussion. It's only possible to mount them on the stern of the SSCV and/or the cranes. This are the only locations with a view on the topside and jacket. In previous system designs the lack of available space was a limiting factor. It is favorable to be not dependent on placing the sensors on the SSCV. Recent developments in drone technology over the past few years show that these flying robots are embraced by different industries. The main advantage of a drone is the ability to get in hazardous or hard to reach locations. A drone can move free in space and deliver butter smooth images thanks to its mechanical 3-axis stabilization gimbal. HMC is therefore interested in the feasibility of using drones as an installation aid during offshore installation activities. Since almost every drone is by default equipped with a camera it is a big advantage if this can be used as the main sensor for the positioning system.

1.3. Research Objectives

Current offshore topside positioning techniques are able to measure the relative distance between a jacket and a topside accurately. However, the existing techniques are limited by its design and should be improved. In order to install topsides unmanned, a universal positioning aid using drones is of interest. The goal of this research is to design and develop a way to use drones to obtain relative information between a topside and a jacket. The main research question that is raised is:

What is the potential of drones as an installation aid during offshore topside installations?

To reach to conclusions about the main research question, this research is divided into several secondary questions. By giving answers to each one of these secondary questions, the main research objective of the project will also be achieved. The secondary questions, that form also the different phases of the study, are related to the several subsystems.

- **What are the requirements and functional specifications for an Unmanned Topside Installation Monitor based on visual object tracking and drones or fixed cameras?** This question will give an overview of the requirements and functional specifications of the system development. It aims to develop a preferred system that meets the operational needs. Attention will be paid to the implementation of the system concept into hardware and software components, their integration into a total system, and the validation of the systems operational capability through a process of developmental and (small scale) operational testing.

- **How can visual object tracking be used to calculate the relative position between a topside and a jacket in 3-DOF?** One of the main challenges is to determine the relative position between a topside and a jacket. A technique based on visual object tracking needs to be created and verified in order to do this. It should be compatible for fixed cameras and drones.
- **How can the combination of drones, fixed cameras and object tracking assist in the installation of offshore topsides at HMC?** Cameras are the main sensor to make visual object tracking possible. These cameras can either be free moving cameras (drones for example) or traditional fixed digital cameras.
- **What are the accuracy's, advantages and limitations of using visual object tracking for topside installations?** The accuracy and precision should be comparable with existing techniques. Since there are already some systems in development the new system should have some advantages over the other. It is also important the be aware of the limitations of the system.

1.4. Thesis Outline

The present document is the final report of a Master thesis conducted in the Department of Maritime and Transport Technology, TU Delft, and in collaboration with the offshore company Heerema Marine Contractors. The theoretical background of this topic was combined with the description of the methodologies used throughout the study and the derived results and they are presented in the following chapters.

The structure of the report is the following:

- In chapter 2, the other systems to enable unmanned topside installations which have been previously developed by HMC are introduced. A brainstorm and concepting phase will be carried out and some small experiments will be done.
- In chapter 3 is discussed how cameras can be used to actively track the relative motion of a topside with respect to a jacket.
- In chapter 4 is discussed how different subsystems can be integrated to the whole system architecture. Two configurations will be presented that use both fixed cameras and drones.
- In chapter 5, an experiment to check both configurations in a simulation setup. Also the accuracy and the precision of the system will be determined.
- and finally in Chapter 6, the discussion, recommendations, and conclusions are given.


GOW02-Z01


GOW02-Z01

2
Concept Exploration

In the previous chapter, the operational problem and the research goal where defined. In this chapter, the two current systems for unmanned topside installation are analyzed to determine their strong and weak points. First, the system requirements are outlined. This chapter will try to give an answer to sub-question 1:

What are the requirements and functional specifications for an Unmanned Topside Installation Monitor based on visual object tracking and drones or fixed cameras?

2.1. System Requirements

The goal of this research is to design a system that is capable of monitoring the relative position between a topside and a jacket. This will be further referred to as 'the system'. Before beginning to develop a new system a detailed analysis of all the requirements must be made. The requirements analysis produces a set of operational requirements (or objectives) that describe what the new system must be designed to do. The principle objective of this exploration phase is to convert the operationally oriented view of the system into an engineering-oriented view. This means that all wishes must be inventoried and quantified. This conversion is necessary to provide an explicit and quantifiable basis for selecting an acceptable functional and physical system concept. [41] In order to come up with a motion monitoring system, HMC made some considerations which will be further described in this chapter. All requirements in this chapter where delivered in writing by HMC. The feedback on the current systems is also well documented and used as a valuable source during the writing of this chapter. Some important requirements for this new development are:

- Any solution should not only work in perfect conditions, but also at the limits to what is still considered a safe situation (where significant movement and impact can be expected).
- Should weather conditions become too dangerous to carry on, the installation can be postponed. This can significantly lengthen the whole installation from lift-off to set-down.
- Robustness is an important pillar as the system shall perform when needed. Should the primary system fail, a back-up system/solution needs to be implemented.

The proposed solution should accommodate any type of topside or jacket as well as any installation method (single or double crane). The system shall function irrespective of vessel type, sea fastening or vessel positioning system. Furthermore, the system shall be robust i.e. work in any environment acceptable for carrying out an installation job. Failure of the system has to be mitigated, as no personnel can be sent to the jacket once installation has started. Wind speeds up to 30 knots (15.34 m/s), sea water exposure, humidity and temperatures of between -10°C to 40°C should not effect the system and its output. [18]

2.1.1. Physical system

The weight of the system will be limited by its use and installation method. Should the system be installed on the jacket and/or topside prior to its transportation offshore, its weight should be limited to 200kg to enable it to easily transfer it by crane (or similar) back to the vessel. Should the system be installed on the jacket and/or topside, offshore, its weight will be limited by the carrying capacity of the available equipment or personnel. If manual labour must be used for the system installation, it can be divided into sections; each of them shall weigh below 25kg and the total system weight shall not exceed 150kg. The dimensions of the system depend on where it will be positioned. The smaller, the better. In any case, its global dimensions should not exceed 1m^3 for practical reasons and to enable it to be easily stored. Should a battery powered system be used, its battery life should at least be sufficient for the duration of the topside installation: up to six hours continuously. A battery-powered system shall be switched-off remotely, should the installation be postponed.

2.1.2. System installation and positioning

The topside positioning strategy is open to suggestions. Currently, the topside is positioned relatively to the jacket. The topside could also be positioned purely on its coordinates (assuming that the topside coordinates are known). In case an offshore installation is necessary, the following two criteria must be considered:

- The overall duration of the installation process must not be extended by the addition of personnel transportation procedures to and from the jacket and/or topside.
- No further risk shall be added to the installation process.

Should emitters and receivers be used on any movable parts (e.g. emitter on the jacket and receiver on the topside). A procedure or subsystem will have to ensure both elements are well positioned, prior to the installation.

2.1.3. Communication

The superintendent (located on the stern of the SSCV during the installation) is the decision maker during the installation process. Any information on the positioning of the topside should be simply and clearly transmitted to him. In the majority of cases, only a minor portion of the jacket and/or topside is visible to him in a continuous way.

2.1.4. Information to be provided

The system to be produced will display simple information to the superintendent, allowing him to take quick decisions. The system should also require minimal amount of training. Any superintendent shall be capable of fully understanding the system and making decisions based on the information provided after four hours of training. All data and their required precision and accuracy is provided in table 2.1.

	Description	**Accuracy**
Concentricity	Position of the axis of the primary and secondary stabbing legs of the topside.	A precision of below 150 mm.
Height	Monitoring of the gap between the lowest topside point (bottom of the primary stabbing cone) to the top of the receiving jacket leg (from 3m to 0m).	A precision of below 150 mm.
Tilt/Attitude (Optional)	Check of the topside's angular position on the x- and y-axis (roll and pitch respectively).	The measurement error shall be such that precision on height is always below 150 mm.
Rotation/Yaw (Optional)	Check of the topside's angular position along the z-axis.	The measurement error shall be such that precision on concentricity is always below 150 mm.

Table 2.1: Information to be provided by the system [18]

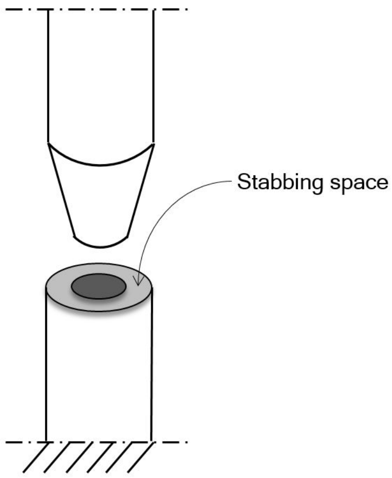

Figure 2.1: Safe margin of stabbing cone

The 150 mm margin is derived from the conical design of the stabbing cone. This is slightly narrower at the bottom. This stabbing space (Fig. 2.1) makes it easier to position the stabbing cone in the receiving bucket.

2.1.5. Other requirements

For a digital system, the minimum measurement frequency shall be 10Hz (i.e. 10 measurements per second). The system to be developed has to be as such as no human intervention will be necessary on the jacket in case of failure. Failure can be described as a complete or partial loss of a sub-system. Maintenance and calibration on the system shall be carried out at a maximum of every six months.

2.1.6. Summary

Several topics for the new system have been discussed. All requirements are summed up in figure 2.2. Based on these requirements two system concepts are currently developed by HMC in cooperation with different subcontractors. These systems will be briefly described in the next section. These systems concepts will be used as a starting point for a new and third system concept which will be further investigated in this research.

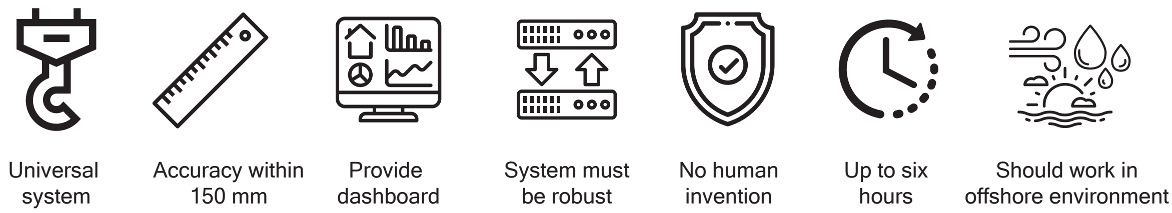

Figure 2.2: General system requirements

2.2. Concepts

In 2014 HMC started with the development and testing of two systems that would be able to carry out an unmanned topside installation. These systems are ”Total Station System” and ”Augmented Reality System”. These systems are respectively referred to as concept 1 and 2 and will be introduced in this section. The third concept will be a new concept to be developed in this research.

2.2.1. Concept 1: Robotic Total Stations

Concept 1 is a solution that uses six robotic total stations to track six prisms and is shown in Figure 2.3. These prisms are located on the topside and jacket. Three total stations track three prisms on the

Figure 2.3: Robotic Total Stations

jacket and three total stations track three prisms on the topside. Information from the six total stations is transferred to a computing device to calculate the relative position between the topside and the jacket. This information can be displayed in real-time. The total stations are located on the stern of the SSCV and their position with respect to the vessel reference frame must be precisely calibrated. This is also necessary for the six prisms. Their 3-D location with respect to the topside or jacket reference frame must be obtained during a dimensional control survey. For the topside, this can be performed onshore at the yard. The prisms on the jacket must be installed offshore prior to the topside installation.

The positioning method of total stations is based on a three-dimensional coordinator measuring technology. The accuracy of this system is within 0.057 m standard deviation for the combined 3-D position. And within 0.066 degrees standard deviation for combined pitch and roll. The accuracy of this system is highly dependent on the precision of the dimensional control survey. This system has been used several times as the primary system for unmanned topside installations. The system works well but requires a lot of preparation to set up. In addition, one does not yet dare to trust this system blindly. Some feedback from a superintendent during an unmanned topside installation was:

- A camera to confirm what you see would be beneficial
- It is still difficult to keep the complete overview when looking at a screen.
- Some kind of visual information would be nice.
- It feels much better to rely on a system which has been confirmed by the crew below the load or my own visual interpretation of reality.

Therefore, a number of back-up tools were requested in addition to the positioning tool. This consisted of four cameras on the jacket and a man in a crew basket that hung next to the topside and passed on information via the radio. Figure 2.4 shows the topside installation interface and the four cameras (on the left) and a man in the crew basket. A more detailed explanation is given in Appendix A.1.

2.2.2. Concept 2: Augmented Reality System

Concept 2 uses cameras to detect, recognize and track objects by means of augmented reality (AR). AR can match and track real world objects and project 3-D predefined CAD drawings on top of it. This is shown in Figure 2.5. A camera is used to film the topside and jacket, the green lines indicate a successful recognition and tracking. For every installation a 3-D CAD model must be prepared in order to facilitate object tracking. The two cameras are connected to a computing device to determine relative position. Despite many efforts this system never worked in an offshore environment. Shadow lines on the structures confused the system which resulted in inaccurate tracking. No statement can be made about the expected accuracy and precision. A more detailed explanation is given in Appendix A.1.

Figure 2.4: Man in basket during topside installation

Figure 2.5: Augmented reality system

2.2.3. Comparison between concept 1 and 2

In the process of engineering a new system it is useful to compare the predecessor systems. The predecessor systems can serve as a point of departure. It is the single richest source of information on the requirements for a new system. [41] Concept 1 and 2 are compared in appendix A. Both concepts were developed to support unmanned installation of topsides. Concept 1, with the robotic total stations, has been used several times as primary system but requires a lot of preparation and is quite expensive, ranging from 75K - 100K USD per installation. Concept 2, the augmented reality system, had a lot of potential but failed to work properly in the offshore environment. There is still a need for a simpler and cost-efficient system that can be operated by HMC itself. The advantage of concept 2 was that a camera was used as the primary sensor. This allows the superintendent to clearly see what happens and interpret the acquired data clearly. For concept 1, the superintendent did not dare to rely entirely on the system and a second system with cameras was a desired backup. A limitation of both systems is that there is not always enough visibility on the jacket from the SSCV. This is the case, for example, if the jacket does not project far above the water level. A system with flexible cameras would therefore be favorable. Internal documents show that there was a lot of attention for the use of drones in 2014. [16] At that time, drones were mostly used as consumer toys. But given the steep technological development that this technology has undergone in recent years, it is interesting to investigate this now. The starting point for the use of drones will be concept 1 and 2. The focus will be on retaining the components that are perceived as positive and improving the points that are experienced as bottlenecks.

2.2.4. New concept: Visual object tracking with fixed cameras and drones

The new concept will use cameras as the primary sensor and is investigated in this thesis. The cameras can either be fixed cameras on the SSCV or flying cameras, often referred to as drones. Compared to the predecessor systems, a major advantage of the use of drones is that they are able to take almost any position in relation to a topside or other object. It is an effective method to remove the person off the jacket, while keeping the same visual. By using fixed cameras, the employability depends on the view from the SSCV. As soon as the topside drops too far below the vessel, the system can no longer follow or track the topside. Moreover, the position of the camera is easy to control via the drone operator. But as a famous Dutch footballer once said: ”Every advantage has its disadvantage”. A disadvantage of the use of drones may be that they still have to be individually controlled by a certified operator. Nevertheless, many parties agree that drones will play an important role in maritime and offshore activities. [45]

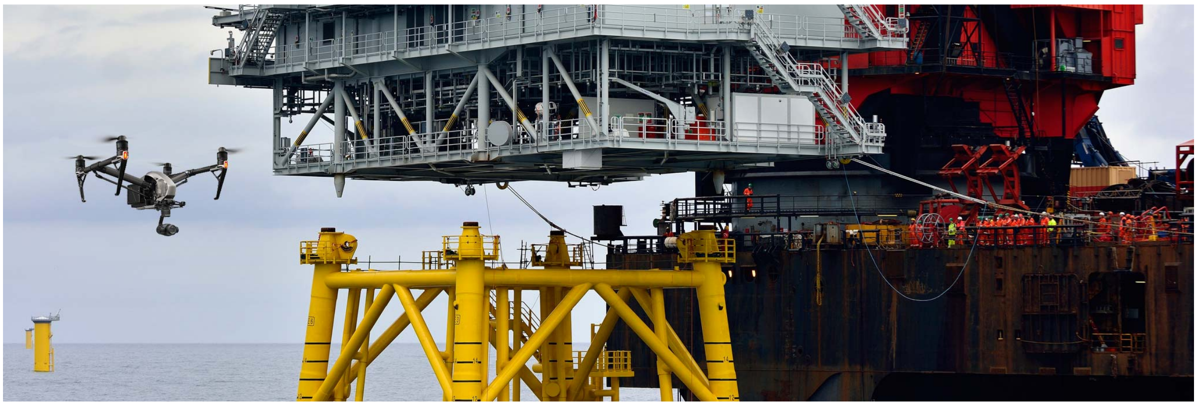

Figure 2.6: Drone as an installation aid during offshore topside installations

Just like in concept 2 this concept will also use cameras to determine the relative position between two objects. These objects can be for instance, but not limited to, a topside and a jacket. In current practice distances where estimated based on experience of the assistant-superintendent and the rigger foremen. To enhance visibility of the stabbing cones and the receiving guides some extra attention could be given to the paintwork to get best contrast possibility when looking with a camera or drone. Another way of distance measurements with a camera is to use a target pattern (physical). The target pattern could be used for alignment. Calculations based on camera images is called computer vision. Computer vision is concerned with electronically perceiving and understanding imagery form cameras. The use of computer vision is much more accurate then human estimations. There are several different computer vision algorithms to use. A robust computer vision technique has to be chosen in order to enable real-time object tracking in offshore conditions. The computer vision technique must be applicable to both drones and fixed cameras on the SSCV. The final concept can use drones, fixed cameras or a combination. In order to increase simplicity, the position of the cameras should not be determined by a spatial control survey.

2.3. Selecting a computer vision technique

A computer vision technique needs to be chosen that makes it possible to determine the relative distance between the jacket and topside. It focuses in particular on optical tracking. Real-time computer vision is a key ingredient to successful augmented-reality tracking and registration. The objective of optical tracking is to determine the pose of an object in the real world relative to a camera. This requires knowledge of cameras and computational algorithms operating on images. In the context of augmented reality, tracking an object means that the object's position and orientation are measured continuously.

2.3.1. Tracking techniques

Three different tracking techniques are considered. The first technique is marker tracking and uses a basic camera representation, contour-based shape detection, pose estimation from homography, and nonlinear pose refinement. The second one is multi-camera infrared tracking. This technique uses multiple cameras in a known configuration to find 2D-2D correspondences in multiple-camera images. Epipolar geometry and triangulation is then used to find absolute orientation. The last and third technique is natural feature tracking by detection. This technique tries to find interest points in images, creation and matching of descriptors and computation of the camera pose from known 2D-3D correspondences. This last technique was also used in the 'Augmented Reality' system.

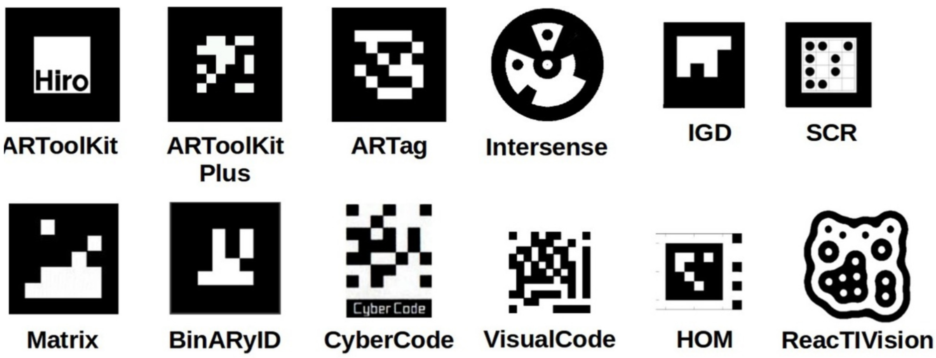

Figure 2.7: Examples of fiducial marker systems [28]

Marker Tracking

Markers are known patterns placed on the surfaces of target objects or known trackable shapes attached to the target objects (see figure 2.7). The markers are designed to make detecting their appearance in the image as easy and reliable as possible. This goal is addressed by choosing shapes that have optimal contrast and are easily detected. The most successful marker designs are circular or square shapes [57]. Circular shapes project onto an ellipsoid in the image, while squares project onto a general quadrilateral. Circular shapes yield only a single centroid point, while squares yield four corner points. Recovering a full 6DOF pose requires a theoretical minimum of three points. A fourth point is required in practical implementations to obtain a unique solution. This requirement implies that circular shapes must always be used in groups with a known configuration, while a single square suffices for detection. However, all four corners of the square must be properly identified. Identification is facilitated by adding a rotation-invariant pattern inside the circular or square shape to discriminate multiple markers and establish marker orientation.

Multiple-Camera Infrared Tracking

This technique requires a minimum of two cameras in a known configuration. The cameras will track rigid body markers composed of four or more retro-reflective spheres. In practice, four cameras set up in the corners of a theoretical square space are a popular configuration. Use of more than two cameras will improve the performance of the system. [34]

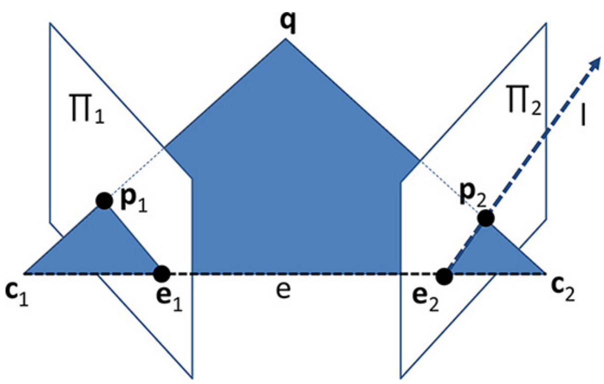

Figure 2.8: Multiple-camera tracking [57]

Figure 2.8 shows the geometry of two cameras with centers c_1, c_2 and image planes π_1 and π_2. A 3D point q projects to p_1 and p_2. With the aid of trigonometric algorithms it is possible to determine the position of point q with respect to the two cameras.

Natural Feature Tracking by Detection

The previous two techniques require the presence of fiducial markers. Besides tracking of markers it is also possible to track 'natural features' to determine the camera pose from observations in the image without instrumenting the environment with markers. First a suitable digital model is reconstructed by scanning the real environment. The tracking model is then matched at runtime to observations from the camera. Natural feature tracking typically requires better image quality and more computational resources. [39] Objects that do not possess much texture can be tracked using edge features, assuming that their outline is easily observable (see figure 2.9). However, a single edge hardly allows a unique identification without additional knowledge, and multiple edges must be jointly interpreted for reliable target detection. Therefore it is necessary to compare these images to some kind of reference model. If such a model is obtained prior to starting the tracking system, this is called the approach of model-based tracking. This approach was also used in the 'Augmented Reality' system.

Figure 2.9: Edge detection [62]

2.3.2. Comparison of tracking techniques

A comparison between the three tracking techniques described in the previous chapter is given in table 2.2. The technique based on natural feature tracking was implemented in the 'Augmented Reality' system. It used natural features as a detection method but this didn't provide accurate results. The other two techniques have not been used yet. The technique with multiple-camera tracking seems to be quite inconvenient if its combined with drones because the orientation between the cameras must be precisely known. It also requires the recognition of at least six markers of which the orientation of the individual markers must be accurately measured beforehand. The technique based on marker tracking, especially square markers, appears to be the most suitable to apply. The relative position between two objects in six degrees of freedom can be obtained from only two markers. The only drawback of this technique is that the markers have to be applied to the structure. Ideally, it would be desirable not to apply markers on the jacket or topside. However this makes it possible to use simple and potentially more robust tracking algorithms and thus increase system accuracy , robustness and usability.

2.4. Marker tracking

The markers that have recently been introduced in chapter 2.3 are binary fiducial markers. These markers are widely used in computer vision techniques for pose estimation. The process of pose estimation is based on finding correspondences between points in the real environment and their 2D image projection. This is usually a difficult step, the use of fiducial markers makes it easier. A fiducial marker system is composed by a set of valid markers and an algorithm which performs its detection in images.

2.4.1. Fiducial marker systems

In literature, several marker systems have been proposed as shown in figure 2.7. The simplest proposals consist of using dots as fiducial markers. These dots can be LEDs, reflective spheres or planar

	Marker Tracking	Multiple-Camera Infrared Tracking	Natural Feature Tracking by Detection
Tracking type	Model-free	Model-free	Model-based
Markers / Natural Features	Marker	Marker	Natural features
Camera orientation	Free moving	Free moving but orientation and position between cameras must be known	Free moving
6DOF between two objects	From 2 markers (1 per object)	At least 6 markers (3 per object)	Correct detection and matching of multiple edges from both objects.

Table 2.2: Comparison between three tracking techniques

dots [25]. Their identification is usually obtained from the relative position of the markers and often involves a complex process. Other approaches use circular markers where the identification is encoded in circular sectors [40]. The disadvantage of this is that only a correspondence point is given (the middle). This makes the use of multiple circular markers necessary for pose estimation. Other types of fiducial markers are based on blob detection. Blob detection methods are aimed at detecting regions in a digital image that differ in properties, such as brightness or color, compared to surrounding regions. Cybercode or VisualCode is derived from 2D-barcodes technology as MaxiCode or QR but can also accurately provide several correspondence points.

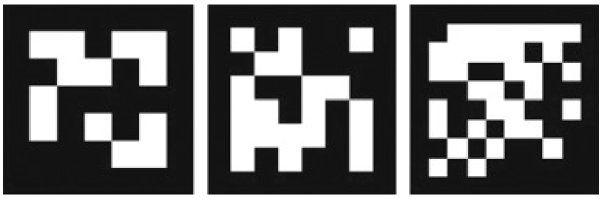

Figure 2.10: Example of markers of different sizes; n=5, n=6 and n=8 [28]

One of the most popular approaches is the use of binary square fiducial markers. The main benefit of these markers is that a single marker provides enough correspondences (its four corners) to obtain the camera pose. Also, the inner binary codification makes them specially robust, allowing the possibility of applying error detection and correction techniques. A popular library for detection of square fiducial markers is the ArUco library. Currently it provides one of the fastest and most reliable methods, which is easy to use and implement too [4]. This method is provided by the Aruco add-on library for OpenCV presented by Garrido-Jurado et al. [28] OpenCV provide a lot of functions which can be used for tracking rigid objects seen by a camera. [11] An ArUco marker is a synthetic square marker composed by a wide black border and an inner binary matrix which determines its identifier (id). The black border facilitates its fast detection in the image and the binary codification allows its identification and the application of error detection and correction techniques. The marker size determines the size of the internal matrix. For instance a marker size of 6x6 is composed by 64 bits.

For this research it was chosen to use the ArUco library since it is considered to be the most evolved, precise and robust tool for generating, detecting and estimating the pose of planar fiducial markers. The library is open source and is built around OpenCV, a reference in image processing and vision computation field. OpenCV and ArUco are available as open source distributions with a BSD license. ArUco was introduced in 2014 and mainly developed for augmented reality purposes. Using ArUco markers to calculate the distance between two bodies can therefore be seen as a novel approach.

2.4.2. Relative position between a topside and jacket

ArUco markers are able to return information about their position relative to a camera reference frame. For two markers it is possible to obtain their relative position by means of vector transformations. The marker itself will be used as a scaling unit since the dimensions of the marker is known. If these markers are positioned on a convenient place on the topside and jacket it would be possible to calculate the relative position between these objects. In theory, one should only need two markers in order to obtain the relative position in six degrees of freedom. An example is given in Figure 2.11.

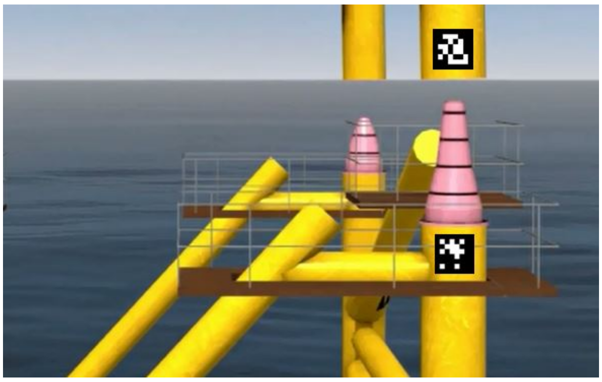

Figure 2.11: Obtain relative position between a topside and a jacket by using ArUco markers

2.4.3. Marker tracking with drones

ArUco markers are mostly used in clean lab environments as a visual navigation aid for robots. [61] There are only a few examples available in literature that use ArUco markers in an outdoor environment. [21] Real-time object tracking of an ArUco marker is an essential part of the proposed concept. If two markers are tracked at the same time it is possible to obtain the relative position between these markers. A small experiment was carried out in order to evaluate the performance of real-time object tracking with a camera attached to a drone.

Experiment setup

For this experiment the author's personal drone is used, a DJI Phantom 4 Pro. The drone is equipped with an Internal Navigation System, an orientable 3-axis gimbaled camera and distance sensors. Two ArUco markers are printed on hard foam to ensure the markers are always flat. The markers are placed side by side on the ground. The drone will fly above these markers with the camera facing down starting at a height of 2 m as can be seen in Figure 2.12.

Figure 2.12: Drone experiment setup

It will ascent to a height of around 30 meters. A video is recorded at a resolution of 1280x720 pixels in black and white. This results in a small sized video which can be easily post processed. The size of the markers are 380 x 380 mm. The distance between the marker centers is 420 mm for the x-axis, 0 mm for the y-axis and 0 mm for the z-axis. An algorithm was developed to obtain the x-, y- and z-offset and their orientation between the marker centers. The measured offsets by the algorithm can be compared with the known offsets. In that way it is possible to obtain the precision and accuracy of a marker based approach.

Results

The results of this experiment are shown in Figure 2.13 and in Table 2.3 for the translations. These results show the measurement error in meters. The green area indicates the 150 mm margin which was introduced in the system requirements. Errors within this margin are considered as acceptable. The graph show the measurement error for x-, y- and z-offset (top to bottom). It is clearly visible that the accuracy of the measured offset decreases with increasing altitude of the drone (height). The graph stops when the algorithm was no longer able to recognize the markers due to small marker size. This was at an altitude of around 25 meters. The x- and y- offset are constantly within the safe margin but get less accurate for smaller marker areas. The accuracy for the z-offset starts fluctuating very soon and gets unacceptable low for smaller marker areas. This result is expected since the measurement accuracy in computer vision depends on the image pixel density.

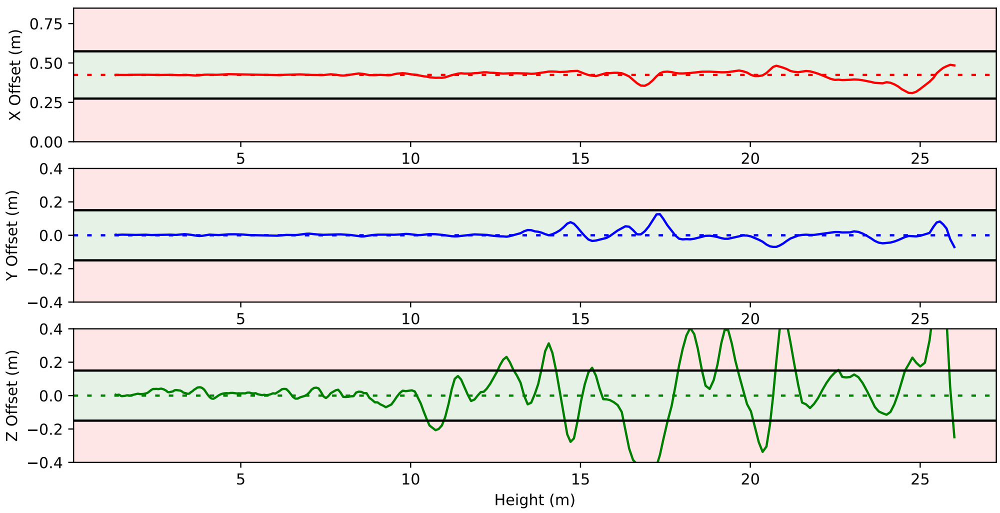

Figure 2.13: Drone experiment results translations

e_{MAE}[m]	$\lvert e\rvert_{MAX}$[m]	σ_e [m]	μ_e [m]
x: 0.012	x: 0.115	x: 0.023	x: 0.000
y: 0.012	y: 0.126	y: 0.023	y: 0.003
z: 0.086	z: 0.781	z: 0.151	z: 0.025

Table 2.3: Drone experiment results translations. e_{MAE} = mean absolute error, $\lvert e\rvert_{MAX}$ = absolute maximum error, σ_e = standard deviation, μ_e = mean error

The results for rotation are shown in Figure 2.14 and in Table 2.4. Figure 2.14 shows that roll and pitch rotations (rotations around the x- and y-axis respectively) are only accurate for bigger marker areas (> 20,000 px^2). Yaw (rotation around the z-axis) is more accurate over the whole range but shows a bump for very small marker areas (< 200 px^2).

From these small experiments it can be concluded that accurate results can expected for the x- and y-offset. Accuracies for z-offset and roll, pitch and yaw heavily depend on the image pixels density and get inaccurate for smaller marker areas.

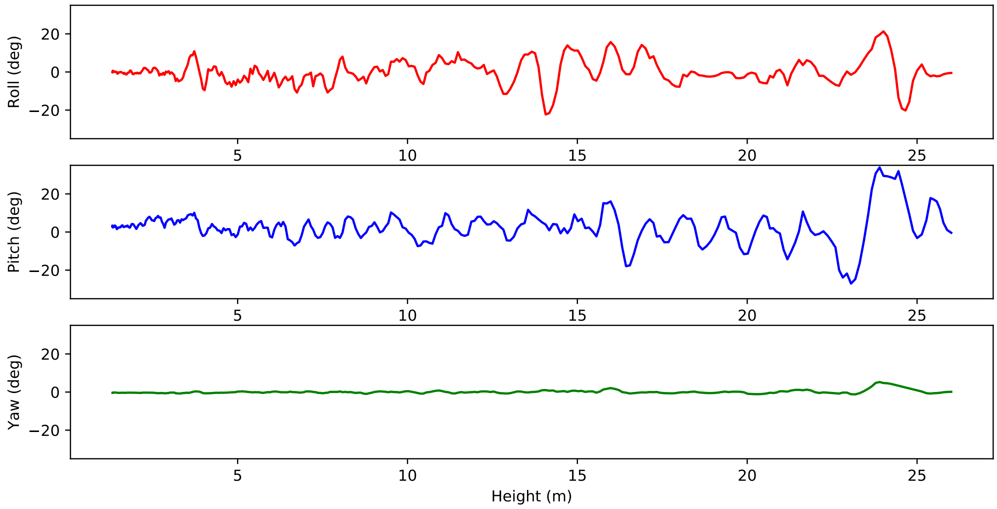

Figure 2.14: Drone experiment results rotations

e_{MAE}[deg]	$\|e\|_{MAX}$[deg]	σ_e [deg]	μ_e [deg]
ϕ: 3.916	ϕ: 22.272	ϕ: 5.857	ϕ: -0.097
θ: 5.468	θ: 33.922	θ: 7.398	θ: 2.646
ψ: 0.497	ψ: 5.264	ψ: 0.849	ψ: -0.011

Table 2.4: Drone experiment results rotations. e_{MAE} = mean absolute error, $|e|_{MAX}$ = absolute maximum error, σ_e = standard deviation, μ_e = mean error

2.4.4. Marker tracking with a multiple camera-setup

The previous experiment in chapter 2.4.3 showed accurate results in the horizontal and vertical direction of the camera plane but inaccurate results for measurements perpendicular to the camera frame (e.g. depth). This problem can be overcome by using an extra camera and an extra pair of markers in a perpendicular orientation. An example is given in Figure 2.15. In this way, distances in all directions can be measured accurately. The previous experiment showed that it was possible to measure distances accurately. A second small experiment will be carried out to check whether it is possible to use two cameras simultaneously in object tracking.

Experiment setup

For this experiment two USB cameras where used. The camera used was the SJ4000. This camera was able to deliver a resolution of 620 x 480 pixels. Tea boxes where equipped with ArUco markers printed on paper with dimensions of 40 x 40 mm. The experiment setup is shown in Figure 2.16. Four unique markers where used to tell the camera which markers it had to track. The algorithm that was used for the previous experiment was not able to recognize a second camera. A new algorithm was developed that used threading. Threading is a way to enable multiple processes at the same time. A separate thread was created for each camera. Both threads where able to communicate with each other to share data. A GUI with a bulls-eye was created to make a top view of the situation. The bulls-eye followed the path of the upper tea box with respect to the lower tea box. The thickness off the bulls-eye indicated the height of the upper tea box. The bulls-eye became smaller when the vertical distance between the boxes increased.

Results

The result of this experiment is shown in Figure 2.17. Three screenshots are shown, two screenshots of both cameras and a screenshot of the GUI with the bulls-eye (red dot). The yellow line which is drawn between the two markers indicate that they are recognized correctly. By moving the upper tea

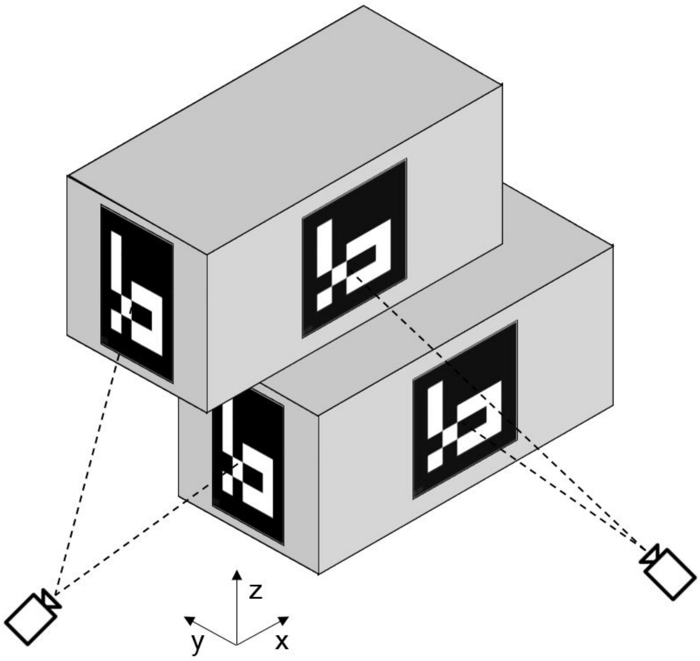

Figure 2.15: Two markers pairs with a perpendicular orientation

box the bulls-eye will start moving and the GUI indicates how the box has to be moved in order to center it again (e.g. move 5 cm east). The main goal of this experiment was to check if it was possible to use two cameras simultaneously and this has been proved. The input to provide imagery can be anything. It can be a camera connected with USB, a video signal coming from a HDMI source, a video file (for post processing) or even a wireless rtmp video-stream from everywhere in the world.

2.5. Summary

An introduction to the previous developed systems was given and the system requirements for an unmanned offshore topside installation monitor are determined. A new system must be able to work for different topsides, endure offshore environments and have a precision of at least 150mm. The concept using visual object tracking with cameras and drones was introduced. Three tracking techniques where presented and marker based tracking seemed to be the most robust method to use. Some small scale experiments have been performed to check its feasibility. The first results provided sufficient confidence that this method will work.

Figure 2.16: Experiment setup

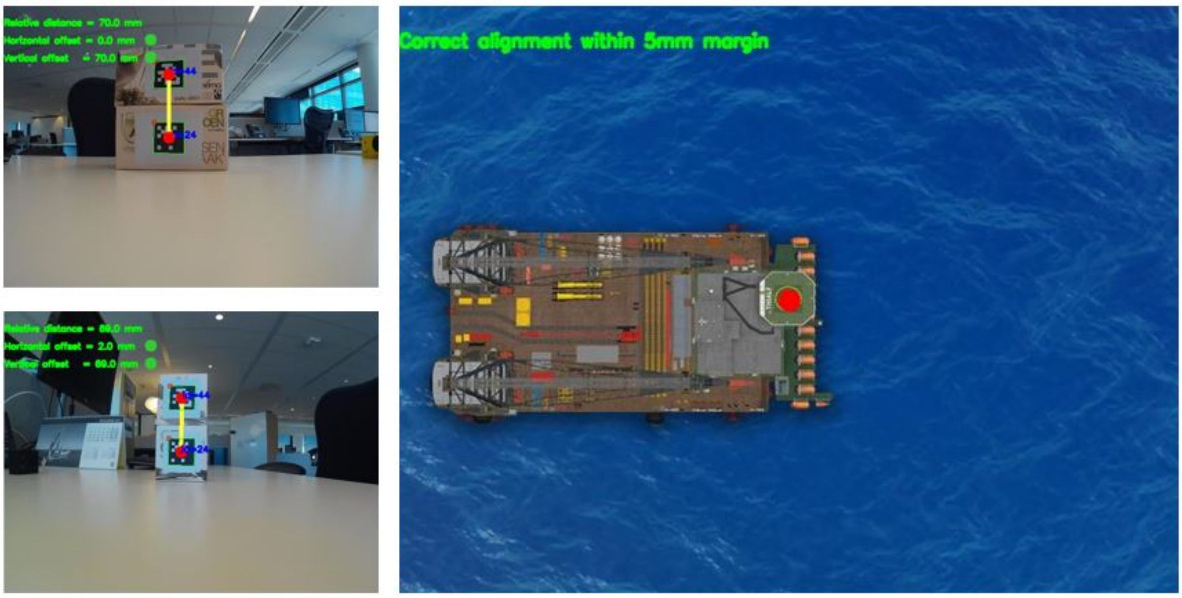

Figure 2.17: User Interface


HEERE
THIALF
PANAMA R.P.
A4


EMA
P4
P4
P4
B4
B4
5
5

3

Real-time motion tracking

This chapter discusses how cameras can be used to determine the relative position between two objects. These objects can be for instance, but not limited to, a topside and a jacket. The detection of the relative motions between the topside and the jacket in real-time is considered a crucial task which has to be solved to carry out the unmanned installation. This chapter tries to give an answer to second sub-question:

How can visual object tracking been used to calculate the relative position between a topside and a jacket in 3-DOF?

3.1. Object tracking with ArUco markers

Each detected ArUco marker returns a vector of four points (corresponding to the four corners), a unique ID, its size and the translation and rotation vector. Markers are comprised by an external black border and an inner region that encodes a binary pattern. This binary pattern is used to identify the marker and its ID. There are different marker dictionaries. Markers can have a different configuration of bits. The more bits, the more words in a dictionary, and the smaller the chance of confusion. However, more bits requires a better resolution for correct detection. So there is a trade off between the accuracy of the marker and the number of bits. The markers are encoded as a $(n+2)$ x $(n+2)$ grid (Fig. 2.10) where the external cells are set as black, creating an external border which is easily detectable. The remaining n x n cells are used for coding. The author of the ArUco library recommends to use the ARUCO-MIP-36h12 dictionary [50], which has 250 different marker patterns with n=6. An example of this marker can be found in figure 3.1.

3.1.1. Camera calibration

An important procedure within the computer vision technology is camera calibration. Camera calibration is the process of obtaining the fundamental parameters of a camera. These parameters are essential to determine where a 3D point in space projects in the camera sensor. The camera parameters can be divided into intrinsics and extrinsics. Intrinsic parameters are:

- f_x, f_y: Focal length of the camera lens in both axes. These are normally expressed in pixels.
- c_x, c_y: Optical center of the sensor (expressed in pixels).
- k_1, k_2, k_3, p_1, p_2: Distortion coefficients.

These parameters describe the relation between the 2D image pixels (x_i, y_i) and the real world coordinates (x, y, z). The relationship between the image pixels and the world coordinates is modeled using the pinhole camera model given by:

$$\begin{bmatrix} x_i \\ y_i \\ w \end{bmatrix} = \underbrace{\begin{bmatrix} f_x & 0 & c_x \\ 0 & f_y & c_y \\ 0 & 0 & 1 \end{bmatrix}}_{K} \begin{bmatrix} x \\ y \\ z \end{bmatrix} \tag{3.1}$$

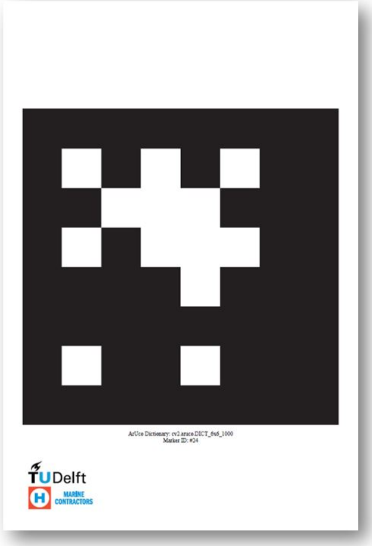

Figure 3.1: Example of ArUco marker: ARUCO-MIP-36h12 dictionary

K is known as the camera calibration matrix which can be found from taking several pictures of a checkerboard and process them using the OpenCV calibration functionality. In addition to calculate the camera calibration matrix K, it is also necessary to remove the radial image distortion.

In an ideal camera, a 3D point (x, y, z) in the space would project in the pixel: $x = (x * f_x/z) + c_x$ and $y = (y * f_y/z) + c_y$. However, camera lenses normally distorts the scene making the points far from the center to be even farther. This is why vertical stripes near the image borders appears slightly bended. As a consequence, the distortion components must be considered to know the projection of a pixel. Distortion can be divided in radial and tangential distortions and these are represented by the parameters: p_1, p_2, k_1, k_2, k_3. The mathematical relationship between the corrected image pixels (x_i, y_i) and the radial distorted pixels (x_d, y_d) is given by:

$$x_i = x_d(1 + k_1r^2 + k_2r^4 + k_3r^6) \tag{3.2}$$

$$y_i = y_d(1 + k_1r^2 + k_2r^4 + k_3r^6) \tag{3.3}$$

$$r = \sqrt{x_d^2 + y_d^2} \tag{3.4}$$

Similarly, another distortion is the tangential distortion which occurs because the image taking lens is not aligned perfectly parallel to the imaging plane. So some areas in the image may look nearer than expected. It is represented as below:

$$x_i = x_d + [2p_1xy + p_2(r^2 + 2x^2)] \tag{3.5}$$

$$y_i = y_d + [p_1 + (r^2 + 2y^2) + 2p_2xy] \tag{3.6}$$

With these parameters it is assumed that the 3D location of a point in relation to the camera reference system is known. But if the projection of a point referred to an arbitrary reference system is required, some extrinsic parameters need to be used. Extrinsic parameters are basically 3D rotations ($Rvec = R_x, R_y, R_z$) and 3D translations ($Tvec = T_x, T_y, T_z$). They are required to translate the camera reference system to the arbitrary one.

These parameters can be calculated with a calibration process of sample images of a well defined pattern, a chessboard in this case. The OpenCV calibration functionality is capable of finding specific points in it. The coordinates in the real world space and the coordinates in the image are known. For the best results, at least ten photos are needed. An example picture is shown in figure 3.2. The chessboard pattern is detected with the function cv2.findChessboardCorners(). It returns the corner points and a return value which will be true if a pattern is obtained. Eventually the found parameters

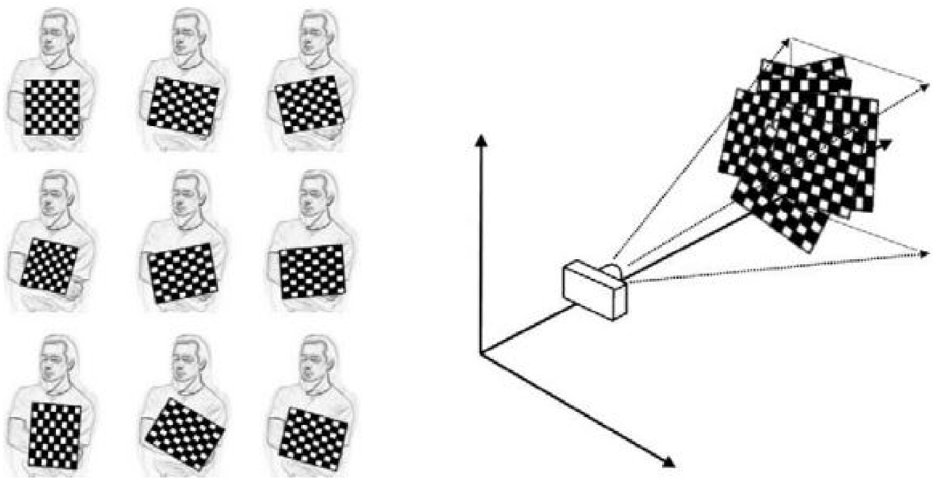

Figure 3.2: Images of a chessboard being held at various orientations (left) provide enough information to completely solve for the locations of those images in global coordinates (relative to the camera) and the camera intrinsics [12]

are stored in a calibration file so that the calibration does not have to be performed again and again. This is an important property. Camera calibration only needs to be performed once. Camera calibration can therefore be carried out far in advance and does not have to be performed during offshore work. [59]

3.1.2. Marker detection

Given an image where some ArUco markers are visible, the detection process has to return a list of detected markers. Each detected marker includes:

- The position of its four corners in the image (in their original order).
- The ID of the marker.

The process is divided into several steps with the aim of detecting the rectangles and identifying the binary code. To achieve this, a gray-scale image is used.

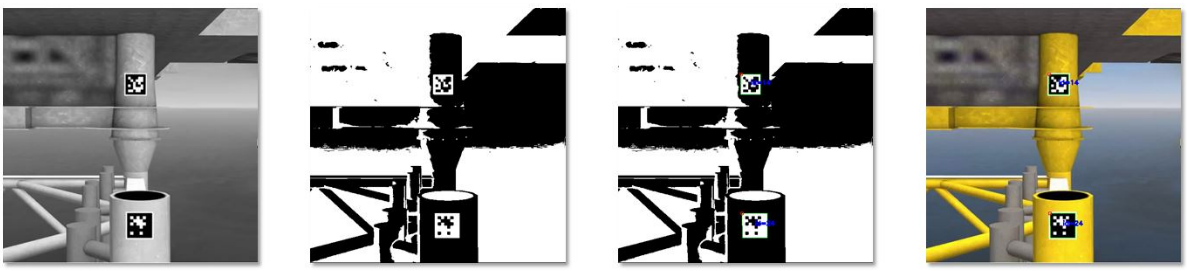

(a) (b) (c) (d)

Figure 3.3: Process of marker detection and identification

While the image analysis is not a novel contribution, the marker code identification and error correction is a new approach specifically designed for the generated dictionaries used in this method. Given the input image transformed into gray-scale (Fig. 3.3a) the following four steps are used for the marker detection:

- **Image segmentation (Fig. 3.3b):** First, the most prominent contours from the gray-scale image are filtered. For this a technique is used based on local adaptive thresholding approach. This technique has proven to be very robust to different lighting conditions.

- **Contour extraction:** The image segmentation is followed by a contour extraction which is performed on the treshold image obtained in the previous step. This contour extraction makes use of the Suzuki and Abe algorithm [60]. The algorithm yields a representation of a binary image, from which one can extract some sort of features without reconstructing the image. After that a polygonal approximation is performed using the Douglas-Peucker algorithm [33]. Since markers are enclosed in rectangular contours, those that are not approximated to 4-vertex polygons are discarded. Finally, the contours are simplified leaving only the external ones.

- **Marker code extraction (Fig. 3.3c,d):** Now its time to analyze the inner region of these contours to extract its ID. The perspective will be removed by computing the homography matrix. The result will be a tresholded image using Otsu's method [47]. Then, the binarized image is divided into a regular grid and each element is assigned the value '0' or '1' (Fig. 3.4) depending on the detection of a black or white square. A first rejection test consists of the detection of the black border. If all the values of the border are '0' then the inner grid is analyzed in the last step.

- **Marker identification:** In the final step it is necessary to determine which of the marker candidates obtained actually belongs to the dictionary and which are just part of the environment. Once the code of a marker is extracted, four different identities are obtained, corresponding to the four possible rotations of the marker. If any of them is found in the specified dictionary, the candidate is considered as a valid marker.

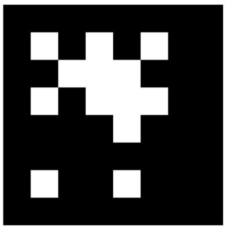

0	0	0	0	0	0	0	0
0	1	0	1	0	1	0	0
0	0	1	1	1	0	1	0
0	1	0	1	1	1	0	0
0	0	0	0	1	0	0	0
0	0	0	0	0	0	0	0
0	1	0	0	1	0	0	0
0	0	0	0	0	0	0	0

Figure 3.4: Bit assignment for each cell

3.1.3. Camera pose estimation

To determine the markers position using computer vision, also known as the camera pose estimation problem, requires to match a set of correspondences. This set is matched at pixel level, on the acquired images. Square fiducial markers, composed by an external wide black border and an inner code (like an ArUco marker), have become the most popular artificial landmarks. Their main advantage is that a single marker provides four correspondence points (its four corners), which are enough to perform camera pose estimation. The pinhole camera model is then used to project 3D points in the image plane using a perspective transformation.

$$s \cdot m' = K[R|t]M' \tag{3.7}$$

or

$$s\begin{bmatrix} u \\ v \\ 1 \end{bmatrix} = \begin{bmatrix} f_x & 0 & c_x \\ 0 & f_y & c_y \\ 0 & 0 & 1 \end{bmatrix}\begin{bmatrix} r_{11} & r_{12} & r_{13} & t_1 \\ r_{21} & r_{22} & r_{23} & t_2 \\ r_{31} & r_{32} & r_{33} & t_3 \end{bmatrix}\begin{bmatrix} X \\ Y \\ Z \\ 1 \end{bmatrix} \tag{3.8}$$

where:

(X, Y, Z)	are the coordinates of a 3D point in the world coordinate space
(u, v)	are the coordinates of the projection point in pixels
K	is a camera matrix, or a matrix of intrinsic parameters
(c_x, c_y)	is a principal point that is usually at the image center
(f_x, f_y)	are the focal lengths expressed in pixel units
s	represents the distance between the camera and the object

Thus, if an image from the camera is scaled by a factor, all of these parameters should be scaled by the same factor. The matrix of intrinsic parameters does not depend on the scene viewed. So, once estimated, it can be re-used as long as the focal length is fixed (in case of zoom lens). In this study prime lenses are used with fixed focal lengths. The joint rotation-translation matrix $[R|t]$ is called a matrix of extrinsic parameters. It is used to describe the camera motion around a static scene, or vice versa, rigid motion of an object in front of a still camera. The latter is the case with a drone flying around an object. That is, $[R|t]$ translates coordinates of a point (X, Y, Z) to a coordinate system, fixed with respect to the camera. The transformation above is equivalent to the following (when $z \neq 0$):

$$\begin{bmatrix} x \\ y \\ z \end{bmatrix} = R \begin{bmatrix} X \\ Y \\ Z \end{bmatrix} + t \tag{3.9}$$

$$x' = x/z \tag{3.10}$$

$$y' = y/z \tag{3.11}$$

$$u = f_x \cdot x' + c_x \tag{3.12}$$

$$v = f_y \cdot y' + c_y \tag{3.13}$$

Figure 3.5 illustrates the pinhole camera model.

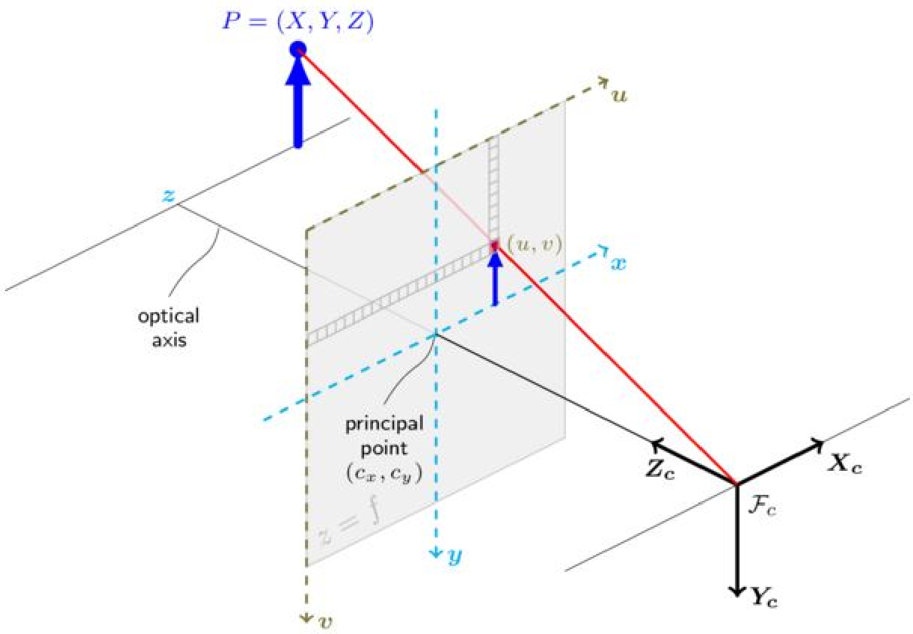

Figure 3.5: Pinhole camera model [11]

3.2. Kinematic model

3.2.1. Model overview

If two markers are correctly detected it is possible to calculate the relative position and orientation between these markers in a world coordinate system. For every detected marker the pose can be estimated as described in chapter 3.1.3. Each marker has six degrees of freedom (DoFs). These degrees of freedom are the output of the function aruco.estimatePoseSingleMarkers. It returns a rotation vector (rvec) that, together with the translation vector (tvec), brings points from the model coordinate system to the camera coordinate system. The translation vector is represented as a shift from one coordinate system to another system whose origin is displaced to another location; in other words, the translation vector is just the offset from the origin of the first coordinate system to the origin of the second coordinate system. Thus, to shift from a coordinate system centered on an object to one centered at the camera, the appropriate translation vector is simply **T** = origin$_{object}$–origin$_{camera}$. The formula for finding the rotation matrix corresponding to an angle-axis vector is called Rodrigues' formula, which is derived in Appendix D. The Rodrigues' formula can be used to transform a rotation vector (returned from the algorithm) to a rotation matrix.

Rotation in three dimensions can be decomposed into a two-dimensional rotation around each axis in which the pivot axis measurements remain constant. If we rotate around the x-, y-, and z-axis in sequence with respective rotation angles $\psi, \phi, \theta,$ the result is a total rotation matrix **R** that is given by the product of the three matrices $R_x(\psi), R_y(\phi)$ and $R_z(\theta)$, where:

$$R_x(\psi) = \begin{bmatrix} 1 & 0 & 0 \\ 0 & \cos\psi & \sin\psi \\ 0 & -\sin\psi & \cos\psi \end{bmatrix}$$

$$R_y(\phi) = \begin{bmatrix} \cos\phi & 0 & -\sin\phi \\ 0 & 1 & 0 \\ \sin\phi & 0 & \cos\phi \end{bmatrix}$$

$$R_z(\theta) = \begin{bmatrix} \cos\theta & \sin\theta & 0 \\ -\sin\theta & \cos\theta & 0 \\ 0 & 0 & 1 \end{bmatrix}$$

The rotation matrix **R** corresponding to the rotation vector **r** (or rvec) such that ||**r**|| $\leq \pi$ can be computed as follows: $\theta =$ ||**r**|| [12]. If $\theta = 0$, then **R** $= I$. Otherwise,

$$\mathbf{u} = \frac{\mathbf{r}}{\theta} \tag{3.14}$$

and

$$\mathbf{R} = I\cos(\theta) + (1 - \cos(\theta))\mathbf{u}\mathbf{u}^T + \mathbf{u}_\times \sin(\theta) \tag{3.15}$$

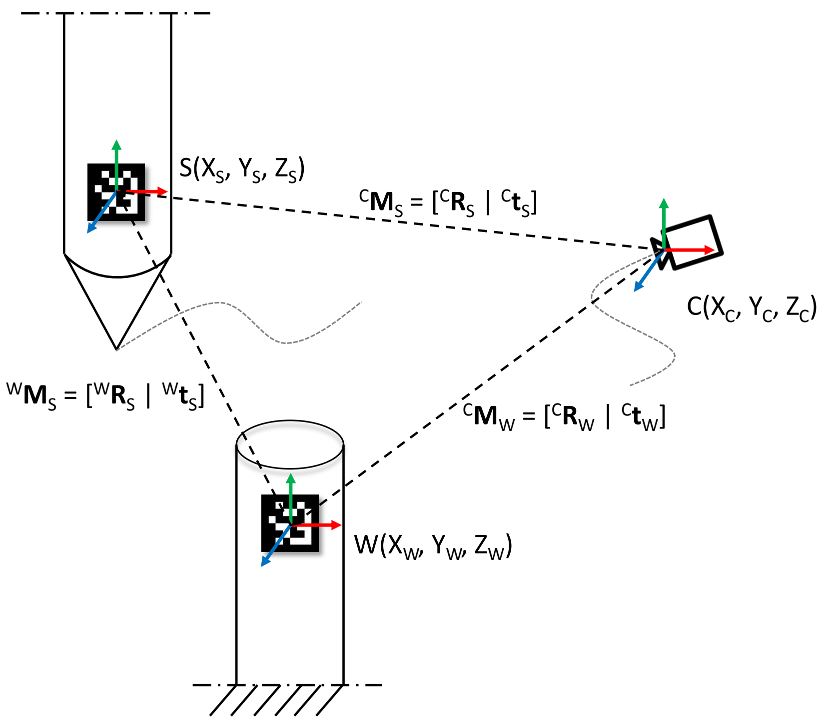

Figure 3.6: Kinematic model

The joint rotation-translation matrix [**R**|**t**] is called a matrix of extrinsic parameters. It is used to describe the camera motion around a static scene, or vice versa, rigid motion of an object in front of a fixed camera. The algorithm is able to find ${}^{C}\mathbf{M}_S$ and ${}^{C}\mathbf{M}_W$ as described in figure 3.7. ${}^{C}\mathbf{M}_S$ is the joint rotation-translation matrix between the camera coordinate system (C) and the coordinate system (S) of the marker on the stabbing cone:

$$ {}^{C}\mathbf{M}_S = [{}^{C}\mathbf{R}_S | {}^{C}\mathbf{t}_S] \tag{3.16} $$

${}^{C}\mathbf{M}_W$ is the joint rotation-translation matrix between the camera coordinate system (C) and the coordinate system (W) of the marker on the jacket receptor leg:

$$ {}^{C}\mathbf{M}_W = [{}^{C}\mathbf{R}_W | {}^{C}\mathbf{t}_W] \tag{3.17} $$

These two matrices in 3.16 and 3.17 can be used to compute the joint rotation-translation matrix between the coordinate system (W) of the marker on the jacket receptor leg and the coordinate system (S) of the marker on the stabbing cone. Therefore we define coordinate system W as the "fixed world". The rotation matrix ${}^{C}\mathbf{R}_W$ and translation vector ${}^{C}\mathbf{t}_W$ need to be inverted. The inverse of a rotation matrix is its transpose, which is also a rotation matrix:

$$ {}^{W}\mathbf{R}_C = {}^{C}\mathbf{R}_W^{-1} = {}^{C}\mathbf{R}_W^{T} \tag{3.18} $$

The inverse perspective transform of a translation vector can be obtained by reversing the direction of the vector and multiply it with the corresponding inverse rotation matrix:

$$ {}^{W}\mathbf{t}_C = {}^{W}\mathbf{R}_C \cdot -{}^{C}\mathbf{t}_W \tag{3.19} $$

Now all parameters are known to obtain the final rotation matrix and translation vector:

$$ {}^{W}\mathbf{R}_S = \left({}^{C}\mathbf{R}_W^{-1} \cdot {}^{C}\mathbf{R}_S\right)^{-1} = \left({}^{W}\mathbf{R}_C \cdot {}^{C}\mathbf{R}_S\right)^{-1} \tag{3.20} $$

$$ {}^{W}\mathbf{t}_S = {}^{C}\mathbf{R}_W^{-1} \cdot {}^{C}\mathbf{t}_S + {}^{W}\mathbf{R}_C \cdot -{}^{C}\mathbf{t}_W = {}^{W}\mathbf{R}_C \cdot {}^{C}\mathbf{t}_S + {}^{W}\mathbf{t}_C \tag{3.21} $$

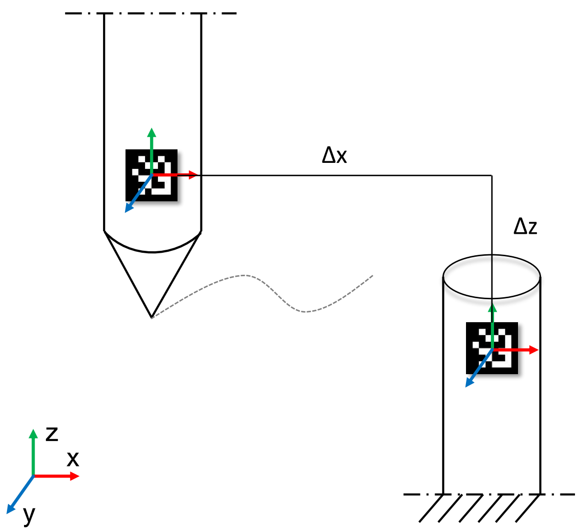

Figure 3.7: Kinematic model, $\Delta x-$, $\Delta z-$offset

$$ {}^{W}\mathbf{t}_S = [\Delta x, \Delta y, \Delta z] \tag{3.22} $$

The final obtained vector ${}^{W}\mathbf{t}_S$ includes information about the vertical offset (Δx, Δy and Δz) between a pair of markers as can be seen in figure 3.7.

3.2.2. Verification

In order to check the created kinematic model some simple calculations with known outcomes will be done. In Figure 3.8 two markers are shown. Lets assume they are filmed by a camera which is perpendicular to the marker plane. The marker on the fixed world is 10 meters away from the camera and has coordinates [2, 4, 10]. The marker on the moving world is 20 meters away and has coordinates [-4, -4, 20]. So the vector of the relative position must be [-6, -8, 10].

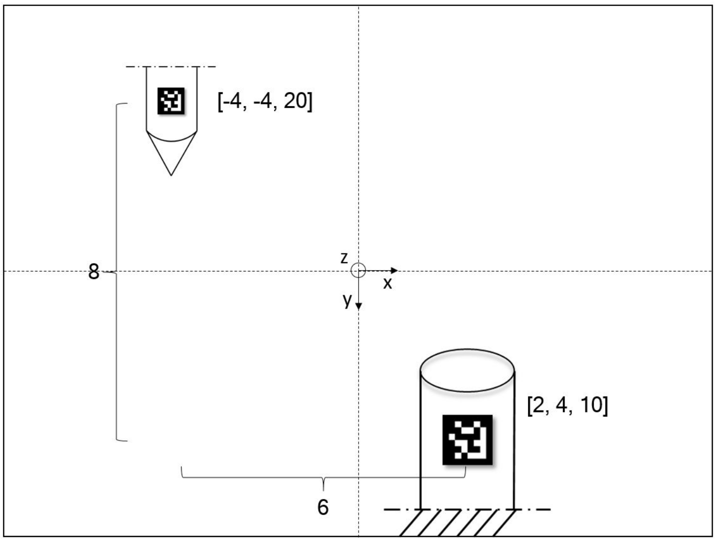

Figure 3.8: Verification, expected values

$$^{C}\mathbf{r}_S = \begin{bmatrix} 0 \\ 0 \\ 0 \end{bmatrix}, ^{C}\mathbf{t}_S = \begin{bmatrix} -4 \\ -4 \\ 20 \end{bmatrix}, ^{C}\mathbf{r}_W = \begin{bmatrix} 0 \\ 0 \\ 0 \end{bmatrix}, ^{C}\mathbf{t}_W = \begin{bmatrix} 2 \\ 4 \\ 10 \end{bmatrix}$$

$^{C}\mathbf{r}_S$ and $^{C}\mathbf{r}_W$ are in vector form. They can be transformed into matrix form with the Rodrigues' formula as derived in Appendix D:

$$^{C}\mathbf{R}_W = \begin{bmatrix} 1 & 0 & 0 \\ 0 & 1 & 0 \\ 0 & 0 & 1 \end{bmatrix}, ^{C}\mathbf{R}_S = \begin{bmatrix} 1 & 0 & 0 \\ 0 & 1 & 0 \\ 0 & 0 & 1 \end{bmatrix},$$

Now the transpose of matrix $^{C}\mathbf{R}_W$ can be calculated which is identical beacause it is already an Identity matrix:

$$^{W}\mathbf{R}_C = ^{C}\mathbf{R}_W^{-1} = ^{C}\mathbf{R}_W^{T} = \begin{bmatrix} 1 & 0 & 0 \\ 0 & 1 & 0 \\ 0 & 0 & 1 \end{bmatrix}$$

$$^{W}\mathbf{t}_C = ^{W}\mathbf{R}_C \cdot - ^{C}\mathbf{t}_W = \begin{bmatrix} 1 & 0 & 0 \\ 0 & 1 & 0 \\ 0 & 0 & 1 \end{bmatrix} \cdot \begin{bmatrix} -2 \\ -4 \\ -10 \end{bmatrix} = \begin{bmatrix} -2 \\ -4 \\ -10 \end{bmatrix}$$

And finally the resulting rotation matrix and translation vector between the two markers can be calculated. Both are exactly what was expected so this is the first proof of the developed algorithm.

$$^{W}\mathbf{R}_S = \left(^{W}\mathbf{R}_C \cdot ^{C}\mathbf{R}_S\right)^{-1} = \left(\begin{bmatrix} 1 & 0 & 0 \\ 0 & 1 & 0 \\ 0 & 0 & 1 \end{bmatrix} \cdot \begin{bmatrix} 1 & 0 & 0 \\ 0 & 1 & 0 \\ 0 & 0 & 1 \end{bmatrix}\right)^{-1} = \left(\begin{bmatrix} 1 & 0 & 0 \\ 0 & 1 & 0 \\ 0 & 0 & 1 \end{bmatrix}\right)^{-1} = \begin{bmatrix} 1 & 0 & 0 \\ 0 & 1 & 0 \\ 0 & 0 & 1 \end{bmatrix}$$

$$^{W}\mathbf{t}_S = ^{W}\mathbf{R}_C \cdot ^{C}\mathbf{t}_S + ^{W}\mathbf{t}_C = \begin{bmatrix} 1 & 0 & 0 \\ 0 & 1 & 0 \\ 0 & 0 & 1 \end{bmatrix} \cdot \begin{bmatrix} -4 \\ -4 \\ 20 \end{bmatrix} + \begin{bmatrix} -2 \\ -4 \\ -10 \end{bmatrix} = \begin{bmatrix} -6 \\ -8 \\ 10 \end{bmatrix}$$

The previous check had no rotation between the markers and the camera frame. In this verification check a rotation off the markers with respect to the camera will be introduced. The configuration of the markers can be seen in Figure 3.9. This illustration represents a top view. The markers are placed 10 meters away from the camera and two meters away from each other. They are rotated 45 degrees around the y-axis. The markers are on the same height. This should result in an x- and z-offset of $2/\sqrt{2}$ m.

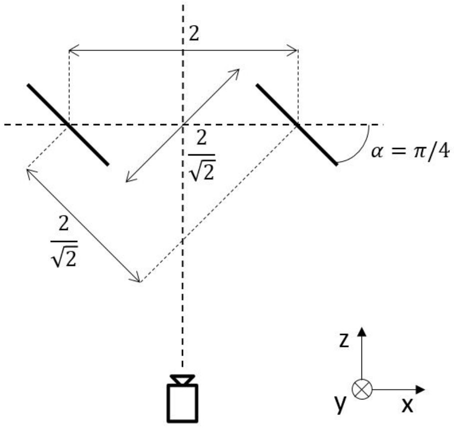

Figure 3.9: Verification, expected values

$$
{}^{C}\mathbf{r}_S = \begin{bmatrix} 0 \\ \pi/4 \\ 0 \end{bmatrix}, {}^{C}\mathbf{t}_S = \begin{bmatrix} -1 \\ 0 \\ 10 \end{bmatrix}, {}^{C}\mathbf{r}_W = \begin{bmatrix} 0 \\ \pi/4 \\ 0 \end{bmatrix}, {}^{C}\mathbf{t}_W = \begin{bmatrix} 1 \\ 0 \\ 10 \end{bmatrix}
$$

${}^{C}\mathbf{r}_S$ and ${}^{C}\mathbf{r}_W$ are in vector form. They can be transformed into matrix form with the Rodrigues' formula as derived in Appendix D:

$$
{}^{C}\mathbf{R}_W = \begin{bmatrix} 1/\sqrt{2} & 0 & 1/\sqrt{2} \\ 0 & 1 & 0 \\ -1/\sqrt{2} & 0 & 1/\sqrt{2} \end{bmatrix}, {}^{C}\mathbf{R}_S = \begin{bmatrix} 1/\sqrt{2} & 0 & 1/\sqrt{2} \\ 0 & 1 & 0 \\ -1/\sqrt{2} & 0 & 1/\sqrt{2} \end{bmatrix},
$$

Now the transpose of matrix ${}^{C}\mathbf{R}_W$ can be calculated which is:

$$
{}^{W}\mathbf{R}_C = {}^{C}\mathbf{R}_W^{-1} = {}^{C}\mathbf{R}_W^{T} = \begin{bmatrix} 1/\sqrt{2} & 0 & -1/\sqrt{2} \\ 0 & 1 & 0 \\ 1/\sqrt{2} & 0 & 1/\sqrt{2} \end{bmatrix}
$$

$$
{}^{W}\mathbf{t}_C = {}^{W}\mathbf{R}_C \cdot -{}^{C}\mathbf{t}_W = \begin{bmatrix} 1/\sqrt{2} & 0 & -1/\sqrt{2} \\ 0 & 1 & 0 \\ 1/\sqrt{2} & 0 & 1/\sqrt{2} \end{bmatrix} \cdot \begin{bmatrix} -1 \\ 0 \\ -10 \end{bmatrix} = \begin{bmatrix} 9/\sqrt{2} \\ 0 \\ -11/\sqrt{2} \end{bmatrix}
$$

$$
{}^{W}\mathbf{R}_S = \left({}^{W}\mathbf{R}_C \cdot {}^{C}\mathbf{R}_S\right)^{-1} = \left(\begin{bmatrix} 1/\sqrt{2} & 0 & -1/\sqrt{2} \\ 0 & 1 & 0 \\ 1/\sqrt{2} & 0 & 1/\sqrt{2} \end{bmatrix} \cdot \begin{bmatrix} 1/\sqrt{2} & 0 & 1/\sqrt{2} \\ 0 & 1 & 0 \\ -1/\sqrt{2} & 0 & 1/\sqrt{2} \end{bmatrix}\right)^{-1} = \left(\begin{bmatrix} 1 & 0 & 0 \\ 0 & 1 & 0 \\ 0 & 0 & 1 \end{bmatrix}\right)^{-1} = \begin{bmatrix} 1 & 0 & 0 \\ 0 & 1 & 0 \\ 0 & 0 & 1 \end{bmatrix}
$$

Now everything is known to calculate the relative position and orientation between both markers. And again the results are exactly the same at what was expected. These two numerical calculations verify the algorithm that is developed.

$$
{}^{W}\mathbf{t}_S = {}^{W}\mathbf{R}_C \cdot {}^{C}\mathbf{t}_S + {}^{W}\mathbf{t}_C = \begin{bmatrix} 1/\sqrt{2} & 0 & -1/\sqrt{2} \\ 0 & 1 & 0 \\ 1/\sqrt{2} & 0 & 1/\sqrt{2} \end{bmatrix} \cdot \begin{bmatrix} -1 \\ 0 \\ 10 \end{bmatrix} + \begin{bmatrix} 9/\sqrt{2} \\ 0 \\ -11/\sqrt{2} \end{bmatrix} = \begin{bmatrix} -2/\sqrt{2} \\ 0 \\ -2/\sqrt{2} \end{bmatrix}
$$

3.3. Motion Tracking Algorithm

Figure 3.10 shows a schematic overview of real-time displacement measurement using digital image processing techniques. An overview can be seen in the top left corner. Here is a jacket leg and a stabbing cone schematically shown. The algorithm will measure and display the distance between this stabbing cone and the jacket leg in the x,y-plane. Also the position of the two calibrated camera positions is shown. Then two representations are displayed that represents the image planes recorded by cameras 1 and 2. Camera 1 records images in the (x,z)-plane and camera 2 records in the (y,z)-plane. The measurement points are marked with a unique ArUco marker as discussed in chapter 2.4. If the markers are positioned in such a way that they are directly above each other in the end position there will be no horizontal offset and only the vertical offset must be known in advance. Because unique markers are used, the vertical offset between a set of two markers can be stored in the database for use at a later stage. This database also stores the calibration matrix of the camera, the size of the markers and the corresponding marker IDs. While capturing image frames, the displacement of the markers is calculated using image processing techniques. The frames from each camera are processed in a separate thread. Running several threads is similar to running several different programs concurrently, but with the following benefits:

- Multiple threads within a process share the same data space with the main thread and can therefore share information or communicate with each other more easily than if they were separate processes.
- Threads sometimes called light-weight processes and they do not require much memory overhead; they are cheaper than processes.

Each frame is converted into a grayscale. Grayscale images require less computing power then colored (RGB) images. Then markers are detected and compared with the marker ID's stored in the database. If a set of markers is found in the image frame their pose and relative position are calculated. This results in an x- and z-offset from camera 1 and an y- and z-offset from camera 2. So the value for z-offset is returned twice. A running average of these offsets with a length of 10 samples is calculated to allow for some noise filtering. In this application the running average is the unweighted mean of the previous data. The moving average is calculated as follows:

$$\Delta\bar{x} = \frac{\Delta x_M + \Delta x_{M-1} + \cdots + \Delta x_{M-(n-1)}}{n} = \frac{1}{n}\sum_{n-1}^{i=0} \Delta x_{M-i} \tag{3.23}$$

$$\Delta\bar{y} = \frac{\Delta y_M + \Delta y_{M-1} + \cdots + \Delta y_{M-(n-1)}}{n} = \frac{1}{n}\sum_{n-1}^{i=0} \Delta y_{M-i} \tag{3.24}$$

$$\Delta\bar{z_1} = \frac{\Delta z_{1M} + \Delta z_{1M-1} + \cdots + \Delta z_{1M-(n-1)}}{n} = \frac{1}{n}\sum_{n-1}^{i=0} \Delta z_{1M-i} \tag{3.25}$$

$$\Delta\bar{z_2} = \frac{\Delta z_{2M} + \Delta z_{2M-1} + \cdots + \Delta z_{2M-(n-1)}}{n} = \frac{1}{n}\sum_{n-1}^{i=0} \Delta z_{2M-i} \tag{3.26}$$

Of the two z-offsets that are obtained, the average is taken:

$$\Delta z = \frac{\Delta z_1 + \Delta z_2}{2} \tag{3.27}$$

This running average will result in a small time delay. If the images are acquired at 30 (FPS) then the running average will result in a delay of 1/3 second. This seems to be an acceptable delay. The running average ensures that the data is displayed more smoothly and fluctuations are filtered out and highlight longer-term trends. Mathematically, a moving average is a type of convolution and so it can be viewed as an example of a low-pass filter used in signal processing. For live data filtering the running average is a very simple, efficient and light weight function to implement.

3.4. Summary

In this chapter the technique of visual object tracking was introduced. The ArUco library has been used for processing. ArUco is intended to compute the position and orientation of a marker with respect to the camera. By combining two markers, one positioned on the jacket and one on the topside, the relative position between these markers can be obtained. These two markers are called a marker pair. Two perpendicular oriented marker pairs on the same target should result in an accurate estimation of the relative position. One camera can be used to capture one marker pair. Two cameras should be simultaneously tracking two marker pairs and combine their data. This data is filtered by using a running average and displayed in a GUI with a bullseye.

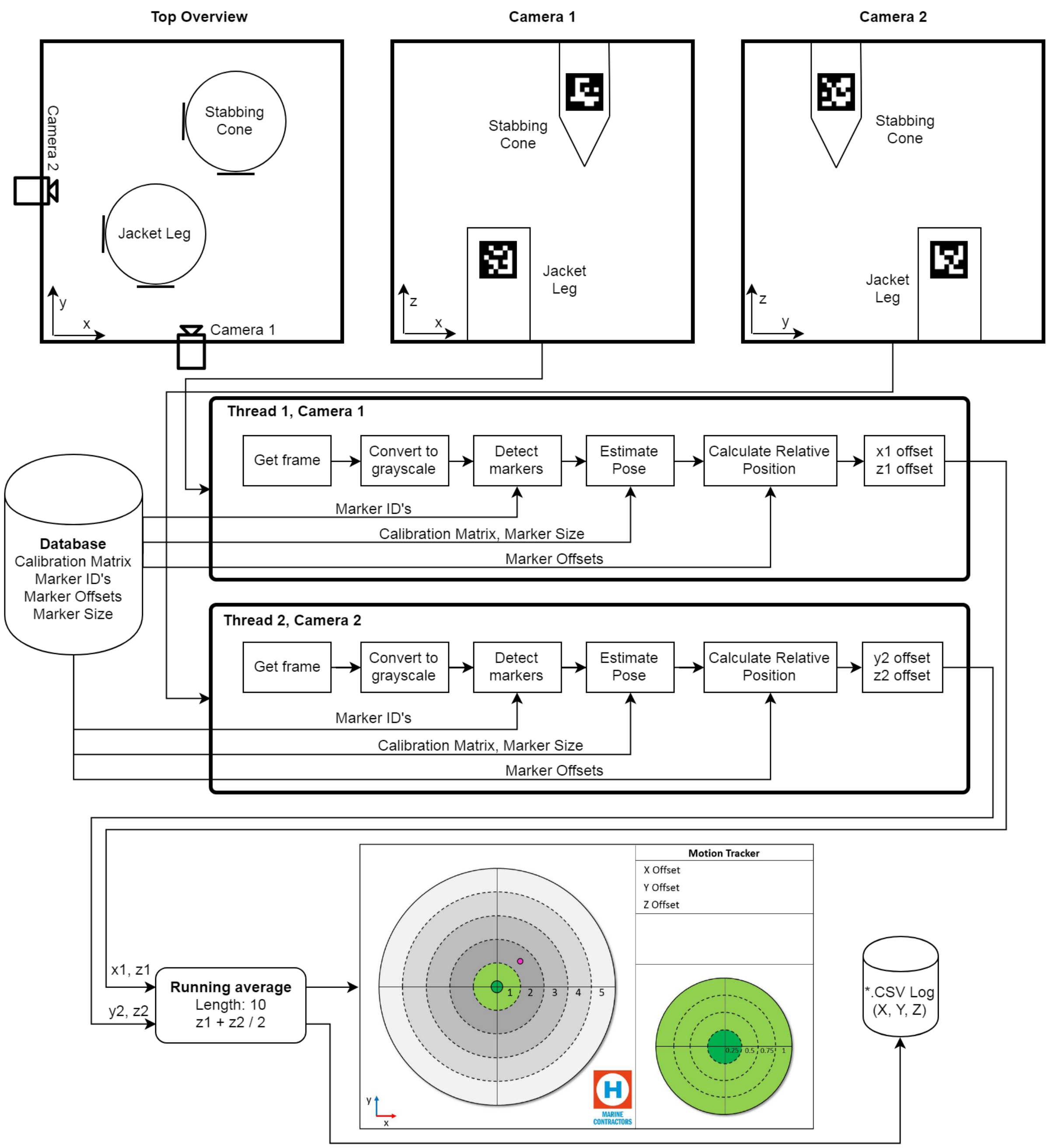

Figure 3.10: Camera and drone configurations


HEEREMA
THIALF
PANAMA R.P.
THIALF
PANAMA R.P.

4

Unmanned Topside Installation

In this chapter, the concept of visual object tracking with fixed cameras and drones will be further developed and explained. The development will focus on how imagery from cameras can be used to determine the relative position between a topside and a jacket. It is also discussed how this can be integrated within the current activities of HMC. The sub-question that is addressed in this chapter is:

How can the combination of drones, fixed cameras and object tracking assist in the installation of offshore topsides at HMC?

4.1. Positioning and orienting

The most important task of the system is to provide information about the relative position between a topside and a jacket. The topside can have a translation, rotation or both with respect to the jacket. This is illustrated in Figure 4.1. The axis definition is also given in this figure with the z-axis pointing positive upwards.

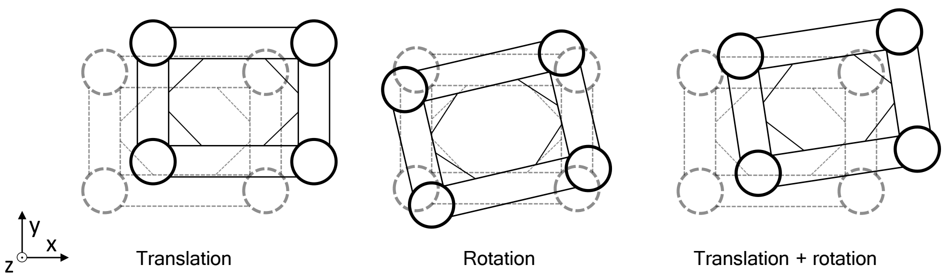

Figure 4.1: Translations and orientations, axis definition

4.1.1. Translations

Small experiments in chapter 2.4.3 showed that translations in the horizontal and vertical plane off a camera frame can be accurately measured for varying marker areas. For translations perpendicular to the camera frame (e.g. depth) these measurements shows inaccurate results for smaller marker areas. It would mean that both markers should always have around 5% of the total camera frame covered to obtain accurate results in all 3-DOF. Very large markers should then be used (around several meters wide). This would not be a realistic solution. Another small experiment in chapter 2.4.4 showed that it is also possible to use multiple cameras. By using multiple cameras, the data can be combined to obtain accurate results for all 3-DOF. The only requirement is that these cameras have to be positioned perpendicular (90 degrees) to each other. Two solutions will be introduced in chapter 4.3 to overcome this problem.

4.1.2. Rotations

A distinction can be made between two types of rotations. Namely, heading (rotation around z-axis) and tilt (combined rotation around x- and y- axis).

Heading

Heading can be calculated when the relative position of two locations is known. In both configurations the relative position of two stabbing cones is determined. These offsets can be used to determine the heading of the topside with respect to the jacket.

Tilt

Information about tilt is not taken into account in the Motion Tracking Algorithm. Tilt could either be determined by rotations between ArUco markers or when the vertical offset of at least three stabbing cones is known. The small experiment in chapter 2 showed that rotational estimations are very prone to errors. Topside tilt is usually around 1-2 degrees. This method would therefore not be accurate enough. In the latter case, when information about three cones is needed, it would increase the system complexity by adding an extra set of markers and cameras for a third stabbing cone. Since tilt is determined by design of the lifting arrangements, and can also not be adjusted once lifting has started, it is not taken into account.

4.2. Marker Location

Two ArUco markers provide information about the relative position between their centers. These markers are called a marker pair. For convenience, the markers must be positioned close to each other to capture them both with a camera. The place where the markers are closest to each other is at the stabbing cone and the receiving bucket. It is also useful if the markers are positioned above each other in the final position. As a result, no correction is needed for a horizontal shift. Only the vertical distance (h) between the marker centers must be known. The vertical distance can be easily calculated as $h = h_u + h_l$. h_u and h_l can be measured after mounting the markers. Distance h can be subtracted from the height measurement obtained between the markers (H). Also the height of the conical part of the stabbing cone (s) must be known to calculate when the stabbing cone enters the receiving bucket (l).

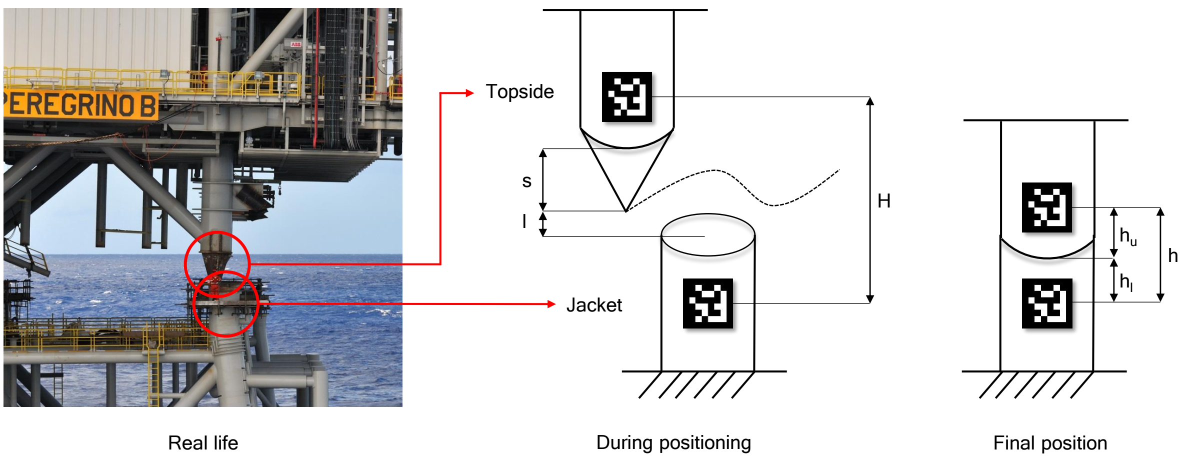

Figure 4.2: Marker locations to be placed on the jacket and topside

The dimensional control survey for these markers is therefore very easy. Distances can be measured with basic tools and no total stations are required. Markers can be clamped or fixed with bolts on a supporting bracket. In this research flat markers with a dimension of 1.00 x 1.00 m are used. Unfortunately it is not (yet) possible to use curved markers and stick or paint them on the round surface.

4.3. Camera Configuration

Now that it's clear that two perpendicular cameras have to track one object some camera configurations can be taught of. Cameras can be fixed on the SSCV or mounted on a drone. In this research two configurations will be introduced. These are hybrid configurations - that is to say, they both use fixed cameras and drones. Both configurations are illustrated in Figure 4.3 and will be further discussed in chapter 4.3.1 and 4.3.2. In both configurations markers on the stabbing cones will be tracked. In most cases, two stabbing cones are longer and are diagonally opposite of each other. These are called the primary stabbing cones (A and D). The other (shorter) ones are called the secondary stabbing cones (B and C).

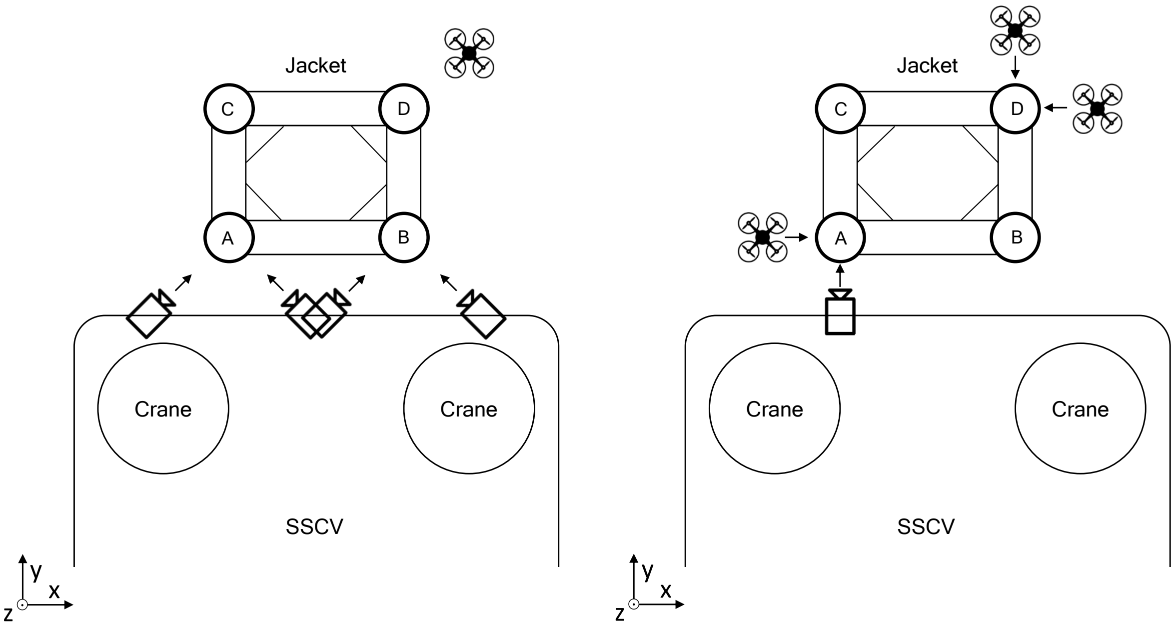

Figure 4.3: Camera configurations

4.3.1. Configuration 1

Configuration 1 primarily consists of four fixed cameras mounted on the stern of the SSCV. Two cameras track stabbing cone A (the primary stabbing cone) and two cameras track stabbing cone B as illustrated in Figure 4.3. When these two stabbing cones line up, the other two stabbing cones should also line up due to geometry. A drone is available to provide visual information about stabbing cone C or D. The visual information can be used by the superintendent as a verification tool. The drone will be able to provide the same information as a person standing on the jacket. It's free to move and can take any position. It should be noted that this configuration is only possible when the jacket is visible from the stern of the SSCV during the complete operation. Special mounts would be needed to lower the cameras from the stern of the SSCV to have enough visibility on the jacket.

4.3.2. Configuration 2

This configuration primarily consists of the use of drones as illustrated in Figure 4.3. One fixed camera is used on the stern of the SSCV. It would be very hard to keep a drone in position on this location. Chances of crashing would be very likely to happen. Drones will track the primary stabbing cones A and D as is customary in current procedures of HMC. The drones can fly near the stabbing cones and automatically keep position. It must be noted that the camera on the SSCV has to be lowered to film the jacket if it is far below the stern of the SSCV. A special bracket (or rails if it is desirable to adjust the height of the camera) should be constructed to enable this.

4.4. Fixed camera

The fixed cameras to be used on board the SSCV should be designed to stream video to a computer. Most digital cameras have video outputs such as HDMI or DVI. A special niche of the camera market are studio cameras. These cameras are specially designed to stream video directly to a computer or studio. This type of camera was also used in the Augmented Reality system as described in chapter 2.2.2. The cameras are already owned by HMC and could be re-used. It are Blackmagic Studio Cameras as illustrated in Figure 4.5. The maximum resolution is Ultra HD (3840 x 2160 pixels) with a frame rate up to 60 frames per second (FPS). The lenses can be changed to adapt for different situations. If the target is close to the camera (5 - 10 m), a wide-angle lens should be used (25 mm for example). If the target is further away (10 - 30 m) a zoom lens should be used (45 or 75 mm). The following formula can be used to estimate the size of the marker in the image plane with a given camera sensor and focal length:

$$h[px] = \frac{h[m] \cdot f[mm]}{l[m] \cdot s[mm]} \cdot s[px] \tag{4.1}$$

f	Focal length in mm
h	Real marker height in m
l	Distance to marker in m
s	Sensor height in pixels and mm

Table 4.1: My caption

If for example a camera is used with a Micro Four Thirds 4/3” sensor which has a sensor height of 13mm, a resolution of 1920x1080 pixels and a lens focal length of 50mm. The camera is 20m away of the marker. Then the marker height in pixels of a marker with dimensions 1x1m is:

$$h[px] = \frac{1 \cdot 50}{20 \cdot 13} \cdot 1080 = 208px$$

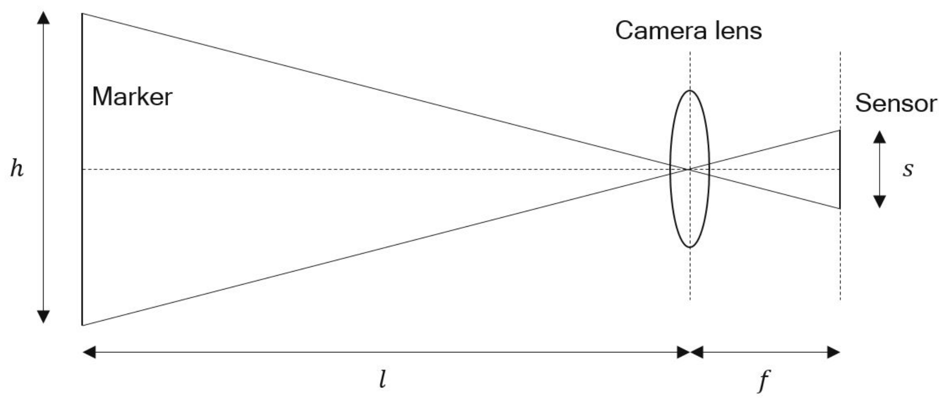

Figure 4.4: Camera lens focal length

All lenses should be able to film in low-light conditions. Therefore, a big aperture is preferred (f1.8 - f2.8). During sunny and bright conditions, polarizing filters can be used to minimize reflections.

A benefit of this camera is that it can be remotely operated by using a control panel as can be seen in Figure 4.6. In this way all cameras that are used on the SSCV can be controlled by one person. Control including iris, shutter speed, white balance, pan/tilt, and ISO is possible.

4.5. Use of Drones

Aerial vehicles that do not carry a human operator, fly remotely or autonomously, and carry lethal or non-lethal payloads are considered as drones. [49] Advances in fabrication, navigation, remote control

Figure 4.5: Blackmagic Studio Camera and lenses

Figure 4.6: Camera Control Panel

capabilities, and power storage systems have made possible the development of a wide range of drones which can be utilized in various situations where the presence of humans is difficult, impossible or dangerous. Growth projections for the sector are significant as drones become cheaper to purchase, smaller in size and easier to operate. In fact, the drone industry is regarded by many as the most dynamic growth sector of the global aerospace industry. [58]

4.5.1. Requirements

In addition to requirements on the positioning system as mentioned in chapter 2.1, the drone itself will also have to meet a number of requirements. These requirements include: safety requirements, operational requirements and data requirements. Extensive research have been done and all results are presented in Appendix C.1. These requirements are derived from the guidance notes on using Unmanned Aerial Vehicles of the American Bureau of Shipping. [3]

4.5.2. Selecting an aerial platform

Figure 4.7 shows the three main classifications and models of drones based on their body shape and flying principles. They can be classified as Fixed Wing, Rotor Wing and Multicopters. Fixed wing

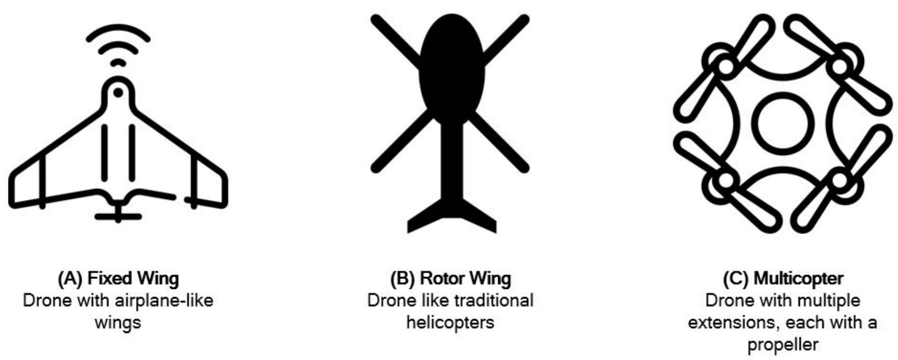

Figure 4.7: Types of drones

drones have advantages in relation to speed, range, endurance and robustness. The disadvantage is the requirement of a runway or launcher for takeoff or landing. Fixed wing drones are also not able to keep position on one location. [14] Rotor Wing (or helicopters) are to be seen in many different configurations, largely driven by the means of counter-action of the rotor torque. This type is characterized that it is extremely asymmetric in all planes which adds to the complication of control and complexity of the algorithms of the flight control system. The tail rotor is relatively fragile and vulnerable to striking ground objects, especially in the smaller size of the machine. [5] Multicopters use multiple rotors to produce thrust. Multicopters are always equipped with an even number of engines. Halve of the motors rotate counterclockwise and the other halve rotate clockwise. The rotor blades are all fixed in pitch and achieve thrust changes on each rotor by changing its speed of rotation. Although multicopters have simple control systems and they are very maneuverable, their main disadvantage is the power consumption. A performance evaluation based an six factors have been carried out in Appendix C.2.

	Fixed wing	Rotor wing	Multicopter
Ease-of-use	++	+	+++
Reliability	++	+	+++
Maintainability	++	+	+++
Time of endurance	+++	++	+
Maintain position	-	++	+++
Payload capacity	++	+++	+

Table 4.2: Comparisons of three types of small aircraft (More “+” implies better)

The results are shown in Table 4.2. This shows that in terms of ease-of-use, reliability, positioning and maintainability the multicopter outperforms the helicopter and the fixed wing aircraft. On the other hand, the multicopter has some disadvantages in terms of time of endurance and payload capacity. But these factors can be comprised or even sacrificed. For example, the time of endurance can be extended by swapping batteries during operations. Multicopters are favored above other competitors in terms of user experience. With the development in battery technology, materials and electric motors the time of endurance and payload capacity will be both improved. Based on this outcome, this research will only focus on the use of multicopters.

4.5.3. Current industrial multicopters

Several industrial drones currently on the market have been compared. A total of five different industrial drones where investigated to compare their suitability for the use in an offshore environment based on the requirements in chapter 2.1. The selected drones are illustrated in Figure 4.8.

The drones where compared based on the following specifications:

1. **Flying time:** longer flying times allow for a more efficient and comprehensive flight plan as it minimizes interruptions to change the drone batteries.
2. **Camera resolution with low illumination:** due to lack of illumination during dusk, dawn, and night the drone camera must be able to capture high-resolution images under low illumination. It can be noted that the illumination can be enhanced by additional flashlights either attached to the drone or on the topside or SSCV itself.
3. **Streaming quality:** the drone must be able to record and stream high-quality videos to perform video-based analyses. Either by a computer or by a human.
4. **Payload capacity:** payload is important as it allows the drone to carry additional attachments such as flashlights, cameras or sensors if needed.
5. **Remote range:** The helideck is located at the bow of the vessel whilst the cranes are located at the aft of the vessel. Therefore, a long-range remote control is required.
6. **Weather conditions:** The drone will operate in offshore conditions and should therefore be able to continue flight in rain and in wind conditions up to 30 knots.

Figure 4.8: Selction of five currently existing professional drones

Considering the aforementioned specifications a comparison has been made in table 4.3. It must

Brand	**DJI**	**ALTURA**	**Intel**	**DJI**	**DJI**
Model	**M210 RTK**	**ZENITH ATX8**	**Falcon 8+**	**Phantom 4 RTK**	**Inspire 1**
Release	Feb 2017	Mar 2014	Oct 2016	Oct 2018	Nov 2014
Flying time	++	++	+	++	+
Camera	++	++	++	+++	+
Payload capacity	+	+++	+	+	+
Remote range	+++	+++	+	+++	++
Weather conditions	++	+++	+	+	+
Robust Positioning	++	-	-	++	-
Price	$15,000	$20,000	$20,000	$7,000	$2,000

Table 4.3: Comparison of different specifications

be noted that drone technologies have rapidly grown in recent years and their development is still at a very high pace. The investment firm Goldman Sachs estimated in January 2017, that businesses will invest $13 billion in commercial drones by 2020, with more than $11 billion in the construction industry. [7] In the comparison it is easy to see that professional drones are getting cheaper. DJI is currently the largest manufacturer of drones and has now secured such a strong position that it is difficult for other companies to enter the market. The RTK module that the DJI M210 and Phantom 4 have is a big advantage for the offshore conditions. RTK is further explained in Appendix C.2.2 but in short it can be explained as a correction method for GPS signals. RTK ensures that drones can keep their position autonomous within 5 cm accuracy. Automation is safer because the drone's sensors are far more sensitive and accurate than an operator working from the ground. Additional technology, which is Obstacle Avoidance (OA), allows the drone to avoid harm to both the vessel, offshore structures, and drone components along with persons and property. The DJI M210 is more than twice as expensive as the Phantom 4 but has a bigger operational range due to its IP43 weather classification. The drones of Altura and Intel do not have an RTK module so they can lose their GPS signal and get drifting. Because robustness is an important pillar, these drones are at a disadvantage compared to DJI's drones. Based on this comparison, the M210 appears to be the best choice for offshore use in the current market.

4.5.4. DJI M210 RTK

The DJI M210 comes with high-performance motors paired with 17-inch propellers to ensure stable flight in strong winds. The new dual-battery power system automatically heats batteries when flying in sub-zero temperatures, while an enclosed design ensures weather and water resistance, so it can fly in a wide range of environments. The dual-battery system also ensures improved reliability. A robust flight autonomy system with front, bottom and upper sensors detect and avoid obstacles while enabling precision hovering so a pilot can fly with confidence. The DJI M210 can be equipped with a wide variety of payloads. The recommended camera for inspection purposes is the DJI Zenmuse X4S camera (figure 4.9). The Zenmuse X4S is a powerful camera featuring a 20 megapixel 1-inch sensor. The lens is compact with low distortion and has a radial dispersion of only 3μm that is equivalent to a 24mm focal length on a 35mm camera. It is therefore very suitable to use with computer vision software.

Figure 4.9: DJI M210 RTK and the Zenmuse X4S 1-inch aerial camera

The DJI M210 is also used in the Ocean Cleanup project. The offshore team performs aerial inspections twice a day. During these flights, they record behavioral data of the system and inspect its integrity. A thermal camera will also be used to monitor sea life in the vicinity of the system. And every once in a while, they snap a stunning sunset image (see Figure 4.10).

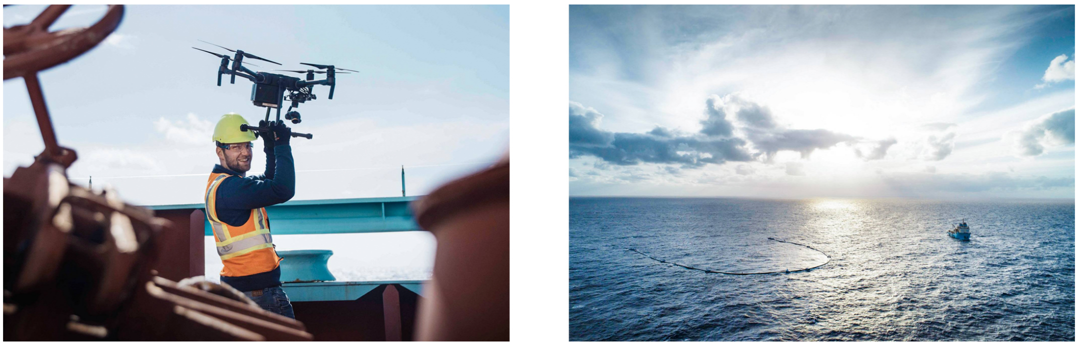

Figure 4.10: DJI M210 RTK used for offshore inspection purposes during the Ocean Cleanup

4.5.5. Flight Plan

Continuous drone flight

The duration of a topside installation can last up to six hours continuously. [18] The DJI M210 RTK has a battery life of max. 35 minutes. This will not be sufficient for the whole operation. The drone will need to return to the SSCV to swap its batteries. It will take several minutes for the drone to fly back, swap batteries and return to the topside again. During this time, tracking of the ArUco markers won't be possible and this in result will delay the operation. A situation that is unacceptable. A possible solution is to alternate between two drones. This concept is illustrated in Figure 4.11 and was tested by Rynne et al. [13] In this research they flew two drones in cyclical deployments. When the battery of the first drone reached its lower limit, the second was launched to relieve it. Both vehicles were programmed autonomously to loiter at the same location to ensure that the observation position was constant. This cycling scheme allowed a drone to be on station almost continuously.

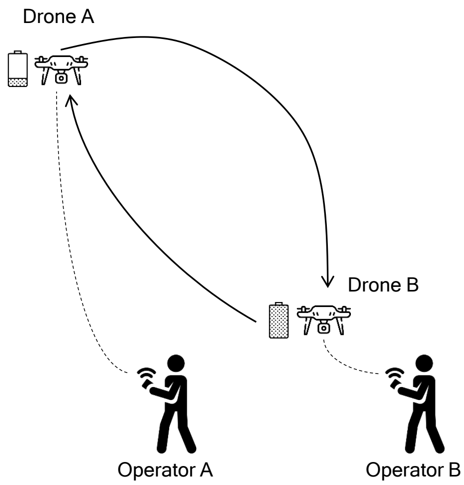

Figure 4.11: Concept of alternating drones

In Figure 4.12 a flight plan is given. Every block indicates a time span of five minutes. It will take max. five minutes for the drone (A) to reach its target position. After the drone reaches its location it is able to hover there for a duration of twenty minutes. After fifteen minutes a second drone (B) is deployed to fly to the target position. Drone B switches position with drone A and drone A will have sufficient remaining battery power to return to the SSCV safely. Drone A will swap its batteries with fully charged ones and the cycle can be executed again.

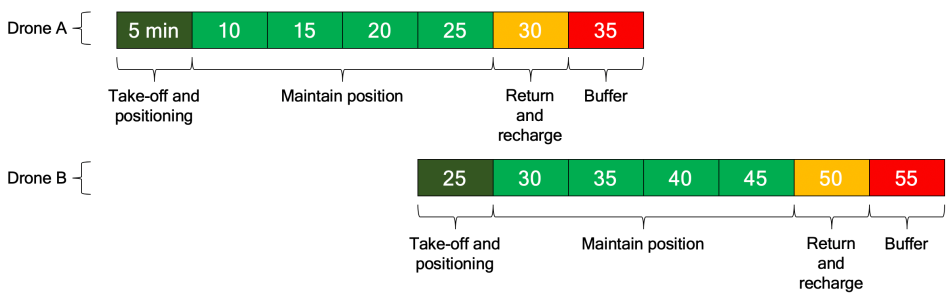

Figure 4.12: Flight plan for continuous drone flights

The duration of the topside installation can be up to 6 hours continuously. [15] One drone is able to provide a continuous stream of 20 minutes. Table 4.4 gives an overview of the number of flights (or battery swaps) is needed to provide a continuous stream to cover the whole installation period. In this calculation it has been assumed that the scheme in Figure 4.12 is used.

So for a continuous drone flight, two drone operators per drone are required. Configuration 1 uses one drone. This means that the minimum required number of operators is two. In most of the times

Flight time (h:mm)	0:30	1:00	1:30	2:00	2:30	3:00	3:30	4:00	4:30	5:00	5:30	6:00
Number of flights	2	3	5	6	8	9	11	12	14	15	17	18

Table 4.4: Number of flights (battery swaps) per drone position for given installation time

offshore crew works in shifts of twelve hours. It is not always known at what time an operation is about to start. It could therefore happen that an operation starts when someones shift is ending and he/she is going to sleep. Offshore crew is therefore often double present. For example, an ROV requires two pilots to operate. During an offshore execution always four ROV pilots are present. This holds the same for drone operations. Therefore, the minimum required drone operators needs to be doubled in order to have enough fit pilots at any time of the day. Configuration 2 uses three drones, thus a minimum of six drone operators. If the shifts are taken into account this means that 12 operators are required. A summary is given in Table 4.5

	Minimum required operators	Required operators with two shifts
Configuration 1	2	4
Configuration 2	6	12

Table 4.5: Required drone operators

Landing zone and operator location
In current HMC procedures a drone is only allowed to take-off from the helideck. [36] On all HMC vessels, the helideck is located at the opposite side of the cranes. The ideal location for a drone operator would be at the aft of the vessel (where the cranes are). At this location the drone operator will have a good visibility on the topside where he/she has to maneuver the drone. Landing and take-off on the helideck is therefore not the best location. The drone operator won't be able to have visual contact with the drone and would therefore have to rely on the on-board camera during take-off and landing. A better option would be to create a designated drone area on the deck of the SSCV where the drones are safe to land and take-off. This area should be as close as possible to the drone operator located at the aft of the vessel. Possible locations are indicated in Figure 4.13 as orange circles. There are no strict regulations about take-off and landing clearances. In the Guidance Notes for Inspection using Unmanned Aircraft Sytems by Lloyd's Register the following is stated: "Take-off and landing zones should be visibly marked and cordoned off to avoid the risk of distraction and collision." [51] A Landing zone with a diameter of 10 meters should be sufficient for safe operations.

4.5.6. Legal conditions

EU has not set forth any detailed rules for the operation of drones, and the Chicago Convention on international Civil Aviation only specifies that flying drones over a foreign State require special authorization. Currently a separate permission for drone operations is required in each country. Which leads to one of the classic issues with the offshore sector – that it operates in areas with several different jurisdictions. According to the Dutch Air Navigation Act, two main conditions must be met for drone flight. First, the drone operator must have acquired a drone license. Second, the drone must be insured. It is also a condition that the drone must be registered and identifiable. Before commencing flight, it may be advisable to apply for exemptions from the requirements. If a flight starts outside the urban area, for instance from a ship, other rules apply. Not considering possible application of the rules of the flag state, the rules on flights outside urban areas will generally apply. [32]

Lloyd's Register has already issued guidelines for offshore use of drones. In view of Lloyd's position on the international market and the potential impact on insurance of drones these guidelines and their development are worth paying attention to.

Something else to take into account is BVLOS and EVLOS:

- **BVLOS:** Flight of a drone beyond the pilot's and any remote observer's visual line of sight. The pilot operates the drone via instrumentation.

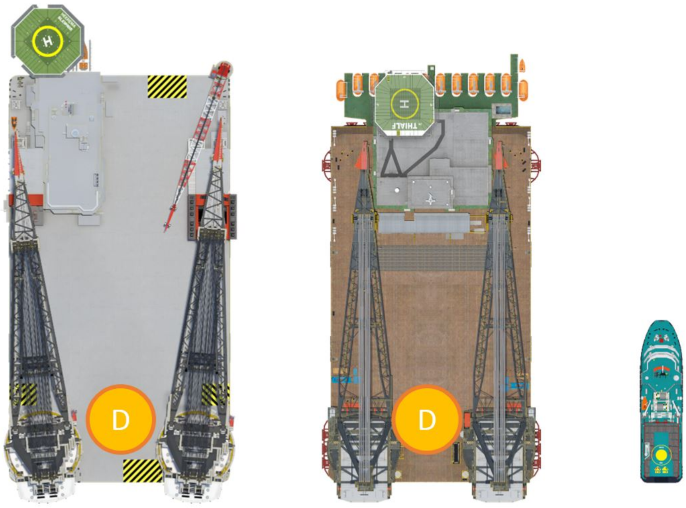

Figure 4.13: Landing zones. Left SSCV Sleipnir, middle SSCV Thialf, right Kolga

- **EVLOS:** Flight of a drone beyond the pilot's line of sight, but within the line of sight of any remote observers. The pilot operates the drone through constant communication and information from the remote observers.

All routine drone operations should occur within visual line of sight. The use of EVLOS or BVLOS for drone operations is subject to regulatory acceptance and risk assessment, and prior approval by the asset owner or shipowner's representatives and the Inspection Data End-User. [51]

4.6. Electronics and software

The main components of the complete system setup will consist of:

- **Imaging devices with camera control:** this will be either drones or fixed cameras.
- **Computing device:** to process camera imagery by means of computer vision.
- **User Interface:** display information in a simple and effective manner.

The basis system lay-out for configuration 1 is illustrated in Figure 4.14. The four fixed cameras and one drone are connected to a Camera Control Panel (CCP). For the fixed cameras on the SSCV this will be a wired connection. The drone will stream its video feed in real-time to the drone controller and a seperate video-stream receiver. This receiver should have a small latency and be able to process at least full HD quality video. An example of such a receiver can be found in Appendix C.2.3. The CCP will be operated by one person who has control over all video settings. In the first instance, camera imagery will be adjusted automatically in terms of brightness and focus. If necessary, these settings can be adjusted to obtain better results. The CCP-operator will also decide which imagery is send to the computing device. As mentioned in chapter 4.5.5, drones will alternate each other to have a continuous view on the topside. When the second drone is ready to overtake the first drone, the CCP-operator will also have to switch the cameras. Camera imagery will then be processed by a computing device. This computing device has to be powerful enough to process five video feeds simultaneously. The computing device could therefore also consist of multiple computers working together. Information from video imagery will be used to calculate the relative position between the topside and the jacket. A Graphical User Interface will display these results in a simple and effective manner to the superintendent or other stakeholder involved in the process. In current offshore installation activities a container is placed at the stern of the SSCV. This container acts as control room where information about the installation is displayed on a desktop computer. The superintendent needs to be inside this container to view the information. When the superintendent is inside the container, he has no view on the activities which are happening outside. A wish of the superintendents is to have this information displayed on a portable device (e.g. a smartphone or tablet).

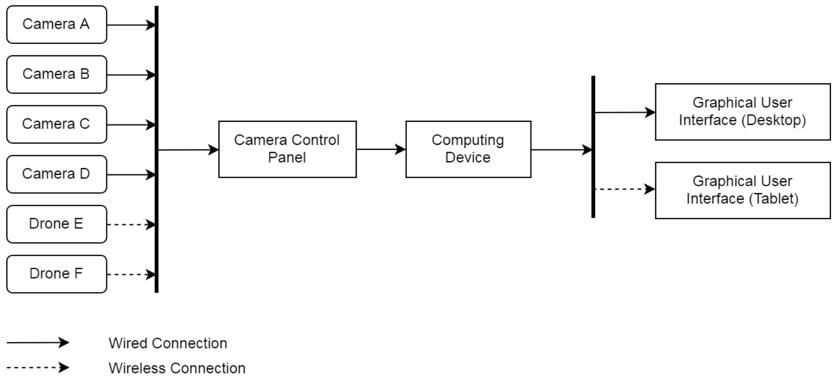

Figure 4.14: System lay-out for configuration 1

The basis system lay-out for configuration 2 is illustrated in Figure 4.15. This configuration uses three drone positions and will therefore consist of six drones (two alternating drones per location). Also one fixed camera is used on the stern of the SSCV as mentioned in chapter 4.3.2.

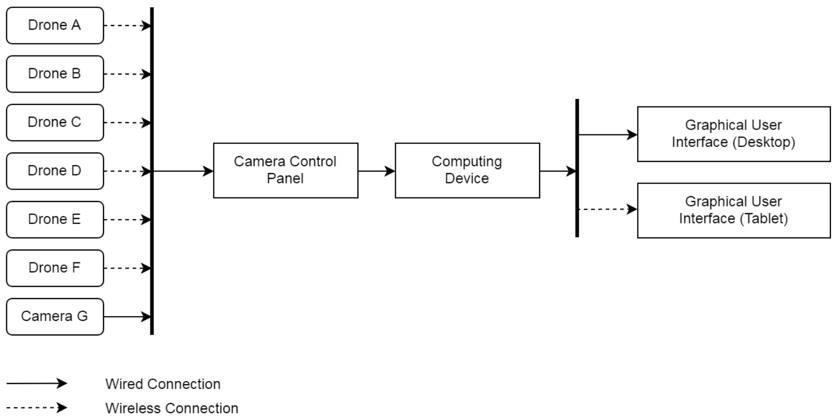

Figure 4.15: System lay-out for configuration 2

4.7. A look into the future: autonomous drones

At present, drones are remotely operated. Chapter 4.5.5 made clear that a lot of drone operators are needed to enable continuous offshore drone flights. The next phase of drone technology will be to deploy 'smarter' machines that can fly autonomously. This technology will allow drones to sense and avoid other objects in their path, recognize features or components through various sensors (including cameras), and achieve situational awareness. As unmanned vehicles become more ubiquitous, the opportunities for more complex autonomous behaviors increases, allowing unmanned systems to transition from being merely remotely-operated assets to autonomous machines. [10]

4.7.1. Concept of operations

In order to support autonomous drone operations offshore a primary or "host" vessel is needed. In the special case of HMC this can be an SSCV or tug. The drones will execute fully autonomous missions from this host vessel. A concept of operations can be explained as follows:

- When a mission needs to be executed, the drone automatically launches from the host vessel.
- The drone uses a preprogrammed flight pattern or flies to a predefined point of interest (POI). The drones use active obstacle avoidance to find its way and streams real-time video to the host vessel. In addition, the drones should also be able to automatically track and follow an object.
- The drones keep track of their own battery status and return to the host vessel if their battery is less then a certain threshold value. Batteries are swapped automatically and the drone returns to continue its mission.
- When the mission is completed, the drones return to the primary vessel and execute an autonomous landing.
- The drone's batteries are swapped or recharged and are ready to repeat the previous steps again.

These operations could be fully automated and repeatedly performed. Missions could be preprogrammed or modified remotely. The basic concept of this operation is illustrated in figure 4.16.

Figure 4.16: Concept of operations

4.7.2. Required Technology Advances

The sketched autonomous execution in the previous section is not yet feasible with the current technology. An analysis of recent studies, however, shows that there is a lot of activity in research in the field of autonomous drone operations. It is therefore not inconceivable that fully autonomous drone operations will become part of maritime / offshore activities. This chapter provides an overview of the required technological advances.

Autonomous take-off and landing Autonomous take-off and landing is a fundamental task for drones. Landing on non-moving objects is already possible on most consumer drones. During take-off the GPS location is recorded and stored as the 'return-to-home' location. Ones the pilot gives a command or the connection to the remote controller is lost, the drone will fly at a specific height to this location and starts descending. The main challenge is to land on a dynamic location such as a vessel. For vision-based take-off and landing, different solutions have been proposed in order to deal with this problem. The authors of [21] used a technique that relies on detection of a special target, state estimation and tracking of the landing target. This system was tested on a vessel and operated in winds up to 20 knots, vessel speeds up to 12 knots, and seas up to 2 meters. This system did not incorporated any GPS or other positioning signal on the host vessel so the drone had to actively search for the pattern. Another vision-based cooperation between a drone and an Unmanned Ground Vehicle (UGV) has been presented in [10]. At which a proportional navigation controller was used for the long-range approach, which subsequently transitioned to a proportional–derivative controller at close range. A central component of this system consists of a Kalman filter to estimate the position of the drone relative to the landing pad, by fusing together measurements from the drone's onboard integrated navigation system, from cameras tracking a visual fiducial marker and from a IMU and GPS unit on the ground vehicle. This system was successfully tested with speeds up to 50 km/h. Another research in [55] was especially focused on landing autonomously on ship deck platforms in extreme weather conditions. As in the previous studies, computer vision was used to recognize the landing zone. That was not a marker in this case, but the pattern that was drawn on the helipad. With the geometry of the 'H' and the white circle that was drawn around it, the drone could then determine its position. The distance to the helipad can be determined with the aid of downward facing ultrasonic sensors. Experiment showed that their approach was appropriately even with contamination on the helipad or light changes. The literature shows that it is possible to autonomously land a drone on a moving target. The best approach seems to use a GPS position of the landing area for the long range approach and a special marker or other recognizable pattern such as a helipad for state estimations at a close range as illustrated in figure 4.18.

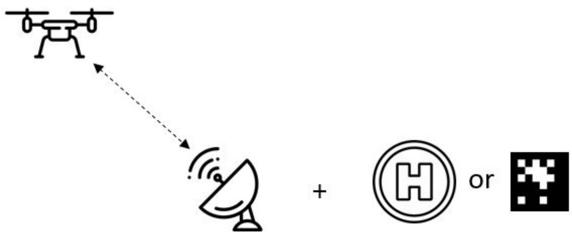

Figure 4.17: Autonomous take-off and landing

Automatic docking and recharging Once the drone has landed after executing a mission it needs to be secured and recharged again. There is already a lot of progress on this problem made by the drone industry. Systems such as DroneBox [38], SkySense [9], UPS's truck-launched drone delivery system [20], and Amazon's patent of a beehive-like structure [54] are aiming to design and build mechanisms to secure, recharge and launch drones. Such a system could be adapted to operate on a SSCV or tug in an offshore environment. All of the mentioned systems use wireless charging techniques to recharge the batteries. With current technology it will take about an hour to fully recharge an empty battery. It will be faster to replace an empty battery for a charged battery. This can be done by hand or with a robotic arm. In this case the drone would be able to fly again within five minutes after landing.

Communications Many drones are designed to use a wireless connection to communicate with the pilot or command center, and once they are out of range, connectivity is lost. The drone remains tied to a single access point and is unable to move beyond that network's range. There are networks that are able to overcome these challenges. Kinetic mesh wireless networks have been deployed in the rugged oil and gas environment because they are highly secure, scalable and mobile, allowing a constant flow of real-time information with no downtime. A drone operating off a standard network is bound to static infrastructure like mounted access points, towers or wireless routers, even though the drones

Figure 4.18: Automatic docking and recharging. From left to right: DroneBox [38], SkySense [9], UPS's truck launch [20] and Amazon's patent [54]

are always on the go. In kinetic mesh, everything is constantly moving – including the infrastructure, allowing an expansive network footprint that functions even in applications such as offshore operations. In a kinetic mesh network, multiple, redundant radio frequencies and any-node-to-any-node capabilities are deployed to continuously and instantly route data via the best-available path and frequency, even over dozens of nodes. If part of the network becomes congested or receives interference, the network leverages this multi-frequency, multi-radio functionality to instantaneously reroute around any obstacle, keeping the drones in the air and on task. [37] The drones are able to pass information in a peer-to-peer network. Mission specific commmands, high resolution imagery and video could therefore be constantly streamed without loss of data. This is illustrated in figure 4.19.

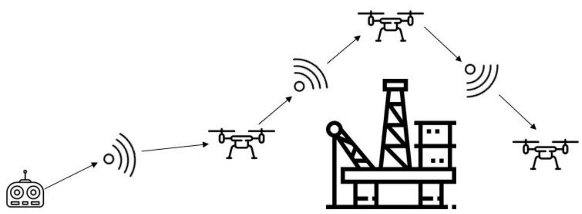

Figure 4.19: Communications

Automatic Tracking Capabilities A great deal of cost savings is derived from the automation of the data capture when compared to similar operations performed by drone pilots. Automating the drone can be accomplished with vision-based navigation. With the rapid development of computer vision and the growing popularity of small drones, the combination of them has been an active area of research [61]. The three main challenges for an autonomous drone are localization and mapping, obstacle avoidance and path planning. Localization and mapping is the key of autonomous navigation, which also provides location and environmental information for drones. Obstacle avoidance and path planning are essential for the drone to safely and quickly get to the target location without collision. Even though drones are sharing similar navigation solution with ground mobile robots, we are still facing many challenges when it refers to vision-based drone navigation. The drone needs to process amount of sensors' information in real time in order to fly safely and steady, especially for image processing which greatly increase the computational complexity. So it has become a major challenge a drone to navigate under constraints of low power consumption and limited computing resources. Besides, drone navigation requires a global or local 3D map of the environment; extra dimension means greater computation and storage consumption. So there is a great challenge when a drone is navigating in a large scale environment for a long time. In addition to that, motion blur caused by fast movement and rotation can easily result in tracking and localization failure during the flight. A more robust way to perform automatic tracking of an object is similar to the case of autonomous landing. Lets say that the drone must automatically track the primary stabbing cone of a topside that is lifted by the SSCV. Presume that the location of the topside relative to the SSCV is known within a certain margin. The drone could then autonomously fly to this location using the GPS coordinates of the SSCV relative to the primary stabbing cone. When it reaches this location the drone has to actively search for the fiducial marker that is attached to the stabbing cone as explained in chapter 3 for more precise tracking. The drone is then able to autonomously keep its position based on the information that is extracted from the fiducial marker. [46]

Hardware improvement for harsh environments Some of the challenges in using drones for offshore applications are the limited energy, short flight time and limited processing capabilities. [29] All these challenges relate to the battery capacity. In recent years the flight time has already doubled from around 15 minutes in 2013 to over 30 minutes in 2018. As the markets for electric applications continue to grow, the technologies that power them continue to evolve today and in the future. A US start-up recently launched their first drone which was designed with a battery-first approach. The company claims the battery of their drone can fly op to two hours on a single charge. It is capable of flying 90 minutes to two hours on a single charge and can recoup 75 percent of the battery with about 45 minutes of charging time. [52]

Regulations In Europe and the US, current regulations significantly restrict operations of drones in order to safeguard the congested airspace and people and property on the ground by, for example, requiring operations to remain within the visual line of sight of a human operator. However, other countries have very different regulations, and, even in the US and the EU, regulations have changed substantially since 2013, when the roadmaps for airspace integration of civil drones were introduced [2] [31]. As stakeholders gain experience in drone technology and as collision avoidance systems mature, it is expected that regulations will be relaxed significantly, thus opening a range of new, attractive applications for drones.

A pilot is the person in direct flight control of the drone. Therefore, his proficiency in drone operations can affect the safety of onsite personnel and the assets. If applicable, the pilot should meet statutory and regulatory flight training requirements to maintain their pilot license. In addition to the statutory and regulatory requirements, the Service Provider or pilot should place a high level of emphasis on their proficiency through training. The pilot should have sufficient ground and flight experience so that expected or observed extreme scenarios (i.e., weather condition changes, functional loss, operation with extra PPE, etc.) can be foreseen and accounted for. If the pilot is not sufficiently familiar with basic maritime and/or offshore asset designs, training should be provided. This training should include maritime and/or offshore nomenclatures in order to communicate effectively with the asset Owner/Operator (in most cases the captain or superintendent).

4.8. Risk assessment

A hazard is any real or potential condition that can cause damage to or loss of a subsystem. For the most engineered systems, hazards are often associated with the unplanned failure of a component, inadvertent misuse, non-standard operations, or the interjection of unforeseen outside influences. Hazards should be identified for all credible situations associated with the used hardware. Severity is an assessment of the worst potential consequence which could occur from a hazard coming to pass. Four categories of hazard severity are defined. [41] See Table 4.6 for a definition of each severity class, specified by degree of level of property damage.

Class	Description	Potential consequences
1	**Catastrophic**	near-complete loss of system
2	**Critical**	major damage to system; loss of major subsystem(s)
3	**Marginal**	minor damage to subsystem, recoverable with minimal impact on operation
4	**Negligible**	systems or components experience more than normal wear and tear; easily recoverable within scope of standard maintenance

Table 4.6: Hazard Severity Classification

Probability is the likelihood that an identified hazard will result in an accident or mishap. There are too many uncertainties to be able to compute a numerical value for the likelihood that a specific cause will occur, and hence it is not useful to attempt to quantify risks beyond a relatively rough measure to assist in their relative prioritization. [41] Five levels of probability are defined. See Table 4.7 for a definition of these probability levels.

Level	Frequency of Occurrence	Definition
A	**Frequent**	Likely to occur often in the life of a subsystem
B	**Probable**	Will occur several times in the life of a subsystem
C	**Possible**	Likely to occur sometime in the life of a subsystem
D	**Remote**	Unlikely but possible to occur in the life of a subsystem
E	**Improbable**	So unlikely, it can be assumed occurrence may not be experienced

Table 4.7: Hazard Probability Levels

The Risk Assessment Value is a numerical expression of comparative risk determined by an evaluation of both the potential severity of a mishap and the probability of its occurrence. It is a number from 1 to 20, assigned from the Mishap Risk Assessment Matrix shown in Table 4.8. The Risk Assessment Value is used to prioritize hazards for risk mitigation actions and to group hazards into risk categorizes, as detailed in Table 4.9.

	Severity			
Probability	**1 - Catastrophic**	**2 - Critical**	**3 - Marginal**	**4 - Negligible**
A - Frequent	**1**	**3**	**7**	**13**
B - Probable	**2**	**5**	**9**	**16**
C - Possible	**4**	**6**	**11**	**18**
D - Remote	**8**	**10**	**14**	**19**
E - Improbable	**12**	**15**	**17**	**20**

Table 4.8: Mishap Risk Assessment Matrix

The next step in the hazard analysis process is development of a risk reduction or mitigation process. There are four mitigation strategies that can be implemented to decrease the risk to an acceptable level.

Risk Assessment Value	**Mishap Risk Category**	**Risk response**
1-5	**High**	Not Acceptable, avoid
6-9	**Serious**	Avoid / Mitigate
10-17	**Medium**	Mitigate
18-20	**Low**	Accept / retain

Table 4.9: Mishap Risk Categories

In Table 4.10 is the hazard study of the marker, drone and fixed camera subsystems shown. Plioutsias et al [48] did a thorough hazard analysis on small drone operations and their work made a big contribution to this chapter. This work complements the existing risk assessment frameworks for small drones, and contributes to the establishment of a commonly endorsed international risk analysis framework.

A risk matrix is presented in Table 4.11. The risks are listed and quantified. Strategies and actions to cope with the risks are presented. What is notable in the table, is that insufficient energy level of a drone is the highest risk.

Subsystem	Generic causal Factors	Detailed Causal Factors	Consequence	Probability	Impact
Marker	**Not all markers visible**	Not all markers are sufficiently lighted	Marker will not be recognized	Probable	Marginal
		Markers (partially) occluded by obstacles			
	Wrong marker ID used	Wrong marker ID used	Marker not recog-nized	Possible	Marginal
	Marker damaged	Marker damaged	Marker not usable	Remote	Critical
	Marker rotated	Marker rotated either 90, 180 or 270 degrees	No consequence	Possible	Negligible
	Wrong marker	Marker confused with other marker during placement	Marker pair will not be recognized	Possible	Marginal
Fixed Camera	**Inadequate functioning of camera**	Inherent technical flaws (i.e. design or production)	Camera will fail or return distorted image	Remote	Marginal
		Excessive environmental conditions (e.g. humidity, high / low temperature)			
		Inadequate maintenance			
	Inadequate communication	Broken cable or connector	Camera will fail or return distorted image	Probable	Narginal
		Wrong settings used			
	No visibility on markers	Bad camera orientation	Marker pair won't be tracked	Possible	Marginal
Drone	**Inadequate functioning of remote control, display, drone**	Inherent technical flaws (i.e. design or production)	Drone will crash or return distorted image	Possible	Critical
		Excessive environmental conditions (e.g. humidity, high / low temperature)			
		Unintentional drop prior to flight			
		Inadequate maintenance			
	Inadequate communication	Signal disruption because of frequency interference	Drone starts hovering and/or returns distorted image	Possible	Critical
		Signal disruption caused by physical impenetrable obstacle			
	Ineffective commu-nication between drone operator and display	Limited visibility of display (e.g. glare, angle of view, reflections of environment)	No or less flight information for operator	Remote	Critical
		Indistinct information on the display (e.g., size of fonts and symbols, colors)			
		Unfamiliarity of operator with terms or language used			
	Inadequate drone operator perfor-mance	Inadequate knowledge or skills in: a) regulations and requirements of the authority, b) operation of the drone, c) the terrain, d) initial weather forecast	Drone will crash or fly-away	Remote	Marginal
		Inadequate a) authority requirements and regulations, b) operating instructions			
		Exceedance of cognitive capacity			
		Effects of emotional state			
		Inadequate weather forecast update			
		Inadequate information about density of operating drones in flying area			
		Chronic, known physiology problems			
		Unanticipated physiology limitations			
	Insufficient energy level; display or remote control	Display battery depleted	Drone will start hovering or return home	Probable	Marginal
		Remote control battery depleted			
	Insufficient energy level; drone	Drone battery depleted	Drone will crash	Probable	Critical

Table 4.10: Hazard study of marker, drone and fixed camera subsystem

Subsystem	Generic causal Factors	Probability	Impact	Risk	Strategy	Action
Marker	**Not all markers visible**	Probable	Marginal	Serious	Avoid/ mitigate	Make a clear plan where markers need to be placed. Be sure to add battery powered LED lighting to background if necessary.
	Wrong marker ID used	Possible	Marginal	Medium	Mitigate	Double check marker IDs during placement. Edit marker ID in algorithm during installation.
	Marker damaged	Remote	Critical	Medium	Mitigate	Make markers from a solid material. Make people aware that a damaged marker may lead to failure.
	Marker rotated	Possible	Negligible	Low	Accept/ mitigate	No impact on system.
	Wrong marker	Possible	Marginal	Medium	Mitigate	Marker IDs have to be adjusted in the algorithm.
Fixed Camera	**Inadequate functioning of camera**	Remote	Marginal	Medium	Mitigate	Test functioning of camera on beforehand. Perform regular maintenance. Make a waterproof housing.
	Inadequate communication	Probable	Narginal	Serious	Avoid/ Mitigate	Check cables and settings before every installation.
	No visibility on markers	Possible	Marginal	Medium	Mitigate	Make a clear plan where cameras need to be positioned. Adjust camera position if necessary.
Drone	**Inadequate functioning of remote control, display, drone**	Possible	Critical	Serious	Avoid/ mitigate	Perform visual and technical checks before every flight. Make sure all components are in top condition.
	Inadequate communication	Possible	Critical	Serious	Avoid/ mitigate	Check for interfering frequencies. Switch frequencies if necessary. Use RTK module or kinetic mesh networks for better performance.
	Ineffective commu-nication between drone operator and display	Remote	Critical	Medium	Mitigate	Use a sun canopy for the display. Use contrasting font color. Be sure operator is familiar with language or switch language.
	Inadequate drone operator perfor-mance	Remote	Marginal	Medium	Mitigate	Make sure operator has enough skills, training and flight hours. Signals of mental or physical problems must be reported to the captain.
	Insufficient energy level; display or remote control	Probable	Marginal	Serious	Avoid/ mitigate	Make sure to check battery status regularly and swap batteries if necessary.
	Insufficient energy level; drone	Probable	Critical	High	Avoid	Always make sure to start landing procedure if remaining flight time is less then 10 minutes.

Table 4.11: Risk register

Most risks have an effect on whether or not the markers can be tracked properly. Whether it is the camera that is not working properly or that a marker is damaged. It should be noted that every stabbing cone uses two marker pairs and two cameras. This has been done to get the most accurate result possible. As mentioned, a configuration with one camera has difficulty in estimating the depth. But this is mainly applicable when the markers occupy a small part of the total camera frame. As soon as the markers become larger, the accuracy increases. There are different stages during the topside installation. During prepositioning the topside is moved towards the jacket. In this stage the marker areas will be small. The next stage will be set down when the topside is lowered onto the supporting jacket. At this time the markers are significantly more close to each other then during prepositioning as can be seen in Figure 4.20. From now the camera can zoom in to increase the area of the markers that are tracked. This in return will lead to an accuracy increase in depth measurements.

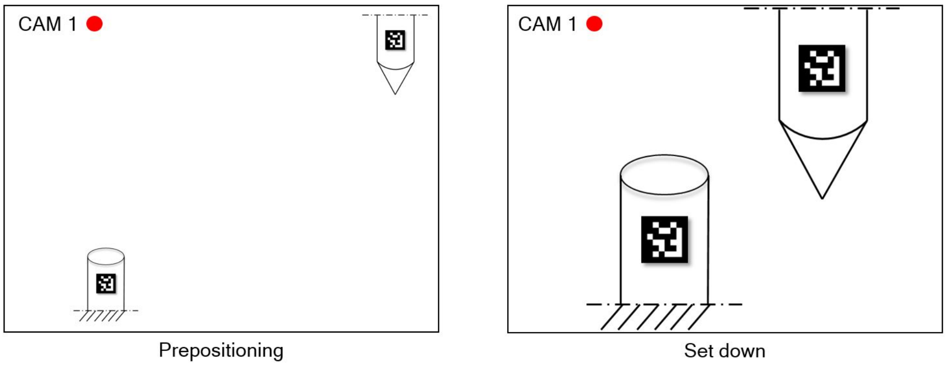

Figure 4.20: Marker area during different stages

Should it ever occur that a marker pair can not be tracked for whatever reason. Then the measurements during prepositioning will not be accurate, but during the set down it is highly possible that one marker pair will provide accurate results. This is also the moment when accuracy is most important. Further testing is required to see if this is true. The failure of a marker pair (per stabbing cone) is obviously not desirable, but will not have a major impact on the installation. If both marker pairs can not be tracked, it is obviously a different story. Then there is no positioning information available and everything will have to be done visually (as is usual now). The superintendent will have to rely again on his or her experience in estimating distances. Drone images are still available from every position and can mimic the role of people on the jacket.

4.9. Summary

The basic characteristics of a topside positioning system were introduced. The primary technology will be visual object tracking with markers. Cameras will be the main sensors to feed the system with data. These cameras can either be fixed cameras or ’flying’ cameras attached to a drone. If use is made of drones, multiple drones will have to alternate each other to provide a continuous data flow. Eventually the DJI M210 RTK was chosen. This drone is designed to fly in extreme weather conditions. Although the drone has to be controlled by a certified pilot, it does have several autonomous systems. This makes it easier for the pilot to carry out flights and assignments. Ultimately, it was examined whether it is also possible to use drones completely autonomously. That is not possible at this moment. In addition to technological challenges, this also has to do with regulations. Nevertheless, there is currently a lot of research into autonomous flying of (groups of) drones. Some developments are already at an advanced stage and some manufacturers have been granted exemption to comply with certain regulations to further develop this technique. But for now, semi-autonomous drone flights are more realistic and this has been successfully demonstrated several times. Drones are able to maintain their position without the intervention of a drone operator. At the moment the operators are only needed to allow the drones to land and take off and to put the drone in position. The moment that drones can be fully autonomously deployed during offshore work will take some time. Until then, improvements can be expected with regard to flight time and other autonomous sub-functions.


LIEBHERR
HESS
SA WHP-N
H-331 PANAMA

5
Experiment

The ArUco library was introduced in April 2014. [28] This fiducial marker system was especially designed for augmented reality applications. Accuracy is not very important in these types of applications. Extensive research have been done to find scientific reports with a focus on the accuracy of this marker system. Some research papers where found ([1], [43], [6], [22], [8]) but a lot of information was missing to make statements about the accuracy of the developed Motion Tracking Algorithm in this thesis. Therefore, an analysis is done to determine the accuracy and precision of the presented algorithm in Chapter 3. In this chapter the tests that are performed are explained and the results are presented. The sub-question that will be answered in this chapter is:

What are the accuracy's, advantages and limitations of using visual object tracking for topside installations?

In order to evaluate the working of the Motion Tracking Algorithm, two experiments will be carried out. The Heerema Simulation Center (HSC) was used to simulate an offshore topside installation. The simulation environment is shown in Figure 5.1.

Figure 5.1: Simulation setup

A topside and jacket where equipped with markers to enable object tracking. Two different experiments are executed and a calibration was performed. In Experiment 1 the accuracy and precision of the Motion Tracking Algorithm is measured. This is done by making several moves with SSCV Thialf on Dynamic Positioning (DP) while having a topside lifted in it's cranes. For this experiment two camera configurations where used as explained in chapter 4.3. The first configuration uses four fixed cameras on the SSCV and one drone position. The second configuration uses three drone positions and one fixed camera on the SSCV. Experiment 2 is a 'proof of principle', where the Motion Tracking Algorithm is used by an assistant superintendent to give instructions for the position of the SSCV and control of the cranes.

5.1. Heerema Simulation Center

HMC has its own Simulation Center to simulate offshore projects. This simulation center allows to run through the project in a virtual world, which brings significant advantages. It is a real-time virtual offshore environment in which project activities can be integrated into a realistic 3D world. DP systems are identical to offshore DP systems. Controls of the crane and environmental conditions can be applied. System simulation is a general type of modelling that deals with the dynamic behaviour of a system and its components. Because of this realistic environment it is inherently less abstract than other forms of modelling such as schematic models or mathematical models. Field tests can be augmented by using simulations to explore system behaviour under a greater variety of conditions. [35]

Virtual reality is considered as a valuable tool for improving and accelerating process development in many industrial applications. It helps to identify and avoid design errors in early stages of the development process, it reduces the number of physical prototypes and saves time and cost. [44]

In a virtual reality simulation a three-dimensional visual environment is presented to the viewer. Spatial virtual simulations require the input to the computer of a detailed three dimensional description of the space and its contents. Also, the viewing position is input into the simulation with a joystick, mouse or predefined location. This can be displayed on a device that is mounted in the viewer's headset or projected on a screen. [41] The HSC consists of multiple rooms representing different locations in the virtual environment. The different rooms and stations are displayed in Figure 5.2.

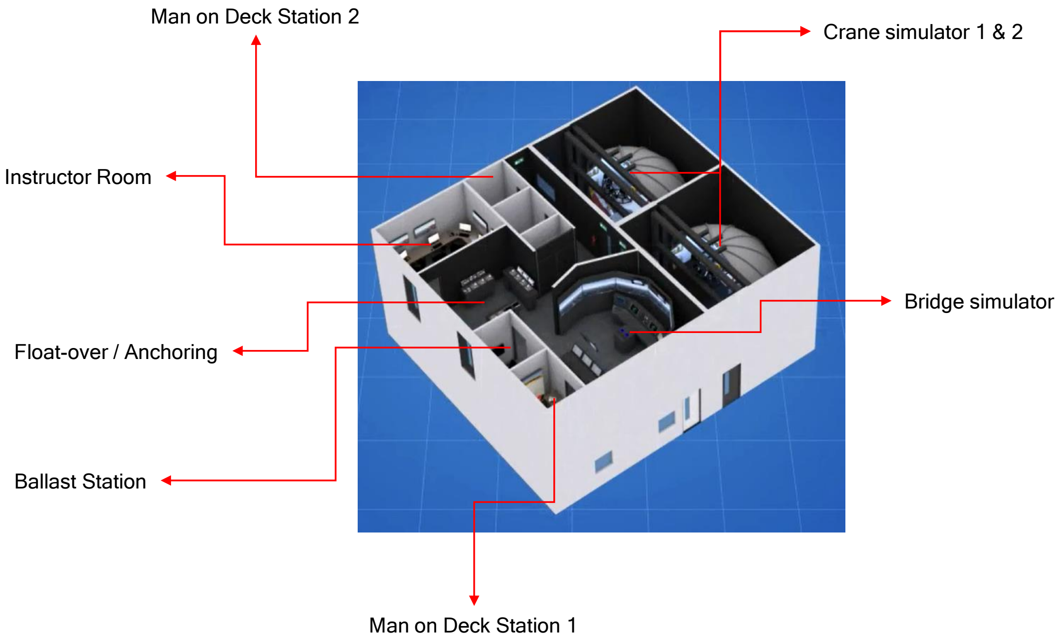

Figure 5.2: Heerema Simulation Center layout

The Simulation Center is designed to adapt a variety of 3D models – such as jackets and topsides – to real component characteristics. These models can be used to run realistic scenarios, including single and dual crane lifts. It can also be used to test new techniques such as the positioning system using drones or fixed cameras. This will allow to actually perform a dry-run of the operation in cooperation with all other relevant people and systems involved.

5.2. Experiment 0: Calibration

5.2.1. Experiment outline

First, the camera of the Simulation Center is calibrated. Camera calibration is a crucial part for the motion tracking algorithm as described in chapter 3.1.1. The software used in the Simulation Center is K-Sim. Because a virtual environment is used it is not possible to use physical camera's. Therefore the calibration will be used to determine how K-Sim renders objects in a virtual environment and measures its distortion. For a successful calibration at least 20 images are required which include a chessboard pattern. [11] An example of this chessboard pattern can be found in Figure 5.3. A set of 30 images where taken from different angles. The output of the calibration is the camera and distortion coefficients matrix. These parameters determine the relation between the camera's natural units (pixels) and the real world units (for example millimeters).

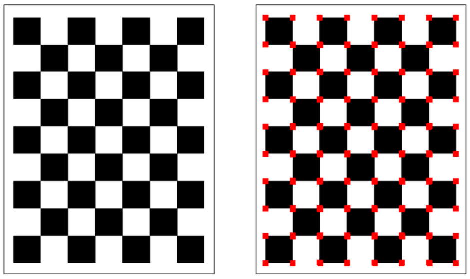

Figure 5.3: Calibration checkerboard

Experiment 0
Goal: calibrate the camera of the simulation software.
Variable: camera angle and distance to chessboard.
Requisites: chessboard picture inserted in simulation environment.
Repetitions: 30 times (number of pictures taken).
Output: Camera matrix and Distortion Coefficients matrix.

5.2.2. Results

Normally one would print a chessboard pattern on paper and take photographs of it in order to perform calibration. In this case that is not possible. The chessboard pattern has to enter the virtual environment. The easiest way was to attach it to an existing object, a container for instance. The camera view can be adjusted to take screenshots from different angles. This was done at the same resolution as experiment 1 and 2 to obtain the most accurate results (see Figure 5.4). The calibration function in Python requires white space (like a square-thick border, the wider the better) around the board to make the detection more robust in various environments. Otherwise, if there is no border and the background is dark, the outer black squares cannot be segmented properly and so the square grouping and ordering algorithm fails. For each image the function draws individual chessboard corners detected either as red circles if the board was not found, or as colored corners connected with lines if the board was found as can be seen on the right in Figure 5.4. In total 30 screenshots where taken from different angles with respect to the calibration chessboard. This resulted in the camera calibration matrix that can be seen in equation 5.1.

$$K = \begin{bmatrix} f_x & 0 & c_x \\ 0 & f_y & c_y \\ 0 & 0 & 1 \end{bmatrix} = \begin{bmatrix} 1258.27 & 0 & 468.746 \\ 0 & 1259 & 296.561 \\ 0 & 0 & 1 \end{bmatrix} \tag{5.1}$$

$$RMS = 0.0198 \tag{5.2}$$

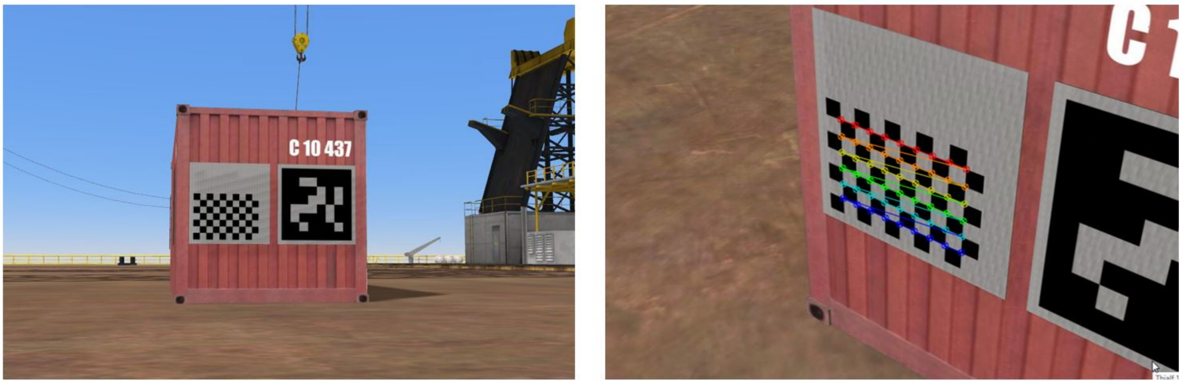

Figure 5.4: 'Camera' Calibration process in K-SIM

OpenCV calculates reprojection error by projecting three-dimensional of chessboard points into the image using the final set of calibration parameters and comparing the position of the corners. A Root-Mean-Square (RMS) error of 0.0198 was found. This means that, on average, each of these projected points is 0.0198 pixels away from its actual position. The objective of the RMS is to approach as close to zero as possible; however, values between 0.1 and 1 are generally considered to be acceptable with respect to accuracy. [11] Therefore, it can be concluded that the accuracy of the obtained results is more than satisfactory. The camera matrix and distortion coefficients are stored using write functions in Numpy (np.savez, np.savetxt etc) for future uses.

Result The calibration of the Simulation Center 'Camera Viewpoint' resulted in an acceptable result. The RMS value is 0.0198 which is considered to be very accurate.

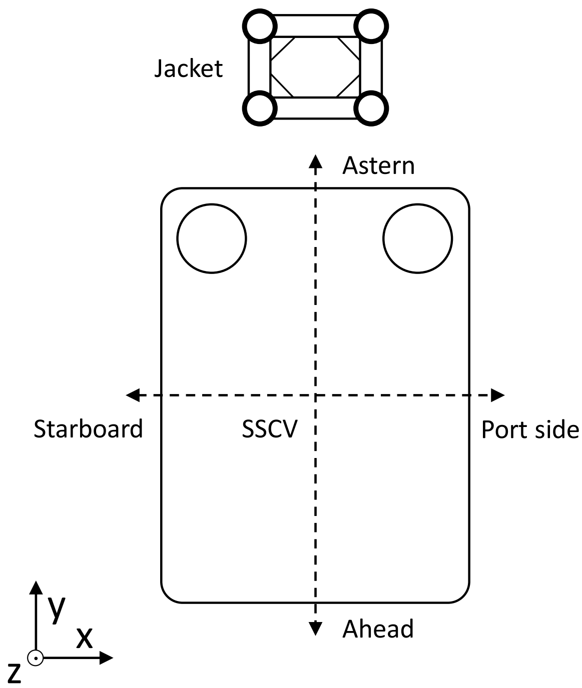

Figure 5.5: Axis definition

5.3. Experiment 1: Algorithm Accuracy and Precision

5.3.1. Experiment outline

In this experiment the accuracy and precision of the Motion Tracking Algorithm is tested. Two concepts will be introduced. The algorithm works on the basis of camera images. However, it does not matter how these images are obtained. This can be done on the basis of fixed cameras on the deck of the SSCV or using drones. The advantage of fixed cameras is that they can be mounted before the start of the installation and it is a relatively simple technique. The advantage of drones is that they can take on any desired position where normal cameras can not or can barely come. Configuration 1 uses four fixed camera positions on the SSCV and one drone position. Configuration 2 uses three drone positions and one fixed camera position. These concepts have been chosen to demonstrate the versatility of the system and where introduced in chapter 4.3. The axis definition for all experiments can be found in figure 5.5.

5.3.2. Configuration 1

In this concept four cameras are positioned on the SSCV. In this case, the stabbing cones that are closest to the SSCV are monitored. If these two are well aligned, the rear cones must also be well aligned. A drone can be used to confirm this. This configuration is shown in figure 5.6. The red bars indicate the positoin of the markers. Each marker pair has one marker on the jacket (bottom) and one marker on the topside (top). Each stabbing cone needs two pairs of markers in order to determine the x-, y- and z-offset.

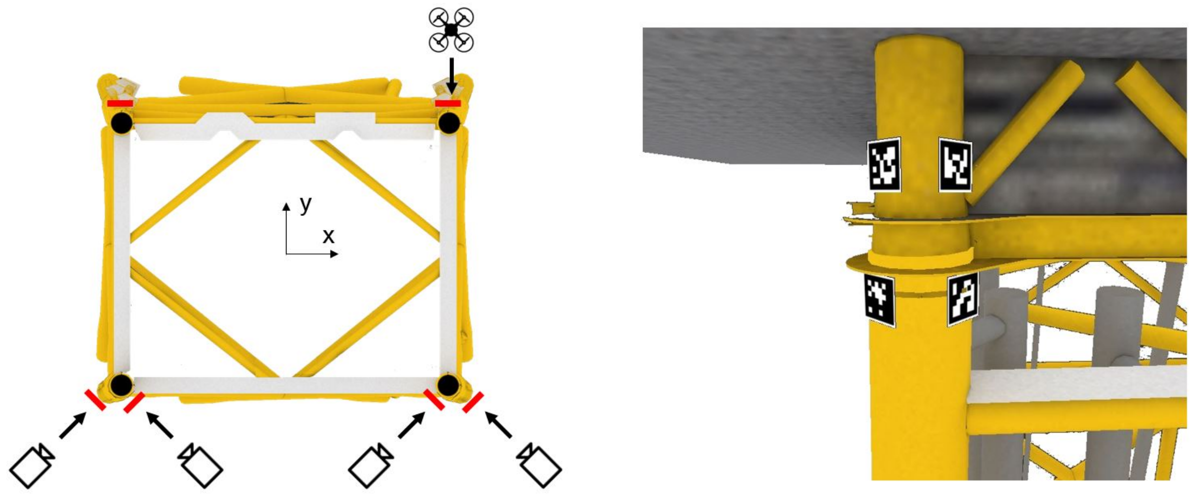

Figure 5.6: Configuration 1

It is also clear that the markers and the cameras are perpendicular to each other, but together make an angle of 45 degrees with respect to the SSCV. In this way, a measurement can be performed from two sides in order to form a 3-dimensional image. This means that in principle no drones have to be used for the positioning. However, a good visibility from the SSCV on the top of the jacket is necessary. In the North Sea this is usually not a problem but can be a problem for the coast of Africa where the jacket sometimes only protrudes a few meters above the water. If this is the case, the cameras need to be lowered from the stern of the SSCV.

Two viewpoints are created in the simulation environment. These viewpoint represents either the fixed camera or one of the drones. These viewpoints are the input for the motion tracking algorithm as described in chapter 3.3. The viewpoints are streamed in real-time to determine the relative position of the topside with respect to the jacket. This data is saved to a *.CSV file and can be compared to the translations that comes out of the simulation log and this way show the positioning error. This will be repeated for different procedures.

In this experiment the precision and accuracy will be measured. In addition, we also look at the limits of the system. This way we look at the maximum distance that can be measured and what happens during movements of the topside caused by sea state and the influence of fog and rain. Table 5.1

shows the procedures that where followed during the experiment.

Procedure	Moves (x, y)	Description
(1)	(0, -20) (0, 0)	Start position 20m ahead, Move 20m astern to final position.
(2)	(0, 0) (10, 0)	Start position above jacket, move 10m to port side.
(3)	(0, 0)	Test performance for: Jonswap: 1m, 8s, heading 135, spreading 4 Fog: 50% Rain: 30%
(4)	(0, 0)	Test performance for: Jonswap: 1m, 10s, heading 135, spreading 4 Fog: 50% Rain: 30%

Table 5.1: Experiment 1 configuration 1: different moves

The first procedure was a move of 20 meters astern towards the jacket. This allows to check when the algorithm starts working and also measures the accuracy and precision. Procedure 2 has the same principle as procedure 1 but in another direction, 8 meters to portside. During procedure 3 and 4 the topside keeps position above the jacket and will be moving due to the vessel motions of the SSCV caused by a Jonswap wave spectrum. Rain and fog will be applied to add some noise to the video footage. These procedures are also visualized in figure 5.7.

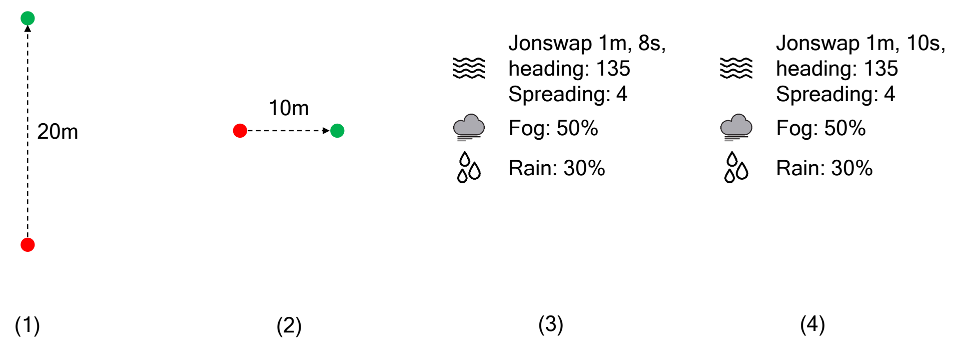

Figure 5.7: Configuration 1 moves

5.3.3. Configuration 2

In configuration 2 the markers are placed on the primary stabbing cones. This is similar to the current method whereby the assistant superintendent and the rigger foreman also stand at the primary stabbing cones. At the stabbing cone closest to the SSCV the markers are filmed by a fixed camera and a drone. The choice of a fixed camera instead of a drone is because of the limited space between the topside and the SSCV and the presence of tugger lines, leaving little room for the drone to maneuver. The markers on the other stabbing cone are filmed by two drones. Here the drones really add value because these images could not possibly be made from the vessel. This configuration is schematically shown in figure 5.8.

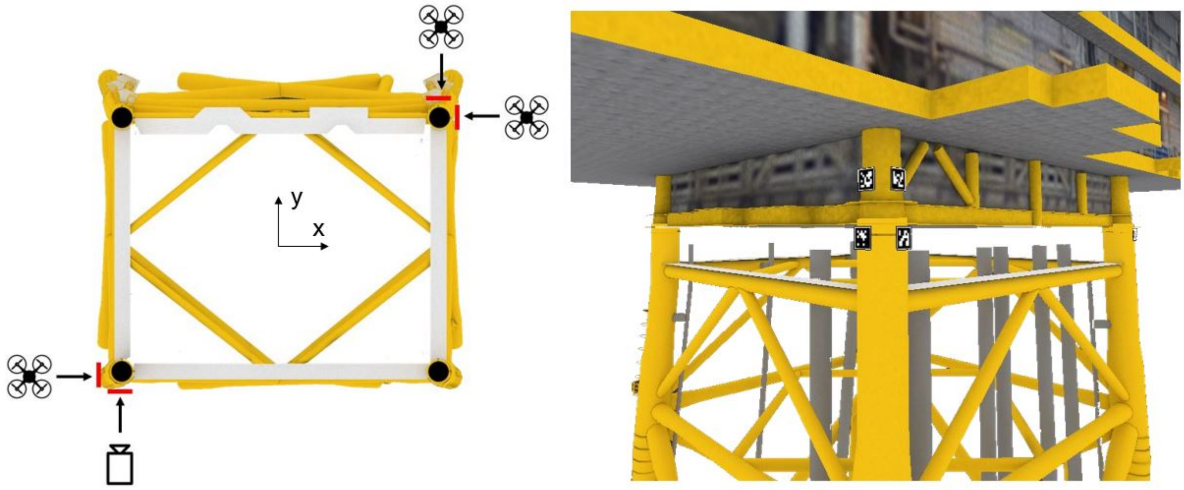

Figure 5.8: Configuration 2

At the previous configuration the system limits and influence of rain and fog where already determined. For this configuration only three procedures are performed to determine the accuracy and precision. All procedures for configuration 2 are given in Table 5.2. Procedure 5 is a translation along the y-axis. The start position is 5 meters away from the jacket. The topside is then moved 5 meters astern to the jacket on DP. Procedure 6 is a translation along the x-axis. Start position is above the jacket. The topside is then moved 5 meters to port side. Then back again 5 meters to starboard. The last and seventh procedure a square pattern was followed. The start position was again above the jacket. The topside was then moved 3 meters ahead, 3 meters to portside, 3 meters astern and again 3 meters to starboard.

Procedure	Moves (x, y)	Description
(5)	(0, -5)	Start position 5m ahead,
	(0, 0)	Move 5m astern to final position.
(6)	(0, 0)	Start position above topside,
	(5, 0)	move 5m to port side,
	(0, 0)	move 5m to starboard to final position.
(7)	(0, 0)	Start position above topside,
	(0, -3)	move 3m ahead,
	(3, -3)	move 3m to port side,
	(3, 0)	move 3m astern,
	(0, 0)	move 3m to starboard to final position.

Table 5.2: Experiment 1 configuration 2: different moves

The moves are also visualized in Figure 5.9.

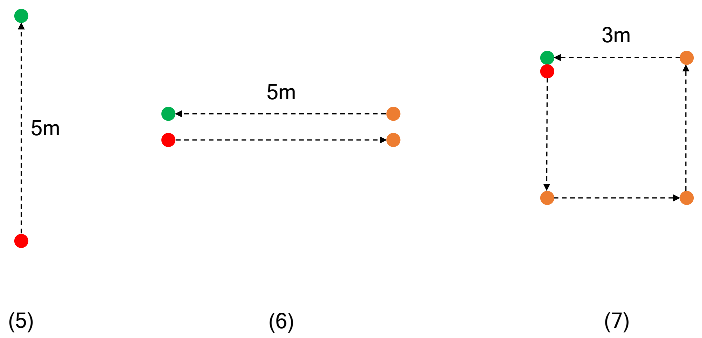

Figure 5.9: Configuration 2 moves

Experiment 1
Goal: test accuracy and precision of moving platform in 3-DOF with different DP moves.
Variable: translation (x, y, z)
Requisites: Motion Tracking Algorithm, Simulator, DP controller, crane controls
Repetitions: 3 times
Output: Resulting translation errors between modelled translations and measured translations.

5.3.4. Results

The advantage of testing in the simulation center is that a log is kept of the movement of each individual object. All markers are inserted as individual objects with the origin in the middle. This is the same position as where the algorithm keeps track of the position. After each simulation run these values can be compared with each other to determine the precision and accuracy. If such a test was to be carried out in practice, another measurement method would be required, for example total stations or ultrasound measurements.

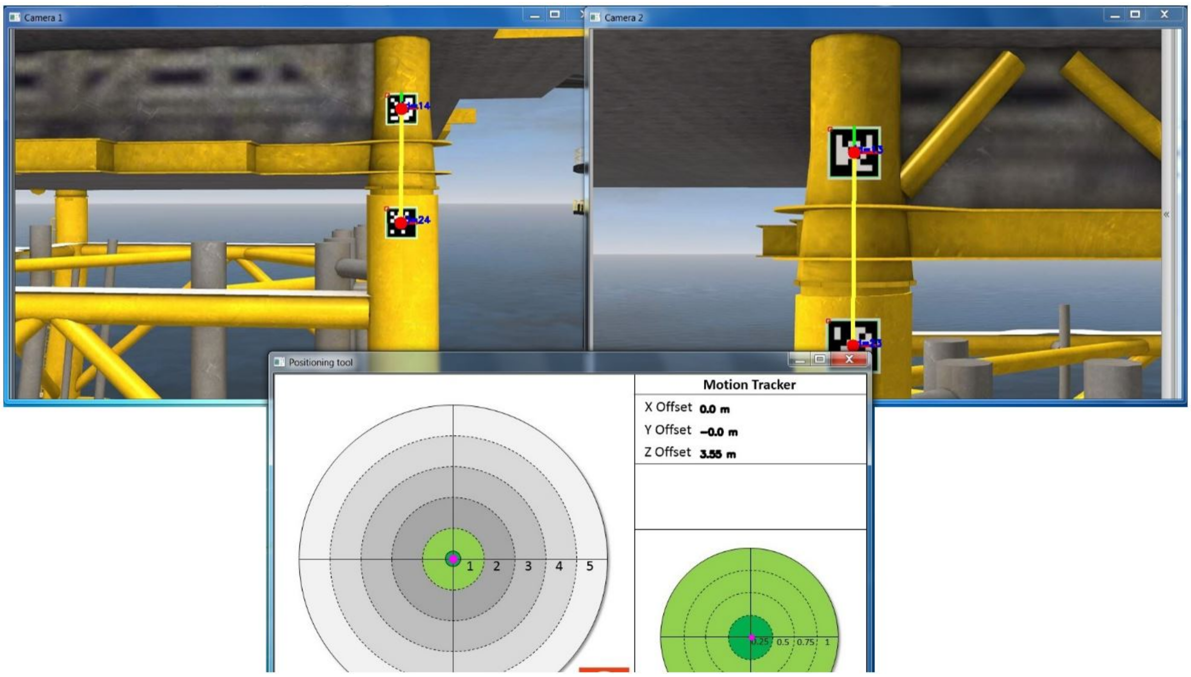

Figure 5.10: Motion Tracking Algorithm - Real Time

This experiment was carried out in the Heerema Simulation Center and the Motion Tracking Algorithm seemed to perform well. A screenshot of the system can be seen in Figure 5.10. In this situation the topside is in its final position. This is also displayed on the motion tracker. Both numerically (in the upper right corner) and visually (on the bullseye). As soon as a marker is recognized, a green border is projected around it. In addition, a coordinate system is projected in the middle of the marker to indicate the orientation. When a marker pair is recognized (two markers between which the distance must be measured) these are connected by a yellow projected line. The SSCV was moved on DP to get the topside in position. The accuracy and precision measurements were performed and the results are expressed as: Mean Absolute Error (e_{MAE}), Maximum Absolute Error ($|e|_{MAX}$), Standard Deviation (σ_e) and Mean Error (μ_e).

As the name suggests, the mean absolute error is an average of the absolute errors $|e_i| = |y_i - x_i|$, where y_i is the prediction and x_i the true value. MAE measures the average magnitude of the errors in a set of predictions, without considering their direction. It's the average over the test sample of the absolute differences between prediction and actual observation where all individual differences have equal weight. In other words, MAE is the average absolute difference between x_i and y_i. For a set of data with n point it is calculated as follows:

$$e_{MAE} = \frac{1}{n}\sum_{i=1}^{n}|y_i - x_i| \tag{5.3}$$

The maximum absolute error is the absolute value of the difference between x_i and y_i. It is a helpful indication of the overall precision and is calculated as:

$$|e|_{MAX} = MAX\,(|y_i - x_i|) \tag{5.4}$$

A standard deviation is a number that tells to what extent a set of numbers lie apart. A standard deviation can range from 0 to infinity. A standard deviation of 0 means that a list of numbers are all equal -they don't lie apart to any extent at all. It is a measure to quantify the amount of variation in the measurement errors. It is calculated as:

$$\sigma_e = \sqrt{\frac{\sum_{i=1}^{N}(e_i - \bar{e})^2}{N-1}} \tag{5.5}$$

The mean error can be compared to the mean absolute error except that the absolute value is not taken (the signs of the errors are not removed), the average error becomes the Mean Bias Error (MBE) and is usually intended to measure average model bias. MBE can convey useful information, but should be interpreted cautiously because positive and negative errors will cancel out.

$$\mu_e = \frac{1}{n}\sum_{i=1}^{n}y_i - x_i \tag{5.6}$$

5.3.5. Configuration 1

In this concept the cameras on the SSCV are rotated 45 degrees with respect to the vessel coordinate system. The camera's are aligned in the x', y' system as illustrated in figure 5.11. This coordinate system has to be rotated 45 degrees in order to match the vessel's reference. There are a few ways to work this out but one of the most convenient options is to use complex numbers. A point (x', y') can be represented by the complex number $x' + iy'$, it can be rotated 45 degrees clockwise by multiplying the complex number $(1 - i)/\sqrt{2}$ and then reading of their x and y coordinates.

$$\frac{(x' + iy')(1 - i)}{\sqrt{2}} = \frac{(x' + y') + i(y' - x')}{\sqrt{2}} = \frac{x' + y'}{\sqrt{2}} + i\frac{y' - x'}{\sqrt{2}} \tag{5.7}$$

Therefore, the rotated coordinates (x, y) are:

$$(x, y) = \left(\frac{x' + y'}{\sqrt{2}}, \frac{y' - x'}{\sqrt{2}}\right) \tag{5.8}$$

In this way the data from the Motion Tracking Algorithm can be properly displayed in the GUI and matched with the data log of the Simulation Center. Now it is also easy to see that the data from both cameras is combined to determine the x- and y-data.

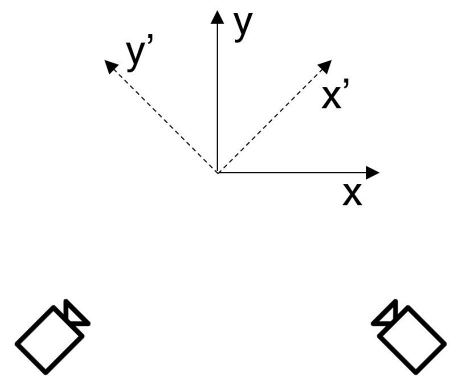

Figure 5.11: Axis rotation

The first two procedures where used to test in what range the algorithm will start working and within what range the results are within the 0.15m error margin. Procedure 1 consisted of an approach 20m astern towards the jacket while the second procedure consisted of a test 10m to port side seen from the jacket. The results are shown in figure E.1 and E.2.

From these figures it can be concluded that the algorithm returns accurate values within 12 meters in y-direction and within 8 meters in x-direction. The results for these procedures (1 and 2) are shown in Table 5.3. The combined mean absolute error of both procedures is 0.048, 0.043 and 0.048 m for x-, y- and z-direction respectively. This is within the acceptable margin of 0.15 m as determined in chapter 2.1.

Procedure	e_{MAE}[m]	$\|e\|_{MAX}$[m]	σ_e [m]	μ_e [m]
1	x: 0.046	x: 0.117	x: 0.034	x: -0.041
	y: 0.039	y: 0.073	y: 0.034	y: -0.028
	z: 0.052	z: 0.104	z: 0.015	z: -0.052
2	x: 0.052	x: 0.137	x: 0.063	x: -0.001
	y: 0.052	y: 0.125	y: 0.031	y: -0.052
	z: 0.039	z: 0.053	z: 0.007	z: -0.039
1, 2 combined	x: 0.048	x: 0.127	x: 0.048	x: -0.028
	y: 0.043	y: 0.099	y: 0.035	y: -0.035
	z: 0.048	z: 0.079	z: 0.015	z: -0.048

Table 5.3: Results procedure 1 and 2 - Configuration 1. e_{MAE} = mean absolute error, $|e|_{MAX}$ = absolute maximum error, σ_e = standard deviation, μ_e = mean error

During procedures 3 and 4 the topside was positioned above the jacket. A Jonswap wave spectrum was applied to the simulation environment to generate waves and induce vessel motions. As a result of vessel motions the topside also starts moving. Previous tests always assumed flat water conditions. In addition, rain and fog were also simulated. The weather conditions caused extra noise in the environment that will also be observed in practice. Rain and fog can be added on a scale of 0 to 100%. This can not be further quantified. The fog was set in such a way that the topside was still visible from the SSCV. It would not be realistic to add just as much fog that the topside is no longer visible because in such a case offshore installation activities would be postponed. The experiment results can be found in table 5.4. Also this experiment returned acceptable values within the 0.15 meters margin. The accuracy of procedure 4 is slightly worse than that of procedure 3. During procedure 3, the movements of the topside were much bigger than during procedure 3. In real life, offshore installation activities would then be postponed to wait for calmer weather. When looking closer to the data of procedure 4 in figure E.9, it can be seen that the errors are mainly caused by a phase difference between the data of the simulation center and the algorithm. This causes the extreme peaks in figure E.10 that fall in the red area. It is probably caused by the running average. There is less effect with lower topside velocities than with higher topside velocities. Figure E.11 is a combination of the error analysis of procedure 3 and 4. The individual error distributions of procedure 3 and 4 can be respectively found in figure E.8 and E.10.

Procedure	e_{MAE}[m]	$\lvert e\rvert_{MAX}$[m]	σ_e [m]	μ_e [m]
3	x: 0.019	x: 0.070	x: 0.022	x: -0.090
	y: 0.019	y: 0.071	y: 0.024	y: 0.003
	z: 0.011	z: 0.037	z: 0.010	z: -0.009
4	x: 0.039	x: 0.295	x: 0.051	x: -0.024
	y: 0.037	y: 0.251	y: 0.048	y: -0.022
	z: 0.020	z: 0.090	z: 0.023	z: -0.012
3, 4 combined	x: 0.032	x: 0.183	x: 0.043	x: -0.019
	y: 0.031	y: 0.161	y: 0.043	y: -0.013
	z: 0.016	z: 0.064	z: 0.019	z: -0.011

Table 5.4: Results procedure 3 and 4 - Configuration 1. e_{MAE} = mean absolute error, $\lvert e\rvert_{MAX}$ = absolute maximum error, σ_e = standard deviation, μ_e = mean error

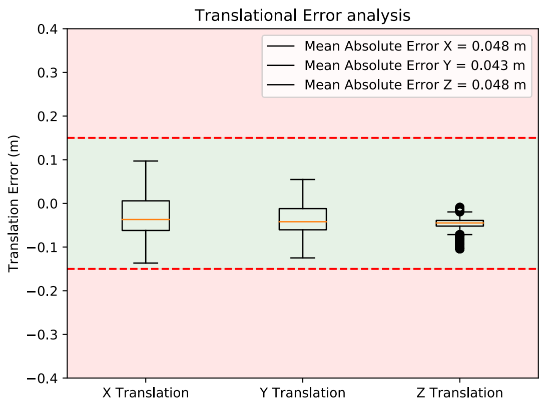

(a) Experiment 1 - Configuration 1, procedure 1 and 2

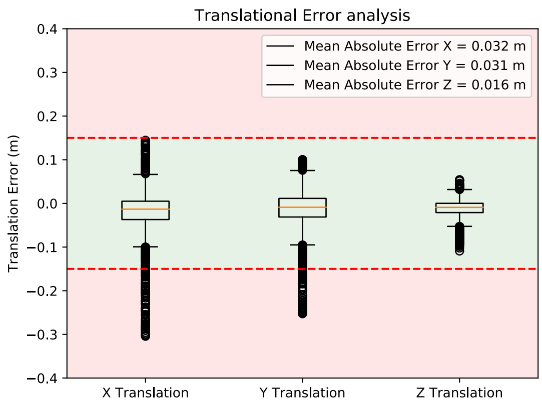

(b) Experiment 1 - Configuration 1, procedure 3 and 4

Figure 5.12: Translational Error Analysis

5.3.6. Configuration 2

The average of the 3 procedures (of the mean absolute error) had an outcome of 0.019, 0.023 and 0.034 m for x, y, and z respectively. A visualization of the mean (non-absolute) error and the extremes is given in figure 5.13. This figure is a combination of procedures 1, 2, and 3. Individual error distributions can respectively found in figure E.12, E.14, and E.16. The maximum tolerable error is 0.15m as established in chapter 2.1. This margin is marked with green, the non-acceptable errors which exceed 0.15m are marked in red.

These outcomes look very promising and would mean the Motion Tracking Algorithm can very accurately determine the relative position between a topside and a jacket. Drones were used in this configuration. The movement of the drone itself is not modeled. This is considered to be negligible and therefore are neglected in further tests.

Procedure	e_{MAE}[m]	$\|e\|_{MAX}$[m]	σ_e [m]	μ_e [m]
5	x: 0.010 y: 0.030 z: 0.055	x: 0.029 y: 0.082 z: 0.079	x: 0.008 y: 0.020 z: 0.006	x: -0.010 y: 0.0030 z: -0.055
6	x: 0.022 y: 0.012 z: 0.040	x: 0.105 y: 0.063 z: 0.082	x: 0.032 y: 0.011 z: 0.017	x: -0.009 y: -0.009 z: -0.039
7	x: 0.026 y: 0.027 z: 0.007	x: 0.082 y: 0.092 z: 0.030	x: 0.026 y: 0.029 z: 0.009	x: -0.017 y: 0.017 z: -0.039
5, 6, 7 combined	x: 0.019 y: 0.023 z: 0.034	x: 0.105 y: 0.092 z: 0.082	x: 0.022 y: 0.020 z: 0.011	x: -0.028 y: -0.035 z: -0.037

Table 5.5: Results procedure 5, 6 and 7 - Configuration 2. e_{MAE} = mean absolute error, $|e|_{MAX}$ = absolute maximum error, σ_e = standard deviation, μ_e = mean error

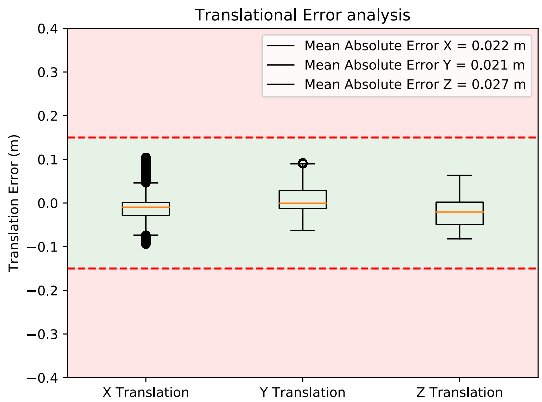

Figure 5.13: Translational Error Analysis: Experiment 1 - Configuration 2

5.4. Experiment 2: Proof of Principle

5.4.1. Experiment outline

In the final experiment the Motion Tracking Algorithm is tested in a simulated offshore topside installation. The experiment allows the immersion of the participants on a completely virtual environment and provides a first approach of the system and the user relation with it. The experiment constitutes an initial exploration on the system in order to address how engineers deal and interact with the motion tracker, and their opinions on the system. First the SSCV was moved in position 20 meters away of the jacket. Then, an assistant superintendent provided instructions to move the vessel and cranes. The vessel and cranes where operated by the same person. This method is different from real topside installations where the assistant superintendent and rigger foreman give information on the position of the topside relative position to the superintendent. The superintendent is then responsible to provide instructions to the captain and crane drivers. A simplified setup was chosen to limit the number of people needed. In addition, the goal is mainly to determine whether the algorithm works and the chosen setup with only one assistant superintendent is therefore sufficient.

First of all, the operation was carried out with the current method whereby people are positioned on the jacket and then give instructions. This has been used as a benchmark. The operation was repeated three times. After this, the motion tracking algorithm was used to determine the position. Figure 5.14 shows how the algorithm was presented to the assistant superintendent. This method was also repeated three times. For each repetition the total time and number of instructions where recorded.

Figure 5.14: Laptop with Motion Tracker provided to the assistant superintendent

Experiment 2
Goal: Test whether the Motion Tracking Algorithm is able to guide an offshore topside installation.
Variable: Translation (x, y, z), crane movement: main hoist and tugger lines haul in/out
Requisites: Motion Tracking Algorithm, Simulator, DP controller, crane controls, assistant superintendent, vessel/crane operator
Repetitions: 3 times per setup
Output: The system usefulness and its usability.

5.4.2. Results

In this experiment the Motion Tracking Algorithm will proof whether it is able to guide an offshore topside installation. Therefore six installations where repeated, three with the current procedure and three with the motion tracking algorithm.

The quantitative data collected during the experiments is shown in table 5.6 and indicates that the positioning time is considerable shorter during the simulation of the new process (the topside positioning using the motion tracker). While positioning the topside in the current simulation process takes about 5:02 min, the motion tracker reduces the time to 4:27 min.

Experiment	Method	Number of operations	Average time
1	People on jacket	9	5:04
	Motion Tracker	6	4:35
2	People on jacket	7	4:40
	Motion Tracker	6	4:20
3	People on jacket	8	5:23
	Motion Tracker	5	4:28
Mean	**People on jacket**	**8**	**5:02**
	Motion Tracker	**5.7**	**4:27**

Table 5.6: Results experiment 2

Concerning the number of operations, the data reveals that the use of the motion tracker can potentially reduce the number of operations. During all rounds of simulations of the current and new process, the number of operations is lower when the simulation includes the use of the motion tracker, from an average of 8 to 5.7. In addition, the assistant superintendent also gained more confidence in his instructions. Unfortunately, no log had been kept of the instructions, but it was noticed during the experiment. With the old method, the commands were cautious. When the motion tracker was used in the second round, the commands became more convincing and accurate.

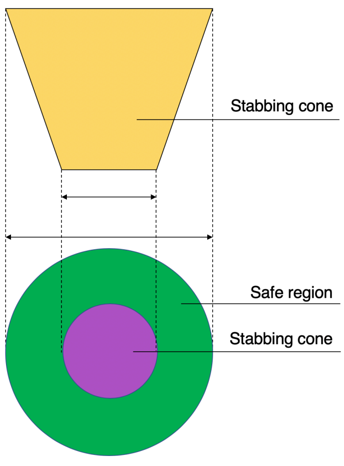

Figure 5.15: Updated motion tracker design

During this experiment the Motion Tracker was considered a useful tool. The information was clear and the video footage gave insight of what is actually happening. An important note is that the assistant superintendent was sometimes more focusing on the video footage and used the motion tracker as a verification tool. This while the motion tracker was actually designed as a primary interface and the video footage had to be considered as a verification tool. Furthermore it was stated that the system is easy to use, easy to control and understandable. Suggested improvements are related to UI design. Currently the interface only shows one stabbing cone at a time. For future use all the tracked stabbing cones should be showed. Another improvement would be to also visualize the vertical clearance between bottom of the stabbing cone and the top of the jacket leg. During the experiment this was only shown as a number. A third improvement relates to the bulls eye design. In the current situation the final 1m was marked green and the final 25cm was marked dark green. The pink tracker was just a moving dot without further dimensions. It only showed the relative position of the stabbing cone. This can be better attuned to each other in a new design. The green area should match the largest diameter of the stabbing cone. The tracker should match the smallest diameter of the stabbing cone. This is illustrated in figure 5.15. In this way it is easy to see when the stabbing cone is located within the final zone to start lowering the topside.

Scientific value The scientific value of this experiment is doubtful and results must be interpret with caution. A topside installation was simulated in around five minutes while in real life it can take up to several hours. It was only tested by one person. Nevertheless, it has yielded interesting results that are worth mentioning. During a real operation, the information will probably also be communicated more efficiently, which leads to a shorter installation time.

5.5. Summary

Precision is how close a measurement comes to another measurement. Precision is determined by a statistical method called a standard deviation. Standard deviation is how much, on average, measurements differ from each other. High standard deviations indicate low precision, low standard deviations indicate high precision. For configuration 1 the mean absolute error was e_{MAE} = 0.048 m and the standard deviation was around $\sigma_e, 1$ = 0.040 m. For configuration 2 this was e_{MAE} = 0.034 and a standard deviation around $\sigma_e, 2$ = 0.020 m. This shows that both configurations meet the requirement of 150 mm precision. If it comes down to precision, configuration 2 is preferred over configuration 1.


HERMOD
PANAMA R.P.
P4
P5
P6

6 Conclusion

In order to install topsides unmanned, a positioning tool is needed. Since the existing methods leave room for improvement, a novel design for the positioning of topsides was created. The final concept was a system based on visual object tracking with fixed cameras and drones. It was designed with the demands and wishes from experts within HMC. A system simulation was performed to proof the concept and estimate the accuracies and precision, which was done in multiple experiments. In this chapter, the process and outcomes are discussed, recommendations for the future are made and conclusions are given.

6.1. Discussion

6.1.1. Simulation validity

The simulation that was used in the experiment serves an essential function in the validation of the Motion Tracking Algorithm. It is necessary that their results represent valid conclusions regarding the predicted behavior of the system. To meet this criterion, it must be determined that they accurately represent the representations of the real world, to the extend required for their intended use. All models used during the simulations had the exact dimensions as in the real world. Also, the camera viewpoints where added on realistic (and thus feasible) positions. In this way, reality has been simulated as well as possible. In addition, performing a physical test was practically unfeasible in the stated time. It is important to remember that it is necessarily only a model, that is, a simplification and approximation to reality. Thus, there is no such thing as an absolutely validated simulation. Despite these cautions, simulations are absolutely indispensable tools in the development of new systems. [41]

6.1.2. Uncertainties

One of the uncertainties is the camera image that the drones will deliver. In the simulator these are simulated as a fixed point in space. In reality, this image will be able to move somewhat. The expectation is that this will have virtually no influence on the results, but it is something to be reckoned with. Another uncertainty is what will happen if there is a drop on the lens of the camera. With fixed cameras, this is easily prevented by using waterproof housings. With the drones this will become a lot more difficult. Measures such as the application of a water-repellent coating could provide a solution. But the effects off drops on the lens are difficult to estimate.

6.1.3. Hardware limitations

All computations where performed on an enterprise laptop. This laptop had sufficient power to get useful results during simulations. However, the frame rate was limited to 15 FPS and a resolution of 920x600 pixels due to the screen size. With an upgrade on installed memory, processor and graphic drive the performance can increase to a 4K resolution (3840x2160 pixels) at 30 FPS.

6.2. Conclusion

The research presented in this report has given an insight in the possibilities and the potential of using drones during offshore topside installations. The knowledge that has been gained is used to formulate a conclusion. This conclusion will answer the research sub-questions that are formulated in chapter 1.

What are the requirements and functional specifications for an Unmanned Topside Installation Monitor based on visual object tracking and drones or fixed cameras? The system requirements that can be set for a positioning monitor during unmanned offshore topside installations are:

- The system must be universal for different topsides and vessels
- Concentricity accuracy within 150mm
- Provide dashboard to superintendent
- System must be robust
- No human invention
- Up to six hours continuously
- Should work in offshore environment

The overall system must be simple. By using cameras, the user sees exactly what is happening and measured. Real-time visualizations of the measurement process takes the guesswork out of the picture because users see exactly what is tracked. Based on the two predecessor systems it can be concluded that unique targets with known position on the topside and jacket are preferred. ArUco markers can be used as a unique target pattern to obtain information about the relative position between two bodies.

How can visual object tracking been used to calculate the relative position between a topside and a jacket in 3-DOF? The relative position between a topside and a jacket is calculated with the use of ArUco markers. ArUco was developed for augmented reality purposes but can also be used as a very robust method to calculate distances. Each ArUco marker returns information about its position and orientation with respect to the camera. Each camera requires a calibration but this only needs to be done once. If two markers are recognized in an image their relative position can be calculated. Distance estimations are based on planar homography and the camera pinhole model. Depth estimations are dependent on the marker area pixel density. Smaller marker sizes result in less accurate results. Therefore two perpendicular cameras are combined to deliver accurate results. Each camera returns information about the horizontal and vertical positions. A Motion Tracking Algorithm has been developed to simultaneously combine these results to obtain positional information about all 3-DOF. When this is done in real-time the results can be displayed in a graphical user interface. A running average is used to display smooth results. All data can be exported to a separate file for post-processing purposes.

How can the combination of drones, fixed cameras and object tracking assist in the installation of offshore topsides at HMC? ArUco markers need to be placed on the stabbing cones and jacket legs. If the markers are positioned in such a way that they are right above each other in their final position, then only information about their vertical offset is needed. This eliminates the need of an extensive spatial survey. Fixed cameras and drones can be used to film the markers on the stabbing cones. A topside normally consist of four stabbing cones of which two cones need to be tracked. A number of configurations are possible. In this research two configurations have been chosen. In configuration 1 four fixed cameras on the stern of the SSCV are used for the motion monitoring. Also one drone is available to deliver real-time imagery of the complete installation. Configuration three uses three drones and one fixed camera from the stern of thee SSCV. In this configuration the drones are not only used to provide imagery but also to track the markers on the stabbing cones. With recent technology drones are limited by their battery capacity. An industrial drone suited for offshore conditions can fly for about 35 minutes. This is not enough for a typical topside installation. To solve this, drones need to alternate each other in order to provide continuous imagery. Therefore, for configuration 1 a minimum of 2 drone operators is required. For configuration 2 this minimum is 6. If offshore shifts are taken into account both amounts will double. Autonomous drone operations could lower or even eliminate the number of required drone pilots. A lot of research is already done to enable this but there is no 'off-the-shelf' solution available yet.

What are the accuracy's, advantages and limitations of using visual object tracking for topside installations? Because ArUco was only distributed in 2014 and meant for augmented reality purposes, there is no literature available for determining accuracies. Since accuracy is an important part of the system requirements, a simulation experiment was performed in the Heerema Simulation Center. A virtual scale model of a jacket, topside and SSCV was used. Markers where added on the topside and jacket just as in configuration 1 and 2. Viewpoints where created to mimic the fixed cameras on the SSCV and the drones. The topside was moved above the jacket following different procedures. Afterwards the results of the motion tracking algorithm could be compared with the log of the simulation environment. These results were used to validate the algorithm and determine its accuracy. For configuration 1 the mean absolute error was $e_{MAE} = 0.048m$ with a standard deviation of $\sigma_e = 0.040m$. For configuration 2 this resulted in $e_{MAE} = 0.034m$ and $\sigma_e = 0.020m$. Based on these results it can be concluded that both configurations deliver results within the required precision of 150mm. But configuration 2 gives slightly better results when it comes to precision. This was the configuration were drones are used to track the markers.

What is the potential of drones as an installation aid during offshore topside installations?

The sub-questions provide supportive results, which are used to answer the main question which was posed in section 1.3 of this thesis. A motion tracking algorithm was designed, developed and tested. The input for this algorithm is camera imagery. This imagery can either be delivered by fixed cameras or flying cameras, often referred to as drones. If these cameras are able to film ArUco markers attached to the topside and jacket, the algorithm is able to determine its relative position.

The motion tracking algorithm performed well during experiments, where the accuracy and the precision was tested for different camera configurations. The spatial position of the cameras is not required to perform calculations, which eases the system initialization. The first configuration used fixed cameras on the stern of the SSCV while the second configuration used drones. Both configurations returned results within the required accuracy but the second configuration - using drones - performed slightly better. A big advantage of drones is the ability to take any desired position with respect to the topside and jacket and are therefore not limited by the view from the SSCV. Drones could therefore be used for any type of operation regardless of the view from the SSCV.

A current limitation in the use of drones is the requirement of a certified operator and the limited power supply. To eliminate the requirement of a certified operator, autonomous drones could be used. Several studies show that there are a lot of opportunities in enabling autonomous drone operations. It will be a matter of time before the first autonomous drones will take off from vessels to carry out specific missions. The power supply of drones is also likely to increase due to a technology push from the automotive and electronic consumer goods industry.

In the meantime drones can be used as a useful visualization tool during topside installations. Drones are able to mimic the presence of people on the jacket and can provide close-ups of every part of the topside or jacket. They eliminate the need for offshore crew to physically access the jacket during installation, which results in a safer work environment.

6.3. System comparison

If configuration 1 of the Motion Tracking Algorithm is compared with the other two systems, the resulting spider diagram can be seen in Figure 6.1.

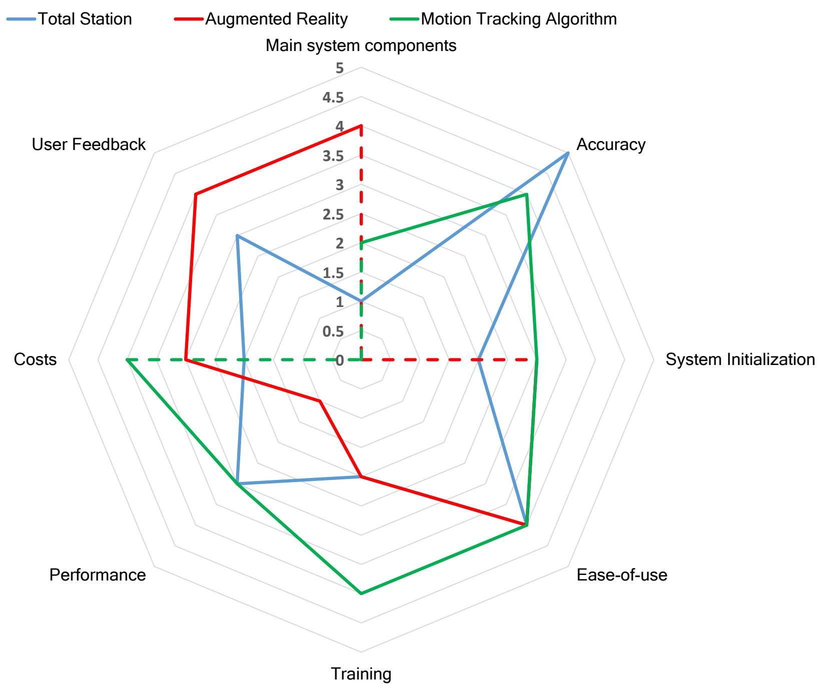

Figure 6.1: Spider diagram

The scores for the total station system and augmented reality system are given in Appendix A.3. The scores for the marker tracking system will be substantiated here. The subjective value method was used to determine raw scores. [41] This method begins with a judgment of the relative utility of each criterion on a scale of 1-5. Thus, 1 = poor, 2 = fair, 3 = satisfactory, 4 = good, and 5 = superior. A candidate that fails a criterion will be given a zero. It is also possible that there is not enough information available about a certain criterion. This is indicated by a dashed line in the spider diagram.

Main System Components: 2 In terms of main system components, this system uses 4 cameras, two drones and 8 markers. It is still necessary to have access to the jacket in order to install the markers. This is also necessary when installing the prisms for the total station system. On the other hand, the surveying process is less invasive when installing the markers compared to the prisms. Therefore, this system scores a 2 out of 5.

Accuracy: 4 In terms of accuracy, it is well within the set precision but slightly less accurate than the total station system.

System Initialization: 3 The markers do not have to be measured. If they are confirmed right under each other, that is sufficient. Only the vertical distance (height) between the markers must be determined as accurately as possible. In addition, the cameras just need to be calibrated once. Calibration can take place in advance.

Ease-of-use: 4 A similar type of GUI as the other two systems can be used.

Training: 4 The motion tracking algorithm can easily be implemented in the simulation center. This allows the crew to practice with this system beforehand. Something that is not possible with the other systems.

Performance: 3 Because the markers are very contrasting, they are still clearly recognizable with bad lighting. The camera can also be adjusted in such a way that it provides optimal results for the marker recognition. In the augmented reality system, many larger parts had to be recognized successfully, which caused a major overexposure or underexposure. As a result, the performance of the motion tracking algorithm will be much better. Only drawback is that a clear line of sight is necessary in order to recognize and track the markers.

Costs: 4 All components of this system are relatively cheap. Furthermore, a minimal amount of preparation is needed in order to calibrate or initialize sub-systems.

User Feedback: 0 The system has not yet been actually tested, so statements about the user feedback would be premature.
Based on the above results, it can be concluded that there is potential in actually using the Motion Tracking Algorithm during real offshore topside installations. In the next section some recommendations are given to further test and improve the system.

6.4. Recommendations

For future research, the following items should be taken into account.

6.4.1. Offshore test

Another recommendation is to perform a test during an offshore installation. The results can then be compared with the data of, for example, a total station. It is then recommended to use a camera with at least full HD resolution. This is the same resolution that drones can stream their images in real-time. In addition, it is already possible to practice a continuous drone flight from an SSCV.

6.4.2. Marker design

First, the design of the marker should be investigated. In this research a flat marker was used. However, it would be more convenient if the marker could also take on a curved shape. In that case the marker could simply be stuck or painted on the stabbing cone. It is also useful to investigate if the marker can be made more robust in case of partial occlusion. If both improvements can be realized, the score for the system initialization as presented in the conclusion can be significantly increased.

6.4.3. Autonomous drones with more endurance

At this moment it requires a lot of resources and manpower to have multiple drones up in the air. However, the drones need to execute a relatively simple mission. Which is take-off from an SSCV, get in position near the topside and automatically alternate a drone low in battery with a fully charged one. If this could be done autonomously it will result in a significant reduction on the number of required drone operators. Numerous researches are focusing on autonomous take-off, landing and path finding. Most of them use a static base station instead of dynamic base station. It would be interesting to investigate if these autonomous operations can also be executed from an SSCV in offshore conditions. This would then result in more flexible camera positions to enable a wider range of installation types.

6.4.4. On-board versus tele-operation

For now it has been assumed that the images are streamed from the drone to a ground station and then analyzed (tele-operation model). The image analysis could also happen on board the drone (on-board model). In case of tele-operation model, video captured by on-board cameras are compressed and are transmitted through a wireless link to a ground station. Video compression, however, is a computation intensive task and has adverse effect on system power consumption. Moreover, compressed image/video data still requires sufficient bandwidth for wireless transmission that increases pressure on system power resources. Video data received on ground station can, therefore, be noisy and delayed.

Tele-operation is commonly used for small unmanned aerial vehicles but at best can only guarantee near real-time operation. In contrast to Tele-operation, On-board vision processing model encourages vision processing to be carried out on-board as shown in Figure 6.2.

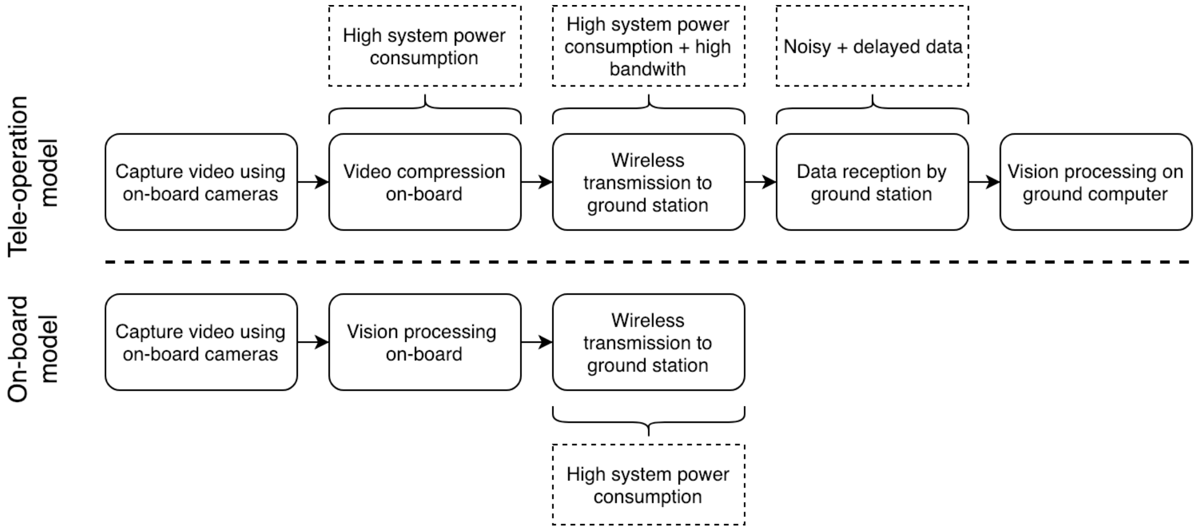

Figure 6.2: Tele-operation versus on-board computation

This model ensures real-time operation and autonomy, but is practically realizable only for simple image processing operations due to extremely restricted on-board computational resources. Even for simple image processing operations, keeping system power consumption with in reasonable limits (usually less than a watt) is a non-trivial task. [27] However, powerful processors are getting smaller and smaller and most UAV's already perform automatic tracking of objects by means of computer vision algorithms. It is therefore an interesting question to find out.


HEEREMA
H
HEEREMA
SLEIPNIR
PANAMA R.P.


HEEREMA
HEEREMA
SLEIPNIR
PANAMA R.P.

Bibliography

[1] Raul Acuña, Rosa Maria Carpio, and Volker Willert. Dynamic markers: Uav landing proof of concept. 09 2017.

[2] Federal Aviation Administration. Integration of civil unmanned aircraft systems (uas) in the national airspace system (nas) roadmap. *Tech. report 2012-AJG-502*, 2013. URL https://www.faa.gov/uas/media/uas_roadmap_2013.pdf.

[3] American Bureau of Shipping. Guidance notes on using unmanned aerial vehicles, 2018. URL http://safety4sea.com/wp-content/uploads/2018/02/ABS-Guidance-Notes-on-Using-Unmanned-Aerial-Vehicles-2018_02.pdf. [Online; accessed September 21, 2018].

[4] Asifr. Object recognition in augmented reality using aruco framework, 2018. URL https://imaginghub.com/blog/20-object-recognition-in-augmented-reality-using-aruco-framework. [Online; accessed November 15, 2018].

[5] R. Austin. *Unmanned Aircraft Systems: UAVS Design, Development and Deployment*. Aerospace Series. Wiley, 2011. ISBN 9781119964261. URL https://books.google.nl/books?id=03gdqhU61C0C.

[6] Andrej Babinec, Ladislav Jurišica, Peter Hubinský, and František Duchoň. Visual localization of mobile robot using artificial markers. *Procedia Engineering*, 96:1 – 9, 2014. ISSN 1877-7058. doi: https://doi.org/10.1016/j.proeng.2014.12.091. URL http://www.sciencedirect.com/science/article/pii/S1877705814031427. Modelling of Mechanical and Mechatronic Systems.

[7] Bart Jansen. Why it's a big deal that commercial drones flew around the atlanta airport, 2017. URL https://eu.usatoday.com/story/news/2017/02/14/drone-flight-atlanta-airport-commercial-use/97748194/. [Online; accessed November 2, 2018].

[8] A. Belhaoua, A. Kornmann, and J. Radoux. Accuracy analysis of an augmented reality system. In *2014 12th International Conference on Signal Processing (ICSP)*, pages 1169–1174, Oct 2014. doi: 10.1109/ICOSP.2014.7015184.

[9] Betsy Lillian. Skysense autonomous drone charging helps security companies with missions, 2018. URL https://unmanned-aerial.com/skysense-autonomous-drone-charging-helps-security-companies-with-missions. [Online; accessed November 13, 2018].

[10] Alexandre Borowczyk, Nguyen Tien, Andre Nguyen, Dang Nguyen, David Saussie, and Jerome Le Ny. Autonomous landing of a quadcopter on a high-speed ground vehicle. *Journal of Guidance, Control, and Dynamics*, 40:1–8, 04 2017. doi: 10.2514/1.G002703.

[11] G. Bradski. The OpenCV Library. *Dr. Dobb's Journal of Software Tools*, 2000.

[12] Gary Bradski and Adrian Kaehler. *Learning OpenCV: Computer Vision in C++ with the OpenCV Library*. O'Reilly Media, Inc., 2nd edition, 2013. ISBN 1449314651, 9781449314651.

[13] Ronald Brouwer, Matthieu De Schipper, Patrick Rynne, Fiona Graham, Ad J. H. M. Reniers, and Jamie Macmahan. Surfzone monitoring using rotary wing unmanned aerial vehicles. *Journal of Atmospheric and Oceanic Technology*, 32:855–863, 04 2015. doi: 10.1175/JTECH-D-14-00122.1.

[14] Roger Clarke. Understanding the drone epidemic. *Computer Law & Security Review*, 30(3): 230 – 246, 2014. ISSN 0267-3649. doi: https://doi.org/10.1016/j.clsr.2014.03.002. URL http://www.sciencedirect.com/science/article/pii/S0267364914000545.

[15] Clement Schuhler. Dev80780 topside set down monitoring functional specifications of the system to be developed, 2014. URL https://instore.hmc-heerema.com/department/innovation/teammanagement/library/Stove/. [Internal document].

[16] Clement Schuhler. Unmanned topside positioning - all ideas, 2015. [Internal document].

[17] Clement Schuhler. Positioning control system for topsides installation: Sounding board 4 session summary, 2016. URL https://instore.hmc-heerema.com/department/innovation/teammanagement/library/SoundBoardSession/. [Internal document].

[18] Clement Schuhler. Dev80780 unmanned topside positioning project, 2016. URL https://instore.hmc-heerema.com/department/innovation/teammanagement/library/DevelopmentProject/. [Internal document].

[19] Clement Schuhler. Topsides positioning controller: Sounding board 5 session summary, 2017. URL https://instore.hmc-heerema.com/department/innovation/teammanagement/library/SoundBoardSession/. [Internal document].

[20] CNBC. Ups tests drone deliveries via high-tech truck, 2017. URL https://www.cnbc.com/2017/02/25/ups-tests-drone-deliveries-via-high-tech-truck.html. [Online; accessed November 13, 2018].

[21] G. Collins, A. Clausse, and D. Twining. Enabling technologies for autonomous offshore inspections by heterogeneous unmanned teams. In *OCEANS 2017 - Aberdeen*, pages 1–5, June 2017. doi: 10.1109/OCEANSE.2017.8085012.

[22] D. A. Cucci. Accurate optical target pose determination for applications in aerial photogrammetry. *ISPRS Annals of Photogrammetry, Remote Sensing and Spatial Information Sciences*, 3:257–262, 2016. doi: 10.5194/isprs-annals-III-3-257-2016. URL http://infoscience.epfl.ch/record/224474.

[23] DJI. Lightbridge 2, 2018. URL https://www.dji.com/nl/lightbridge-2. [Online; accessed January 15, 2019].

[24] DOF Subsea. Borkum riffgrund uti topside dimensional control survey report, 2018. [Internal document - HMC PROJECT NUMBER – I/0464].

[25] Klaus Dorfmüller and Hanno Wirth. Real-time hand and head tracking for virtual environments using infrared beacons. In Nadia Magnenat-Thalmann and Daniel Thalmann, editors, *Modelling and Motion Capture Techniques for Virtual Environments*, pages 113–127, Berlin, Heidelberg, 1998. Springer Berlin Heidelberg.

[26] DroneView Technologies. Droneview technologies signs agreement with abs group to inspect aerial wind turbines, 2016. URL https://www.droneviewtech.com/blog-and-news/2016/7/6/droneview-technologies-signs-agreement-with-abs-group-to-inspect-aerial-wind-tur [Online; accessed August 9, 2018].

[27] Shoaib Ehsan and Klaus D. McDonald-Maier. On-board vision processing for small uavs: Time to rethink strategy. *CoRR*, abs/1504.07021, 2015. URL http://arxiv.org/abs/1504.07021.

[28] S. Garrido-Jurado, R. Muñoz-Salinas, F.J. Madrid-Cuevas, and M.J. Marín-Jiménez. Automatic generation and detection of highly reliable fiducial markers under occlusion. *Pattern Recognition*, 47(6):2280 – 2292, 2014. ISSN 0031-3203. doi: https://doi.org/10.1016/j.patcog.2014.01.005. URL http://www.sciencedirect.com/science/article/pii/S0031320314000235.

[29] Masoud Gheisari, Javier Irizary, and Bruce N. Walker. Uas4safety: The potential of unmanned aerial systems for construction safety applications, 05 2014.

[30] Ferran Giones and Alexander Brem. From toys to tools: The co-evolution of technological and entrepreneurial developments in the drone industry. *Business Horizons*, 60(6):875 – 884, 2017. ISSN 0007-6813. doi: https://doi.org/10.1016/j.bushor.2017.08.001. URL http://www.sciencedirect.com/science/article/pii/S0007681317301210. THE GENERATIVE POTENTIAL OF EMERGING TECHNOLOGY.

[31] RPAS Steering Group. Roadmap for the integration of civil remotely-piloted aircraft systems into the european aviation system. *Final report from the European RPAS Steering Group*, 2013. URL https://www.sesarju.eu/sites/default/files/European-RPAS-Roadmap_Annex-1_130620.pdf.

[32] Gustav Olson, Peter and Hebsgaard Muff, Steffen. Using drones offshore, 2017. URL https://www.njordlaw.com/knowledge/using-drones-offshore/. [Online; accessed January 11, 2019].

[33] Douglas David H. and Peucker Thomas K. *Algorithms for the Reduction of the Number of Points Required to Represent a Digitized Line or its Caricature*, chapter 2, pages 15–28. Wiley-Blackwell, 2011. ISBN 9780470669488. doi: 10.1002/9780470669488.ch2. URL https://onlinelibrary.wiley.com/doi/abs/10.1002/9780470669488.ch2.

[34] Nils Hasler. *Motion Capture*, pages 495–498. Springer US, Boston, MA, 2014. ISBN 978-0-387-31439-6. doi: 10.1007/978-0-387-31439-6_21. URL https://doi.org/10.1007/978-0-387-31439-6_21.

[35] Heerema Marine Contractors. Simulation center brochure, 2016. URL https://heerema-production-content.s3.amazonaws.com/HMC/Media/Brochures/Simulation20Center20Brochure20R10.pdf. [Online; accessed September 26, 2018].

[36] J. Rotgans. Drones operations wi 05.02.19 provide guidelines for the use of drones on vessels, 2015. URL https://instore.hmc-heerema.com/knowledge/msd/WorkInstructions/. [Internal document].

[37] Josh Parker. Eyes in the sky: Using aerial drones to power offshore operations, 2016. URL https://www.oedigital.com/subsea/item/14001-eyes-in-the-sky-using-aerial-drones-to-power-offshore-operations. [Online; accessed November 13, 2018].

[38] Kelsey D. Atherton. Dronebox is a nest for drones, 2016. URL https://www.popsci.com/dronebox-is-nest-for-drones. [Online; accessed November 13, 2018].

[39] G Kipper and J Rampolla. Augmented reality: An emerging technologies guide to ar. pages 1–158, 11 2012.

[40] Vladimir A. Knyaz and Alexandr V. Sibiryakov. In *The Development of New Coded Targets for Automated Point Identification and Non-contact 3 D Surface Measurements*, 1998.

[41] Sweet William N. Seymour Samuel J. Biemer Steven M. Kossiakoff, Alexander. *Systems Engineering Principles and Practice (2nd Edition)*. John Wiley & Sons, 2011. ISBN 978-0-470-40548-2. URL https://app.knovel.com/hotlink/toc/id:kpSEPPE006/systems-engineering-principles/systems-engineering-principles.

[42] M Lemmens. Total stations: The surveyor's workhorse. *GIM International: the worldwide magazine for geomatics*, 30:20–25, 10 2016. URL http://resolver.tudelft.nl/uuid:f2e09112-3e18-4478-968f-22f10e57c68d.

[43] Alberto Lopez-Ceron and Jose M. Canas. Accuracy analysis of marker-based 3d visual localization. 07 2016.

[44] Dengzhe Ma, Jrgen Gausemeier, Xiumin Fan, and Michael Grafe. *Virtual Reality & Augmented Reality in Industry*. Springer Publishing Company, Incorporated, 2011. ISBN 3642173756, 9783642173752.

[45] Marianne Harbo Frederiksen and Mette Præst Knudsen. Drones for offshore and maritime missions: Opportunities and barriers, 2018. URL https://offshoreenergy.dk/sites/default/files/publications/drones_for_offshore_and_maritime_missions_sdu_spring_2018.pdf. [Online; accessed December 7, 2018].

[46] Phong Ha Nguyen, Ki Wan Kim, Young Won Lee, and Kang Ryoung Park. Remote marker-based tracking for uav landing using visible-light camera sensor. *Sensors*, 17(9), 2017. ISSN 1424-8220. doi: 10.3390/s17091987. URL http://www.mdpi.com/1424-8220/17/9/1987.

[47] N. Otsu. A threshold selection method from gray-level histograms. *IEEE Transactions on Systems, Man, and Cybernetics*, 9(1):62–66, Jan 1979. ISSN 0018-9472. doi: 10.1109/TSMC.1979.4310076.

[48] Anastasios Plioutsias, Nektarios Karanikas, and Maria Mikela Chatzimihailidou. Hazard analysis and safety requirements for small drone operations: To what extent do popular drones embed safety? *Risk Analysis*, 38(3):562–584, 2018. doi: 10.1111/risa.12867. URL https://onlinelibrary.wiley.com/doi/abs/10.1111/risa.12867.

[49] Q. Quan. *Introduction to Multicopter Design and Control*. Springer Singapore, 2017. ISBN 9789811033827. URL https://books.google.nl/books?id=M3opDwAAQBAJ.

[50] Rafael Muñoz-Salinas. Mapping and localization from planar markers, 2014. URL http://www.uco.es/investiga/grupos/ava/node/57/. [Online; accessed November 15, 2018].

[51] Register, Lloyd's. Guidance notes for inspection using unmanned aircraft systems, 2016. URL file:///C:/Data/Downloads/Guidance_Notes_for_Unmanned_Aircraft_Systems_Mar_2016.pdf. [Online; accessed January 11, 2019].

[52] Reuters. New drone has five times longer flight time, claims ex-tesla inventor, 2018. URL https://www.timeslive.co.za/news/sci-tech/2018-09-10-new-drone-has-five-times-longer-flight-time-claims-ex-tesla-inventor/. [Online; accessed November 14, 2018].

[53] Safety 4 Sea. Lr releases guidance note for drone inspections, 2016. URL https://safety4sea.com/lr-releases-guidance-note-for-drone-inspections/. [Online; accessed August 9, 2018].

[54] Sam Levin. Amazon patents beehive-like structure to house delivery drones in cities, 2017. URL https://www.theguardian.com/technology/2017/jun/26/amazon-drones-delivery-beehive-patent. [Online; accessed November 13, 2018].

[55] Jose Luis Sanchez-Lopez, Jesus Pestana, Srikanth Saripalli, and Pascual Campoy. An approach toward visual autonomous ship board landing of a vtol uav. *Journal of Intelligent & Robotic Systems*, 74(1):113–127, Apr 2014. ISSN 1573-0409. doi: 10.1007/s10846-013-9926-3. URL https://doi.org/10.1007/s10846-013-9926-3.

[56] Sarah Whittaker. Meet elios, the industrial drone for ship surveys inspired by insects, 2018. URL https://dronebelow.com/2018/03/20/elios-industrial-drone-inspired-by-insects/. [Online; accessed August 9, 2018].

[57] Dieter Schmalstieg and Tobias Höllerer. *Augmented Reality - Principles and Practice*. Addison-Wesley Professional, United States, 6 2016.

[58] Allianz Global Corporate & Specialty. Rise of the drones: Managing the unique risks associated with unmanned aircraft systems uas [white paper]. *N/A*, 2016. URL https://www.agcs.allianz.com/assets/PDFs/Reports/AGCS_Rise_of_the_drones_report.pdf.

[59] A. Spizhevoi and A. Rybnikov. *OpenCV 3 Computer Vision with Python Cookbook: Leverage the power of OpenCV 3 and Python to build computer vision applications*. Packt Publishing, 2018. ISBN 9781788478755. URL https://books.google.nl/books?id=TrZTDwAAQBAJ.

[60] Satoshi Suzuki and KeiichiA be. Topological structural analysis of digitized binary images by border following. *Computer Vision, Graphics, and Image Processing*, 30(1):32 – 46, 1985. ISSN 0734-189X. doi: https://doi.org/10.1016/0734-189X(85)90016-7. URL http://www.sciencedirect.com/science/article/pii/0734189X85900167.

[61] Richard Szeliski. *Computer Vision: Algorithms and Applications*. Springer-Verlag, Berlin, Heidelberg, 1st edition, 2010. ISBN 1848829345, 9781848829343.

[62] Tyler Cole. Shannon edge detector for grayscale images, 2015. URL https://nl.mathworks.com/matlabcentral/fileexchange/51124-shannon-edge-detector-for-grayscale-images. [Online; accessed September 19, 2018].

[63] Jun Wu, Jigui Zhu, Zhijing Yu, Jingchang Zhuge, and Bin Xue. A total station spatial positioning method based on rotary laser scanning and ultrasonic ranging. *Review of Scientific Instruments*, 87(11):115104, 2016. doi: 10.1063/1.4966982. URL https://aip.scitation.org/doi/abs/10.1063/1.4966982.

A

Predecessor systems

A.1. Concept 1: Total Station system

HMC proposes to install topsides unmanned by using high resolution optical ranging sensors or robotic 'Total Stations' tracking both the topside and jacket position simultaneously. The relative position of the topside with respect to the jacket will be visualized with XYZ-offsets from the topside stabbing cones towards the jacket legs. 360° prisms (fig. A.2) are installed on the jacket and topside in preparation for the unmanned topside installation. The system consists of six total stations (fig. A.2) and the Topside Installation Monitor (TIM) software (fig. A.1) produces real time Topside position and orientation to sub-centimetre accuracy. The TIM software is exclusively developed by DOF subsea. Prior to installation the six total stations are mounted on a suitable location on the installation vessel. Three Total Stations track three prisms on the jacket and three Total Stations track three prisms on the Topside. The information from the six Total Stations is transferred to the TIM software to calculate a relative position between the jacket legs and topside stabbing cones which is displayed real time during installation. The system configuration is visualized in figure B.1.

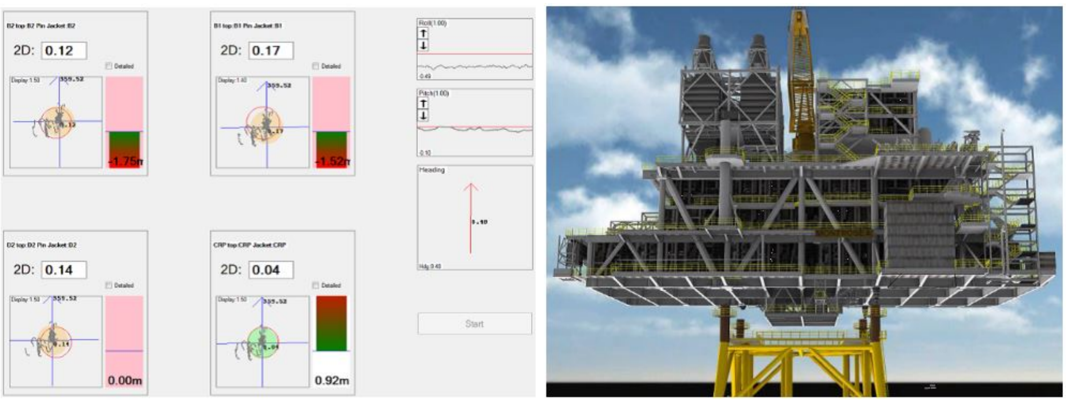

Figure A.1: Positioning information from the total station system displayed live in both 2D and 3D

In 2015, data was gathered on GodeWind and Flyndre to develop systems for live offshore testing. In spring 2016, live tests were carried out on Montrose and Clair Ridge with the Total station system. The second Clair Ridge topside (DPWM) was positioned using the total station system as the primary system. Banksmen were on the jacket and confirmed the position given by the system. Positive feedback on the total station system was received from superintendents on the Thialf for both projects.

Topside preparation To facilitate the installation of the topside a dimensional control survey of the topside needs to be carried out. The dimensional control survey is required in order to determine the position and alignment of the installation aids fitted to the structures. During the dimensional control

Figure A.2: Total Station and 360° prism

survey carried out at the fabrication yard utilizing a Total Station, the prism positions relative to the central reference point (CRP) and therefore the jacket legs are established. The topside CRP will be the geometric centre of the topside. The geometric centre is defined by the diagonal lines running between the centre of diagonally opposite topside legs. 360° prisms are installed on the topside. A dimension control survey is carried out utilizing a total station to determine the prism positions relative to the stabbing cones/topside columns. In figure A.3 an example of these prism locations is given. The XYZ offsets are determined relative to the topside CRP in a local coordinate system. Survey observations are put into a software tool called SC4W to return these offsets. The topside installation aids (360° prisms and u-bolt clamps) are not removed after the survey. The installation aids are marked and left fitted securely to the topside and will remain in place until after the topside has been installed offshore.

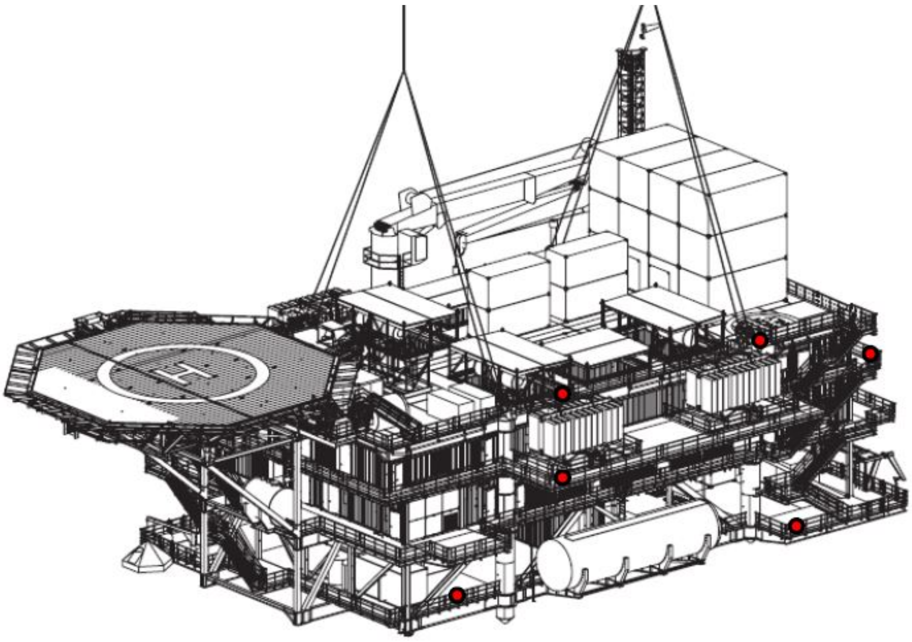

Figure A.3: Topside Prism Location Diagram

Jacket preparation In contrast to the topside, the prisms which are located on the jacket are installed offshore prior to the topside installation. The installation is carried simultaneously with the removal of the jacket leg covers. A survey team will have to install five 360° prisms with U-bolt clamps in the following locations of the jacket (fig. A.4):

- Two of the u-bolt prism clamps and 360° prisms will be installed on the jacket hand-rail

- Three of the u-bolt prism clamps and 360° prisms will be mounted on scaffold poles that extend outboard of the jacket by approximately two meters towards the SSCV

The three u-bolt prism clamps and 360° prisms mounted on scaffold poles will be outboard of the jacket to ensure that there is a line-of-sight between the total stations onboard the SSCV and the 360° prisms during the entire topside installation. It is noted that the topside overhangs the jacket during installation and set-down, and prisms mounted on the hand-rail would likely be obscured.

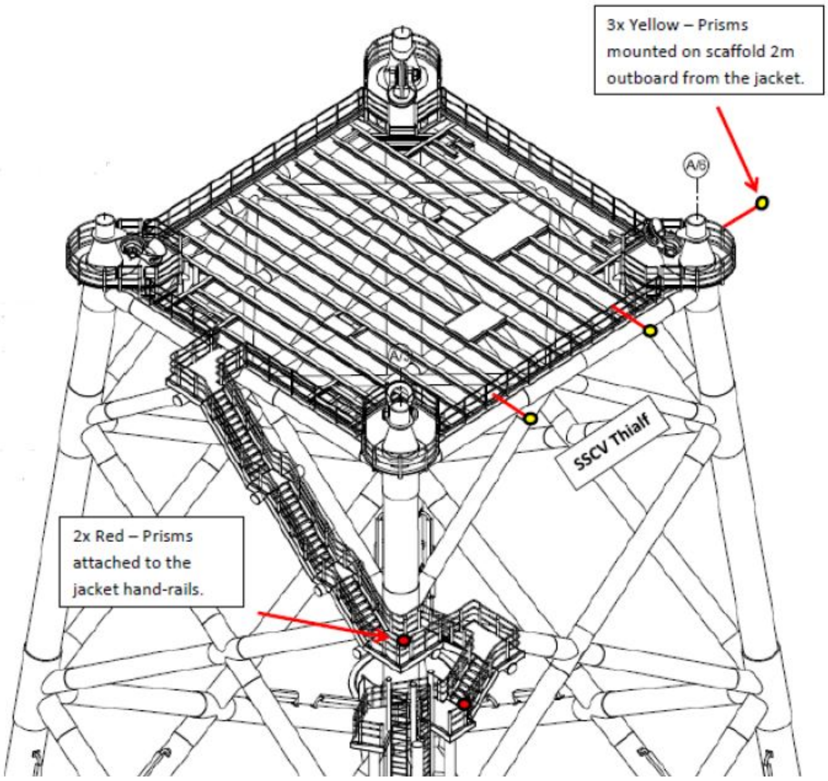

Figure A.4: Jacket Prism Location Diagram

Prior to the topside installation and on completion of the installation of the five 360° prisms onto the jacket the survey team will complete a dimensional control survey of the jacket. The dimensional control survey is required to determine the five 360° prisms XYZ offsets relative to the jacket and confirm the final XYZ offsets of the top of the jacket legs at the final cut-off height. The survey will be completed by means of a Total Station with the same principal of the topside survey. The survey team will set-up and configure the TIM software in the survey container on the back deck. On completion of the TIM software set-up and configuration in the container, the six total stations will be set-up and tested to ensure data is received and decoded by the TIM software. The final configuration, testing and quality control of the TIM software will take place after completion of the jacket dimensional control survey and the results are available for input to the TIM software.

A.1.1. Working principle

The positioning method of total stations is based on a three-dimensional coordinator measuring technology. A laser beam is launched to track a measured target point and then obtains the horizontal and vertical angles of the point through code discs or prisms. [63] When getting the slope distance between the point and the laser tracker via electronic distance measurement (EDM), the coordinates of the measured point can be solved. EDM units employ electromagnetic (EM) energy for measuring the slope distance to a target point. The precision ranges between sub-millimetre to sub-centimeter level. The EM signal will be reflected by any surface it meets. Only when the surface is perpendicular to the path will most of the signal reflect in the direction of the instrument. To overcome this issue a prism is used. A prism consists of multiple mirrors which reflect beams back in the direction of the source, but shifted (see figure A.5. The total station is equipped with an inbuilt microprocessor to process the observations. It can determine angles, horizontal distances and x,y,z, coordinates of the target point in a preferred Earth-related reference system. [42]

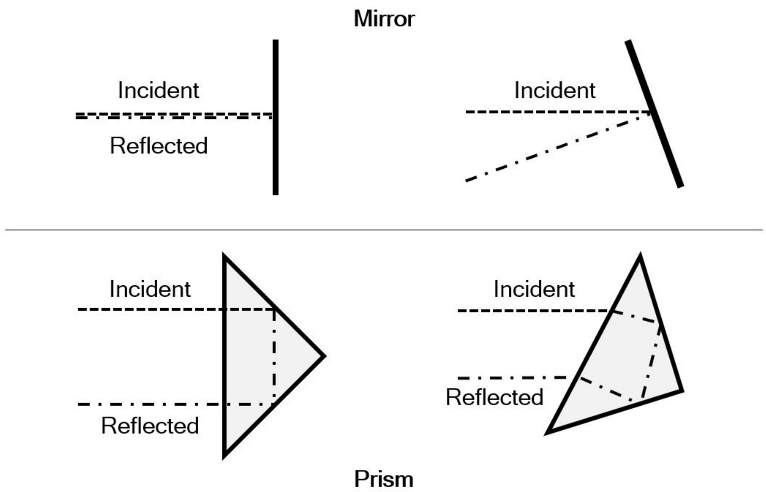

Figure A.5: Sketch illustrating how an EM beam reflects on a mirror and on a prism

A.2. Concept 2: Augmented reality system

The Augmented Reality (AR) system was under development from 2016 until 2018. The system was developed by TWNKLS, a Dutch company specialized in augmented reality applications. Augmented Reality is an interactive experience of a real-world environment whereby the objects that reside in the real-world are ”augmented” by computer-generated perceptual information. AR can match and track real world objects and project 3D predefined CAD drawings on top of it. This process should make it possible to use AR as a positioning tool to determine distances between objects. The tool that TWNKLS was developing for HMC should be able to recognize jacket and topside structures and match them with a 3D model.

The system consisted of using 2 cameras mounted on the stern of the SSCV to track the structures through the recognition of markers that are attached on them. Once the markers are recognized it is possible to perform calculations on distances through image recognition techniques. Figure A.6 shows a succesful recognition of the structure during a test at the fabrication yard. The green lines are rendered on top of the camera image as a virtual dimensioning.

The system comes with two interfaces: a Management Interface and a User Interface. The Management Interface is used to monitor the process and is displayed on a PC. It is used by an administrator and deals with the setup and control. The User Interface is the actual tool that provides information about the topside-jacket relative position. The User Interface is used by the (assistant) superintendent and will support him or her to give instructions to the crane operator and skipper to position the topside.

The Management Interface is used to initialize the matching process of a topside and a jacket real and virtual images. An administrator needs to manually assign points in the real world to points in the virtual world. These points are markers that are located on the real structure and their corresponding virtual marker. Once the system is correctly initialised, it will display a 2D real-time interface that provides information about distances, heights and rotations of the topside with respect to the jacket. The tool also graphically displays this information as a bulls-eye from above (fig. A.7).

The inner white circle indicates the jacket leg and the red dot the stabbing cone. The red dot is followed by a white track indicating the previous positions. The stabbing cones are correctly positioned when the red dot ends up in the middle of the white circle. The red dot then changes to a green dot. In addition to a visual display, the XYZ values are also given as numeric values. Finally, a 3D representation is also available at the bottom right of figure A.7.

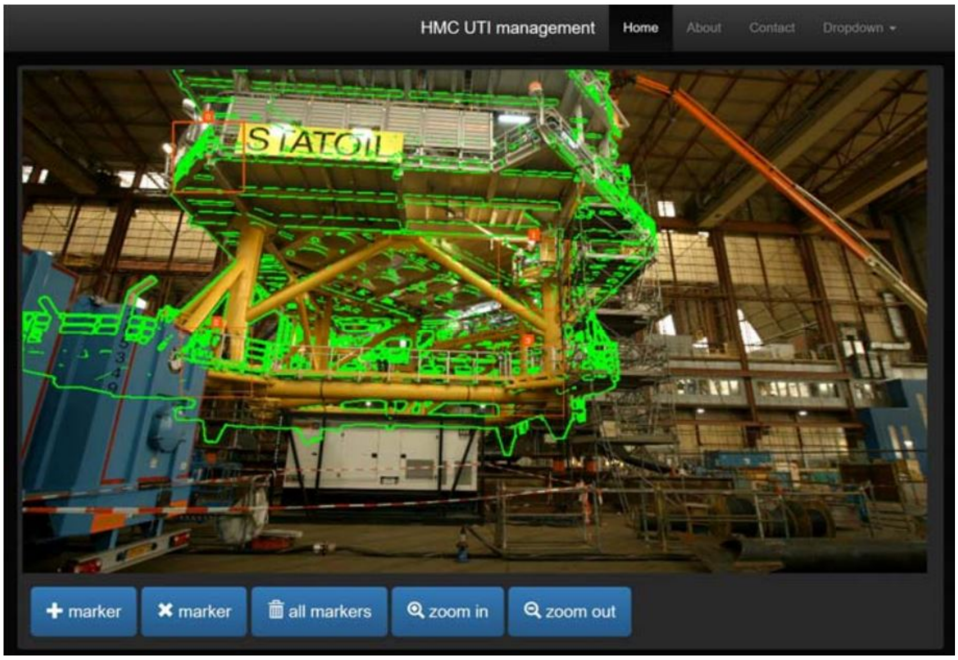

Figure A.6: Recognition of structure

Despite efforts by both HMC and TWNKLS, this system has unfortunately never functioned properly. After two years of development, it was decided to stop the project. Tracking in unprepared environments remains a challenge, and calibration of AR devices is still a complex process. The recognition of structures proved to be a difficult task in offshore conditions. During a test offshore on the Juniper project the system got confused by nice shadow lines on the jacket braces, and started tracking it instead of the actual edge of some braces. In addition, it was difficult to get the system accurate enough. The system had to be scaled by drawing the CAD drawings on the recognized structure. Due to deviating sizes between drawings and as-built reality, there were too many differences here.

A.3. System Comparison

In the process of engineering a new system it is useful to compare the predecessor systems. The predecessor systems can serve as a point of departure. It is the single richest source for information on the requirements for a new system. The users of the predecessor system are usually the best source of information of what is needed in a new system. A predecessor system will impact the development of a new system in three ways [41]:

- The deficiencies of the predecessor system are usually recognized, often being the driving force for the new development. This focuses attention on the most important performance capabilities and features that must be provided by the system.

- If the deficiencies are not so serious as to make the current system worthless, its overall concept and functional architecture may constitute the best starting point for exploring alternatives.

- To the extent that substantial portions of the current system perform their function satisfactorily and are not rendered obsolete by recent technology, great cost savings (and risk reduction) may be achieved by utilizing them with minimum change.

Given the above, the average system development will almost always be a hybrid, in that it will combine new and undemonstrated components and subsystems with previously engineered and proven ones. The predecessor systems are described in chapters A.1 and A.2. Both systems will be compared based on eight different system characteristics. These characteristics include: Main system components, accuracy, system initialization, ease-of-use, training, performance, costs, and user feedback.

Figure A.7: User Interface

The subjective value method was used to determine raw scores. This method begins with a judgment of the relative utility of each criterion on a scale of 1-5. Thus, 1 = poor, 2 = fair, 3 = satisfactory, 4 = good, and 5 = superior. A candidate that fails a criterion will be given a zero.

A.3.1. Main system components

The main system components required for the system to function give an indication of the complexity. A large number of different components indicates a more complex system.

’Total Station’ system The main components of this system are six Total Stations, at least 12 360° prisms (six are located on the jacket and six are located on the topside), a Topside Installation monitor, and some subsystem to connect all components together. These systems need to be installed by a subcontractor. Due to the large amount of components and the necessity of a subcontractor the ’Total Station’ system scores a 1 out of 5.

‘Augmented reality’ system The main components of this system consists of two 4K cameras, a prepared 3-D CAD model, a Management Interface, and a User Interface. Due to its simple setup this system scores 4 out of 5.

A.3.2. Accuracy

The accuracy of the system indicates how reliable the data obtained is. Because the system is used to make decisions about a very critical operation, good accuracy is desirable.

’Total Station’ system The accuracy of this system depends on the calibration of the prisms and the calibration of the Total Stations. The subcontractor responsible for the system givens an error budget for every installation. An example error budget for the Borkum Riffgrund project is given in figure B.2. The combined accuracy for position is 0,057m and for heading an attitude 0,036 degrees and 0,066 degrees respectively. This is very accurate for offshore operations and within the required accuracy as mentioned in chapter 2.1. Therefore, the system will score a 5 out of 5.

‘Augmented reality’ system There is no information available about the accuracy of the ’Augmented Reality’ system. The system therefore scores a 0 but this is indicated with a dashed line in the spider diagram.

A.3.3. System Initialization

System initialization indicates which preparation is required for it to function. Ideally, as much as possible should be prepared onshore because offshore activities are very dependent on weather conditions. Preparations that are necessary for the system should not delay the operation.

’Total Station’ system This system requires the 360° prisms to be installed and calibrated correctly. Installation on the topside is usually done at the yard prior to transit. Installation and calibration is done by the subcontractor. Installation on the jacket is usually done offshore. In most cases the jacket is already installed a couple months prior to the topside installation. It is therefore not always possible to install the prisms at the construction yard of the jacket. The positions of the prisms are determined in the local coordinate system of the structure were they are installed on. These locations need to be inserted into the software tool in order to calculate the relative positions between the topside and the jacket. Next to the prisms also the Total Stations have to be installed on the stern of the SSCV. Final step is to connect all the Total Stations and start tracking the prisms. Because there are quite a number of steps involved at different locations and different times this system scores a 2 out of 5.

‘Augmented reality’ system This system uses a 3D CAD model to extract information about relative positions. This CAD model has to match the as-built dimensions of the structures. The CAD model is usually a very detailed drawing and therefore increases the required computational power and slows down the update frequency. The CAD model need to be simplified in order to speed up this process. In order to increase accuracy it is necessary that the dimensions do not deviate too much from the as-built situation. In reality, these dimensions will never exactly match. It is therefore necessary to have some primary components that are important for the correct recognition of the structure being re-measured in order to increase the accuracy. It can also happen that some parts off the topside are not specified on the drawing (scaffolding for instance). If this is the case, final corrections to the model need to be made offshore prior to installation. Because the preparation of the CAD model and the measuring of important components can be a time consuming process, this system scores a 3 out of 5.

A.3.4. Ease-of-use

The superintendent is provided with a tablet which displays information about the offsets of all 4 stabbing cones. A 2D graphical interface shows a bulls-eye to track the stabbing cone above the jacket lag. A second interface shows the 3D representation with the possibility to zoom in and rotate the scene. The interface of both systems are almost the same. Superintendents and other users of the system were satisfied with the information provided by the system. Therefore both systems score a 4 out of 5.

A.3.5. Training

HMC has at its own simulation center where the situation on the vessel can be simulated in detail. Important components such as the bridge and crane cabins are reconstructed 1-to-1. Prior to an offshore topside installation the vessel management team is trained to carry out the process. Integrating the topside installation monitor would be a very useful addition to familiarize the crew with the operation and controls of the system.

’Total Station’ system At this moment the users of the system are provided with a user manual and a training from the subcontractor. The system is not yet implemented in the simulation centre. Therefore, the only option to test the system is during real offshore topside installations.

‘Augmented reality’ system Users of the system are provided with a user manual and a training from the subcontractor. Plans were made to see if the system was able to track structures from rendered images in the simulation centre but this was never tested because the project was stopped. Because both systems are not integrated with the simulation center, they score a 2 on the scale of 5.

A.3.6. Performance

The performance of the system is understood in which weather conditions it can be used, what the redundancy is in the case of (sub) system failure and what other limiting factors can be.

’Total Station’ system This system tracks six prisms with six Total Stations. There are twelve prisms in total which can be tracked. This means that six prisms can be used as a back-up in case a prism can’t be detected. In addition, there is one spare Total Station in case of failure. The system has already been used as a primary system during Unmanned Topside Installations. Feedback from the users is positive. Fog and tugger lines can cause disturbances in the detection of the prisms. The Total Stations need to be accessible to make adjustments to the settings. In some cases it is desirable to lower the total stations from the stern of the SSCV to increase line of sight on the jacket. This is not possible as the total stations cannot be operated remotely. Rain and poor lighting conditions (night) seem to have no big influence on the performance of the system. This system therefore scores a 3 out of 5.

‘Augmented reality’ system The system was tested twice in offshore conditions and did not provide accurate results. The system got confused by nice shadow lines, and started tracking it instead of the actual edge of some braces. During another test it was too dark for the system to track enough objects. Based on these results the system in its current state scores a 1 out of 5.

A.3.7. Costs

Since competition in the offshore Oil&Gas sector is increasing. The costs will have to be kept to a minimum. It must be stated that unmanned topside installation can also have economic benefits. If there is no need to bring crew to the jacket there is also no need for a rescue vessel in the vicinity (during the operation if personnel cannot be reached by crane). Also the number of access ladders on the jacket can be reduced. This will imposes savings for the client in jacket installation aids related to access from sea. [19]

’Total Station’ system Subcontractor is needed in order to install and calibrate the prisms and to install the complete set-up. Total costs are around $ 75K - $ 100K per installation. In most cases access to the jacket is still necessary. Proposed savings due to reduction of access ladders can therefore not be made. The system therefore scores a 2 out of 5.

’Augmented Reality’ system The development costs were around $ 700K. Costs per installation should be significantly less than the ‘Total Station’ system but no accurate estimates are available. [19] Also, a specialized engineer need to prepare the 3D-CAD model. This can take up quit some time. But total costs are expected to be less than for the ’Total Station’ system. Therefore this system scores 1 point better than the other system.

A.3.8. User feedback

Ultimately, everything is related to the attitude of the users towards a certain system. When trust or interest is lacking, this can have major consequences for the implementation of a system.

’Total Station’ system Superintendents are satisfied with the system but they expressed that a visual system is needed for contingency. The main drawback of the system is its complexity and the need of calibrating all prisms. The overall user experience is considered as ’good’ and therefore scores a 3 out of 5. [17]

’Augmented Reality’ system Superintendents are interested in the system. Edge tracking seems too difficult to use in an offshore environment. Scaling problems resulted in inaccurate results. Nevertheless were the superintendents willing to use the system if these problems could be overcome. [17] It is also very clear to sea what is happening since calculations are based on visual information. Therefore, this systems scores 1 point better: 4 out of 5.

B

Total Station System lay-out and accuracies

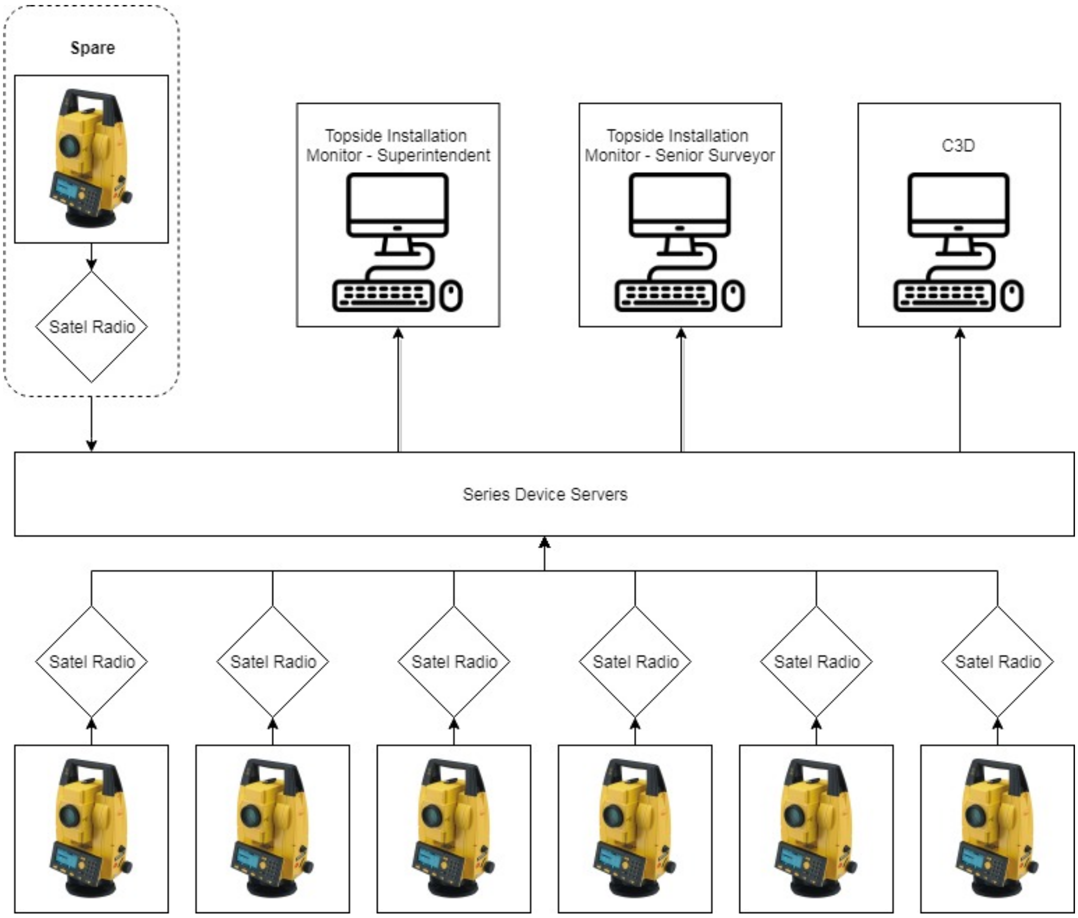

Figure B.1: Total Station system configuration

Typical Position Standard Deviation of the Moving Structure - Borkum Riffgrund Topside				
Description	**Equipment**	**σ (68.3%)**	**2σ (95%)**	**3σ (99%)**
X [m]	UTI System	0.006m	0.012m	0.015m
Y [m]	UTI System	0.018m	0.035m	0.046m
Z [m]	UTI System	0.011m	0.022m	0.028m
Typical Position Standard Deviation of the Fixed Structure - Borkum Riffgrund Jacket				
Description	**Equipment**	**σ (68.3%)**	**2σ (95%)**	**3σ (99%)**
X [m]	UTI System	0.002m	0.004m	0.005m
Y [m]	UTI System	0.003m	0.006m	0.008m
Z [m]	UTI System	0.002m	0.004m	0.005m
Typical Position Standard Deviation of the Fixed & Moving Structure - Borkum Riffgrund Jacket				
Description	**Equipment**	**σ (68.3%)**	**2σ (95%)**	**3σ (99%)**
Combined 3D Position [m]	UTI System	0.022m	0.044m	0.057m
Typical Heading Standard Deviation of the Fixed & Moving Structures - Borkum Riffgrund Jacket & Topside				
Description	**Equipment**	**σ (68.3%)**	**2σ (95%)**	**3σ (99%)**
Prism baseline of 20m [D.ddd°]	UTI System	0.014°	0.027°	0.036°
Typical Pitch Standard Deviation of the Fixed & Moving Structures - Borkum Riffgrund Jacket & Topside				
Description	**Equipment**	**σ (68.3%)**	**2σ (95%)**	**3σ (99%)**
Prism baseline of 20m [D.ddd°]	UTI System	0.014°	0.027°	0.036°
Typical Roll Standard Deviation of the Fixed & Moving Structures - Borkum Riffgrund Jacket & Topside				
Description	**Equipment**	**σ (68.3%)**	**2σ (95%)**	**3σ (99%)**
Prism baseline of 15m [D.ddd°]	UTI System	0.022°	0.043°	0.056°
Typical Attitude Standard Deviation of the Fixed & Moving Structures - Borkum Riffgrund Jacket & Topside				
Description	**Equipment**	**σ (68.3%)**	**2σ (95%)**	**3σ (99%)**
Combined Pitch & Roll [D.ddd°]	UTI System	0.026°	0.051°	0.066°
Position [m]		**0.022m**	**0.044m**	**0.057m**
Heading [D.ddd°]		**0.014°**	**0.027°**	**0.036°**
Attitude [D.ddd°]		**0.026°**	**0.051°**	**0.066°**

Figure B.2: Total Station Topside Installation Error Budget [24]

C

Drone Specifications

C.1. Aerial system requirements

In addition to requirements on the positioning system, the drone itself will also have to meet a number of requirements. For example, the use of drones will have to comply with local and national regulations. In addition, the use of such a system must comply with the safety guidelines of the customer and HMC itself. The mission type obviously determines the measurement procedure to be completed (in terms of flight type, sensing payload and measurements to take). Payload is defined as all the elements of a drone that are not necessary for flight but are carried for the purpose of fulfilling specific mission objectives. All these applications need tools to accelerate and partially automate the creation of missions, the calculation of the optimal trajectories and the automatic execution of parts of the mission with the least human intervention, in order to obtain cost effective solutions. In addition to the requirements related to the positioning, requirements will also have to be imposed on the aerial platform. These requirements can be subdivided on the basis of safety, operability, and acquisition, review, and security of data. [3]

Safety requirements In terms of safety, the following requirements will be set:

- The drone and any onboard modules should be rated for its intended operational (offshore) environment (e.g., intrinsically safe in hazardous areas, operational wind speed, temperature, humidity, etc.)
- The drone should have critical component redundancy in the case of a malfunction or failure
- The drone should have multiple operational modes (e.g. GPS mode, height mode and manual mode) in the case of a malfunction or failure
- Fatique Management Program: It is recommended that the daily operating time for each pilot is limited to eight hours, and the continuous operating time for each task is limited to three hours

Operational requirements With respect to operability the following requirements should be considered:

- The drone has a control system that allows the pilot to easily operate the drone
- The drone has onboard flight control modules that allows for the maintenance of stable and accurate positions
- The drone has onboard localization and navigation modules (e.g. GPS for outdoor activities)
- The drone is able to operate for a sufficient amount of time relevant to the operation being conducted

- The maximum operating range of the drone should be accurately defined (e.g. in terms of flight height, distance from the pilot)
- Dimensions of the drone allows for access and navigation within the intended space (size of the landing site and structural limitations)
- The drone should provide and maintain an interference-resistant communication channel
- The system should include reliable connectivity equipment to maintain constant communication amongst all personnel involved during operations

Data requirements There are also requirements in terms of acquisition, review and security of data:

- Integrity of the raw data should be maintained during the data storage process
- The raw data and related metadata should be stored separately from any post-processed data
- The drone has an onboard camera that provides adequate visual quality of still images, live-stream videos, and recorded videos. It is recommended the drone camera possess a High-Definition (HD) resolution
- The drone system should include an appropriate platform to display and replay visual data including still images, live-stream videos, and recorded videos
- All frequencies used to support safety-critical drone functionality should be coordinated and reported to the vessel captain
- There should be data security policies and procedures in place for verification that data collected during the operation and any data analyses are captured, transmitted, and stored in a secure way that has a minimum vulnerability to unauthorized manipulation and distribution

C.2. Selecting an aerial platform

In this chapter chapter the functional and physical characteristics of the aerial platform will be defined. It is proposed to meet the operational need defined in the preceding chapters. The decisions in the process of concept definition center on the selection of a particular system configuration or concept and the definition of the functions it is to perform. The decisions will be made by a structured process that considers the relative merit of a number of alternatives before any one is selected. This process is called ”trade-off-analysis” and is used in decision making process throughout system development. The objective of trade-off studies is to assess the relative ”goodness” of alternative system concepts with respect to operational performance, cost and risk.

Three different types of drones where introduced. A performance evaluation of these types of drones can be carried out from the following six factors:

- **Ease-of-use** Driving a multicopter is the simplest because it is able to land and take off vertically. In addition, the multicopter is also able to remain in a fixed position. The controller consists of only two joysticks with which all movements can be controlled. This makes the operation of the multicopter very simple. In general, an adult would be able to control this within a few hours. The controller parameters can also be easily set so that it is possible to adjust the reaction speed. The difficulty in controlling a helicopter lies in strongly coupled modes and highly nonlinear dynamics. These also make the autopilot design difficult. Moreover, it is hard to tune the controller parameters. The flying operation of a fixed-wing aircraft needs to be performed in a large air space. Since it cannot stay still in the air, the remote pilots have to perform the control actions frequently. For model helicopters and model airplanes, both of them will cost users a long time to learn to operate and control. Based on the analysis above, the multicopter has the best ease-of-use performance.
- **Reliability** The multicopter has a high reliability when it comes to the mechanical structure. In contrast to the fixed-wing aircraft and the helicopter, the multicopter has no rotating joints. As a result, there is virtually no mechanical wear.

- **Maintainability** Multicopters are easiest to maintain. They have a simple structure and can therefore easily be put together. Conversely, both fixed-wing aircraft and helicopters have more components and complex structures. As a result, their assembly is not easy.
- **Endurance and payload** The energy conversion efficiency of multicopters is the lowest. So their flight time and payload capacity do not have any advantages compared with the fixed-wing aircraft and helicopters. Their overall performances are shown in Table C.1.

	Fixed wing	Rotor wing	Multicopter
Ease-of-use	++	+	+++
Reliability	++	+	+++
Maintainability	++	+	+++
Time of endurance	+++	++	+
Maintain position	-	++	+++
Payload capacity	++	+++	+

Table C.1: Comparisons of three types of small aircraft (More “+” implies better)

Table C.1 shows that in terms of ease-of-use, reliability, positioning, and maintainability the multicopter outperforms the helicopter and the fixed-wing aircraft. On the other hand, the multicopter has some disadvantages in terms of time of endurance and payload capacity. But these factors can be comprised or even sacrificed. For example, the time of endurance can be extended by swapping batteries during operations. Multicopters are favored above other competitors in terms of user experience. With the development in battery technology, materials, and electric motors the time of endurance and payload capacity will be both improved.

C.2.1. Current industrial multicopters

This chapter will provide some insight in the currently available industrial drones. A total of 5 different professional drones were investigated (see figure C.1 and table C.8) to compare their suitability for the use in an offshore environment.

Figure C.1: Selction of five currently existing professional drones

To efficiently select a drone, the following considerations were studied.

1. **Flying time over 20 min:** longer flying times allows for a more efficient and comprehensive flight plan as it minimizes interruptions to change the drone batteries.

2. **Camera resolution with low illumination:** due to lack of illumination during dusk, dawn, and night the drone camera must be able to capture high-resolution images under low illumination. It can be noted that the illumination can be enhanced by additional flashlights either attached to the drone or on the topside or SSCV itself.

3. **Streaming quality:** the drone must be able to record and stream high-quality videos to perform video-based analyses. Either by a computer or by a human.

4. **Payload capacity:** payload is important as it allows the drone to carry additional attachments such as flashlights, cameras or sensors if needed.

5. **Remote range:** The helideck is located at the bow of the vessel whilst the cranes are located at the aft of the vessel. Therefore, a long-range remote control is required. Interference from metal structures and radio interference from VHF antennas must also be taken into account.

6. **Weather conditions:** The drone will operate in tough offshore conditions and should therefore be able to continue flight in rain and in wind conditions up to 30 knots.

From these five selected professional drones the DJI Inspire 1 must actually be classified as a consumer drone. All vessels of HMC are already equipped with this drone for filming and photography purposes. It is added to the list to compare it with the other considered drones. All drones are ready to fly (RTF) out of the box.

Flying time The flight time depends mainly on the battery capacity and the weight of the drone. Every gram you save is a few extra seconds in the air. A more powerful battery will also result in extra weight, its a constant trade-off in the design process. The maximum flight times are presented in table C.2.

	DJI	**ALTURA**	**Intel**	**DJI**	**DJI**
	M210 RTK	ZENITH ATX8	Falcon 8+	Phantom 4 RTK	Inspire Z3
Max flight time (min)	35	35	16-26	30	22
Batteries					
Amount	2	1	2	1	1
Capacity (mAh)	7660	20000	4000	5870	4500
Voltage (V)	22.8	22.2	14.8	15.2	22.2
Type	LiPo 6S	LiPo	LiPo	LiPo 4S	LiPo 6S

Table C.2: Max flight time and battery specifications

Camera The DJI drones come with their integrated camera and 3-axis gimbals. The drones from Altura, Intel, and Microdrones can be equipped with different camera's from third parties. There are some considerations to use a drone that comes with a built-in camera or supports and add-on camera. The pros of a drone with an integrated camera include:

- **Ease-of-use:** A drone with a built-in camera does not require much setup or configuring beyond chargin batteries and plugging in a storage device like a USB drive or SD card.

- **Flight-sepcific filming features:** Drones with integrated cameras typically have advanced features like object tracking and visual navigation.

- **Lightweight:** Built-in cameras often require no extra battery or processor but can use the power supply and computing power from the drone.

The cons of a drone with an integrated camera include:

- **No different lenses:** in most cases it won't be possible to change the camera lens. This could be useful for some operations. Most drones are equipped with a wide-angle camera. In some cases, a zoom lens might be more convenient.

- **Battery life:** Integrated cameras typically feed off of the main battery. Adding additional batteries will add additional weight and thus reduce fly times.

The different camera specifications are listed in table C.3.

	DJI	**ALTURA**	**Intel**	**DJI**	**DJI**
	M210 RTK	ZENITH ATX8	Falcon 8+	Phantom 4 RTK	Inspire Z3
Camera model	DJI X5S	Sony Alpha 7R	Sony Alpha 7R	DJI 1”	DJI X3
Sensor	M 4/3	Full-frame	Full-frame	1” CMOS	1/2.3” CMOS
Focal length	9mm-45mm	35mm	35mm	24mm	20mm
Megapixels	20.8	36	36	20	12.4
Streaming quality	1080p	1080p	1080p	1080p	720p

Table C.3: Camera specifications

It must be stated that the Phantom 4 RTK a special lens distortion recording process. Each Pahntom 4 RTK camera goed through a calibration process that measures the distortions of the lens, and records the corresponding OPEN-CV parameters. This can be very useful if the camera must be used for computer vision purposes.

Payload capacity The payload capacity is mainly influenced by the propeller size and the power output of the electric motors. Payload capacity might be an important factor if additional sensors need to be installed on the drone. The different payload specifications are listed in table C.4.

	DJI	**ALTURA**	**Intel**	**DJI**	**DJI**
	M210 RTK	ZENITH ATX8	Falcon 8+	Phantom 4 RTK	Inspire Z3
Weight (kg)	4.42	6.65	1.2	1.39	3.06
Max take-off weight (kg)	6.14	9.65	2.8	1.39	3.5
Max payload (kg)	0.99	3	0.8	0	0.4

Table C.4: Payload specifications

Remote range The remote range for controlling function and video link as well as the used frequencies are shown in table C.5. The effective transmission distance depends on the method of operation (such as the antenna position) and actual flight environment. The maximum distances are based on an unobscured environment.

	DJI	**ALTURA**	**Intel**	**DJI**	**DJI**
	M210 RTK	ZENITH ATX8	Falcon 8+	Phantom 4 RTK	Inspire Z3
Controller frequency	2.4 GHz; 5.8 GHz	2.4 GHz	2.4 GHz	2.4 GHz	2.4 GHz; 5.8 GHz
Video frequency	2.4 GHz; 5.8 GHz	5.1 - 5.8 GHz	5.1 GHz	2.4 GHz	2.4 GHz; 5.8 GHz
Video link range (km)	7	1	0.5	7	5
Controller range (km)	7	18	1	7	5

Table C.5: Remote range and frequency specification

Weather conditions The weather requirement is that the drone can operate in rain and with wind speeds up to 30 knots (15.43 m/s). The IP Code consists of the letters IP followed by two digits. It classifies the degrees of protection provided against the intrusion of solid objects (including body parts like hands and fingers), dust, accidental contact, and water in electrical enclosures. The standard aims to provide users more detailed information than vague marketing terms such as waterproof. The IP numbers are further explained in table C.6. The overall weather specifications are listed in table C.7.

IP Number	First digit (Solids)	Second digit (Liquids)
IP43	Protected from tools and small wires greater than 1 millimeter.	Protected from water spray less than 60 degrees from vertical.
IP55	Protected from limited dust ingress.	Protected from low pressure water jets from any direction.

Table C.6: IP Classifications

	DJI	**ALTURA**	**Intel**	**DJI**	**DJI**
	M210 RTK	ZENITH ATX8	Falcon 8+	Phantom 4 RTK	Inspire Z3
Max wind (m/s)	12	16	12	12	10
Weather	Dry to light rain or snowfall	Dry to light rain or snowfall	Dry	Dry	Dry
Rating	IP43	IP55	N/A	N/A	N/A
Operating temperature (Celsius)	-20° to 45° C	-5° to 40° C	-5° to 40° C	0° to 40° C	-10° to 40° C

Table C.7: Weather conditions

C.2.2. Real-time Kinematic (RTK)

Two drones from DJI have the term RTK behind their name. RTK stands for Real-Time Kinematic. It is a positioning and navigation system that offers precise centimetre accuracy for drones. It uses GPS and GLONASS or GPS and BeiDou, dependent on the region, and a ground station to achieve RTK results. It is an addition to the usual GPS system that ensures the position determination of a drone. The RTK system on the aircraft communicates with the ground station and satellites to provide the exact real-time location of the aircraft which will stay up to date during the flight (see figure C.2). The ground system's location must be updated every time it is moved in order to give the required results and cannot be moved if the aircraft is in the air. It could be positioned on a fixed structure such as a jacket, monopile, or other fixed offshore structure. Thanks to an extra GPS receiver the drone will receive a correction signal, which not only greatly improves the positioning accuracy, but also makes the drone no longer dependent on the digital compass for determining orientation. The key benefit of a drone using RTK is the pinpoint accuracy during flight. The drone know it's specific location at all times resulting in exact hovering, even during high winds. It allows pilots to operate in small spaces and close to objects. Further to the centimetre accuracy, the RTK provides protection from interference from radio frequency (RF) and electromagnetic fields (EMF). Interference of this kind may occur when flying close to the vessels radar, antennas and large metal structures. Interference from RF and EMF can cause a loss of GPS, resulting in the drone entering ATTI mode. ATTI mode can cause significant disruption to the flight and could result in a flyaway or crash. Another useful feature of RTK is the accurate geotagging of the information the drone captures. This includes both images and video which will be tagged with precise location for post-processing purposes. To summarize, having a drone with built-in RTK has special benefits for offshore users. Not only is the drone more accurate in vertical and horizontal flight whilst moving and hovering, it can also go in areas that would previously have interfered with a drone.

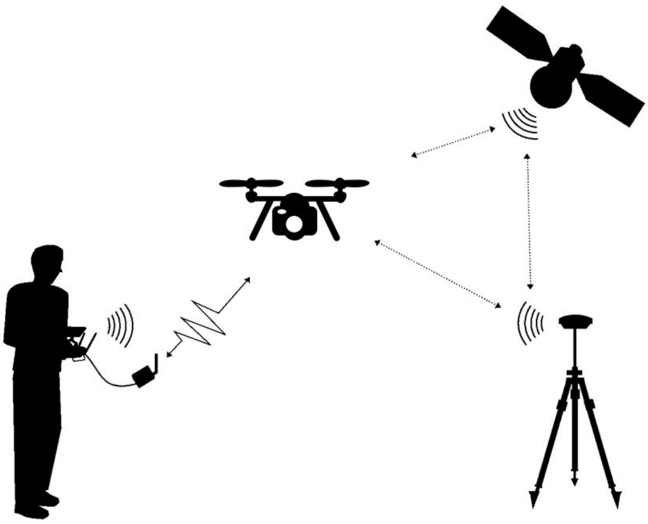

Figure C.2: RTK Explained

C.2.3. Lightbridge

The DJI Lightbridge 2 has been designed to meet the requirements of professional broadcasting at high frame rates and HD clarity. USB, mini-HDMI and 3G-SDI ports support video output at up to 1080p/60fps. Total latency has been significantly reduced to as low as 50ms. Lightbridge 2 is intelligent. It automatically adapts in real time to keep latency low while maintaining a strong signal. For uninterrupted transmission, a high-speed processor chooses the best channel and bandwidth based on current distance and electromagnetic environment. [23]

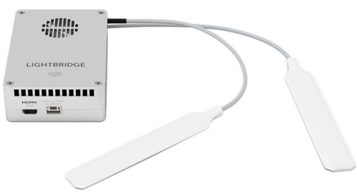

Figure C.3: DJI Lightbridge 2

C.2.4. Overview

Brand	**DJI**	**ALTURA**	**Intel**	**Microdrones**	**DJI**
Model	**M210 RTK**	**ZENITH ATX8**	**Falcon 8+**	**md4-1000**	**Inspire Z3**
Dimensions					
Height (mm)	408	470-570	160		
Width (mm)	887	600	768	1030	581
Length (mm)	880	600	817	1030	581
Weight (kg)	4.42	6.65	1.2	2.65	3.06
Max take-off weight (kg)	6.14	9.65	2.8	6	3.5
Max payload (kg)	0.99	3	0.8	1.2	
Flight Time					
Max flight time (min)	24-32	40	16-26	45	22
Batteries					
Amount	2	1	2	1	1
Capacity (mAh)	7660	20000	4000	13000	4500
Voltage (V)	22.8	22.2	14.8	22.2	22.2
Type	LiPo 6S	LiPo	LiPo	LiPo 6S2P	LiPo 6S
Flight Performance					
Max speed	82.8 kph	72 kph	65 kph	43 kph	79 kph
Power plant	4x brushless electric motor	8x brushless electric motor	8x brushless electric motor		4x brushless electric motor
Propellers	4x 17 inch	8x 17 inch	8x 8 inch		4x 13 inch
Collision avoidance	YES	YES	NO	NO	YES
Hovering accuracy					
Vertical (m)	0.1 (RTK enabled)	?	2-5		0.5
Horizontal (m)	0.1 (RTK enabled)	?	1-3		2.5
Weather Conditions					
Max wind speed in GPS mode (m/s)	12	16	12	12	10
Weather	Dry to light rain or snowfall	Dry to light rain or snowfall	Dry	Dry to light rain or snowfall	Dry
Rating	IP43	IP55	N/A		
Operating temperature (Celsius)	-20° to 45° C		-5° to 40° C	-5° to 40° C	-10° to 40° C
Frequencies					
Controller	2.400-2.483 GHz; 5.725-5.825 GHz	2.4 GHz	2.4 GHz		2.400-2.483 GHz; 5.725-5.825 GHz
Video frequency	2.400-2.483 GHz; 5.725-5.825 GHz	5.1 - 5.8 GHz	5.1 GHz		2.400-2.483 GHz; 5.725-5.825 GHz
Video link range (km)	7	1	0.5		5
Controller range (km)	7	18	1		5
Camera					
Model	X5S	Sony Alpha 7R	Sony Alpha 7R	Sony Alpha 7R	X3
Sensor	M 4/3	Full-frame	Full-frame	Full-frame	1/2.3” CMOS
Focal length	9mm-45mm	35mm	35mm	35mm	20mm
Megapixels	20.8	36	36	36	12.4
Streaming quality	1080p	1080p	1080p	1080p	720p

Table C.8: Comparison of identified drone specifications

D

Rodrigues' rotation formula

To got the relative position from a marker in the world coordinate system to a marker in another coordinate system there is a need to rotate points or objects by certain angle around a given axis. One way to do it is to use Rodrigues' rotation formula.

$$\mathbf{R} = \mathbf{I} + [\vec{n}]_{\times} sin(\alpha) + [\vec{n}]_{\times}^{2}(1 - cos(\alpha)) \tag{D.1}$$

Where $[n]_x$ is a skew symmetric of normalized vector of the rotation axis and α is the rotation angle in radians. The result is a 3x3 rotation matrix R. In general, the most basic way of representing a rotation are Euler Angles. Any rotation in space is represented by three 2D rotations in planes xy, yz, and xz as shown in equation D.2.

$$\mathbf{A} = \begin{pmatrix} cos\phi & sin\phi & 0 \\ -sin\phi & cos\phi & 0 \\ 0 & 0 & 1 \end{pmatrix}, \mathbf{B} = \begin{pmatrix} 1 & 0 & 0 \\ 0 & cos\theta & sin\theta \\ 0 & -sin\theta & cos\theta \end{pmatrix}, \mathbf{C} = \begin{pmatrix} cos\theta & 0 & -sin\theta \\ 0 & 1 & 0 \\ sin\theta & 0 & cos\theta \end{pmatrix} \tag{D.2}$$

The rotation matrix is a product of the three discrete 2D rotations: $R = ABC$. In computer vision algorithms the Euler Angles rotation is not really practical. Rotation is not smooth (small changes in position can result in dramatic change of one or more Euler Angles). The use of angle axis rotations can solve this problem. There is now a proof of the formula in equation D.1 on the basis of a short example. Here, a point V is rotated about axis $\vec{n}$ at a given angle α to the final position U as can be seen in figure D.1.

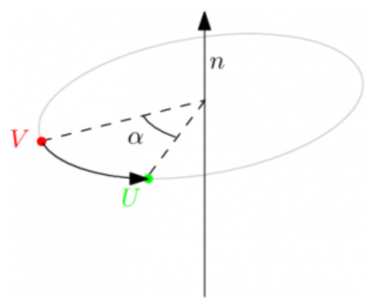

Figure D.1: Point V rotated with angle α around axis $\vec{n}$

A vector $\vec{v}$ is defined from the origin to the point V and a plane in the origin perpendicular to the axis of rotation $\vec{n}$. The vector representing the axis of rotation is also normalized so that $|\vec{n}| = 1$ (fig. D.2a).

The next step is to project the vector $\vec{v}$ on the axis of rotation and also on the plane in the origin. The vector projected on the axis of rotation is called $\vec{v_p}$. It is calculated as:

$$\vec{v_p} = (\vec{n} \cdot \vec{v})\vec{n} \tag{D.3}$$

Vector $\vec{v_r}$ is obtained by simply subtracting $\vec{v_p}$ from $\vec{v}$. This vector is called the vector rejection:

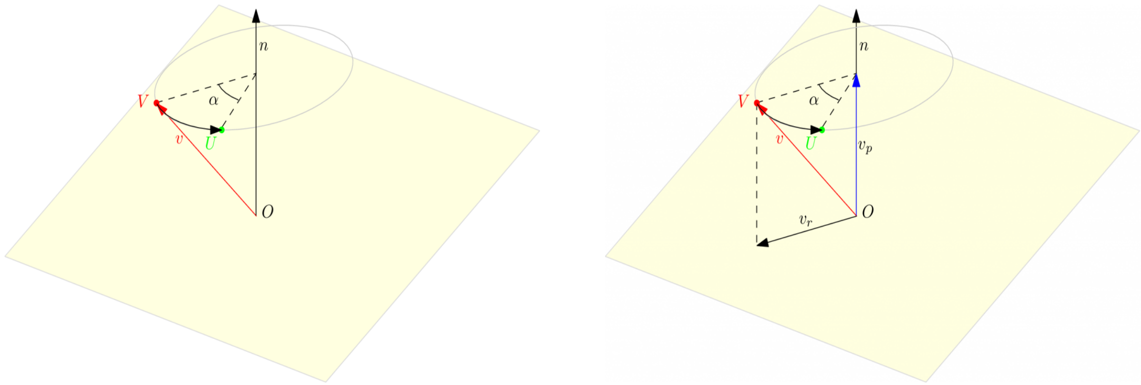

(a) Vector $\vec{v}$ from origin to point V

(b) Projection vector $\vec{v_p}$ and rejection vector $\vec{v_r}$

Figure D.2: Introducing vector projection

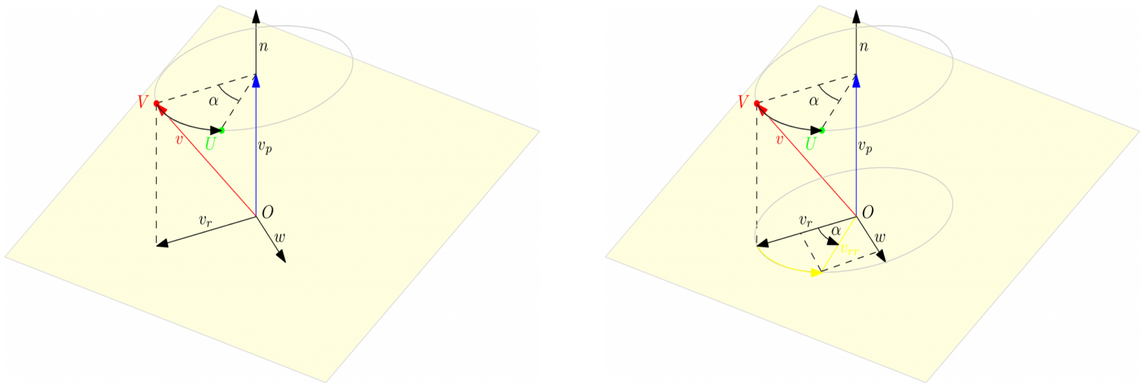

(a) Vector $\vec{w}$ perpendicular to $\vec{v}$ and $\vec{v_p}$

(b) 2D rotation, vector $\vec{v_{rr}}$

Figure D.3: 2D rotation of vector $\vec{v_r}$

$$\vec{v_r} = \vec{v} - \vec{v_p} \tag{D.4}$$

Then, a vector $\vec{w}$ is created which is perpendicular to $\vec{v}$ and $\vec{v_p}$. This vector will be used to rotate $\vec{v_r}$ by the anlge α on the plane in the origin:

$$\vec{w} = \vec{n} \times \vec{v} \tag{D.5}$$

The cross product between unit vector $\vec{n}$ and the vector $\vec{v}$ has the same length as the vector rejection $\vec{v_r}$ (fig. D.3a).

A 2D rotation of the vector $\vec{v_r}$ is performed in the plane $\vec{v_r}, \vec{w}$. This new vector is called $\vec{v_{rr}}$:

$$\vec{v_{rr}} = \vec{v_r} cos(\alpha) + \vec{w} sin(\alpha) \tag{D.6}$$

The last step consists of summing vectors $\vec{v_{rr}}$ and $\vec{v_p}$. This is needed to get from the plane in the origin to the point U.

$$\vec{u} = \vec{v_{rr}} + \vec{v_p} \tag{D.7}$$

If equations D.3, D.4, D.5, and D.6 are substituted in equation D.7 the following result is obtained:

$$\vec{u} = (\vec{v} - (\vec{n} \cdot \vec{v})\vec{n}) cos(\alpha) + (\vec{n} \times \vec{v}) sin(\alpha) + (\vec{n} \cdot \vec{v})\vec{n}$$
$$\vec{u} = \vec{v} cos(\alpha) - (\vec{n} \cdot \vec{v})\vec{n} cos(\alpha) + (\vec{n} \times \vec{v}) sin(\alpha) + (\vec{n} \cdot \vec{v})\vec{n}$$
$$\vec{u} = \vec{v} cos(\alpha) + (\vec{n} \cdot \vec{v})\vec{n}(1 - cos(\alpha)) + (\vec{n} \times \vec{v}) sin(\alpha)$$

This result can be simplified by converting the dot and cross products to multiplications. Given the fact that all vectors are column vectors the dot product can be calculated as:

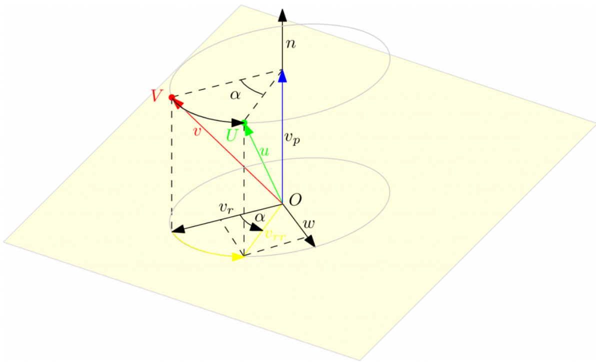

Figure D.4: Vector $\vec{u}$ from plane in origin to point U

$$\vec{v_p} = (\vec{v} \cdot \vec{n})\vec{n} = (\vec{n}^T \vec{v})\vec{n} = \vec{n}\vec{n}^T \vec{v}$$

To calculate the cross product a skew-symmetric matrix is used. First of all the n vector is concerted into a skew-symmetric matrix and the multiplied with vector v. The vector n in the skew-symmetric matrix form is:

$$[\vec{n}]_x = \begin{pmatrix} 0 & -n_3 & n_2 \\ n_3 & 0 & -n_1 \\ -n_2 & n1 & 0 \end{pmatrix}$$

$$\vec{w} = \vec{n} \times \vec{v} = [\vec{n}]_x \vec{v}$$

Substituting the dot and cross product equations the Rodrigues' formula is obtained:

$$\vec{u} = \vec{v} cos(\alpha) + \vec{n}\vec{n}^T \vec{v}(1 - cos(\alpha)) + [\vec{n}]_\times \vec{v} sin(\alpha) \tag{D.8}$$

Equation D.8 can be used to rotate point $\vec{v}$ around rotation axis $\vec{n}$ by angle α. To get the rotation matrix **R** this equation must be split in the **R** and $\vec{v}$ components.

$$\vec{u} = \mathbf{R}\vec{v}$$

thus

$$\vec{u} = \left(\mathbf{I}\, cos(\alpha) + \vec{n}\vec{n}^T (1 - cos(\alpha)) + [\vec{n}]_\times sin(\alpha)\right) \vec{v}$$

$$\mathbf{R} = \mathbf{I}\, cos(\alpha) + \vec{n}\vec{n}^T (1 - cos(\alpha)) + [\vec{n}]_\times sin(\alpha) \tag{D.9}$$

This can be simplified by using the identity of the outer product.

$$\vec{n}\vec{n}^T = [\vec{n}]_\times + \mathbf{I}$$

Where **I** is the identity matrix. This identity can be proved with a few simple steps.

$$\vec{n}\vec{n}^T = \begin{bmatrix} n_1 \\ n_2 \\ n_3 \end{bmatrix} \begin{bmatrix} n_1 & n_2 & n_3 \end{bmatrix} = \begin{bmatrix} n_1^2 & n_1 n_2 & n_1 n_3 \\ n_1 n_2 & n_2^2 & n_2 n_3 \\ n_1 n_3 & n_2 n_3 & n_3^2 \end{bmatrix}$$

This looks familiar with the skew-symmetric matrix as in equation D. By squaring this matrix the result is:

$$[\vec{n}]_\times^2 = \begin{bmatrix} -n_3^2 - n_2^2 & n_1 n_2 & n_1 n_3 \\ n_1 n_2 & -n_3^2 - n_1^2 & n_2 n_3 \\ n_1 n_3 & n_2 n_3 & -n_2^2 - n_1^2 \end{bmatrix}$$

At this point only the diagonal is different. Therefore the last step is to turn the diagonal of $[\vec{n}]_\times^2$ to the diagonal of $\vec{n}\vec{n}^T$. Since the vector $\vec{n}$ has the unit length, it is possible to add 'one' to the $[\vec{n}]_\times^2$ diagonal to get $\vec{n}\vec{n}^T$. For example:

$$n_1^2 + n_2^2 + n_3^2 = 1 \;\Rightarrow\; n_1^2 = -n_2^2 - n_3^2 + 1$$

This can be rewritten to:

$$\begin{bmatrix} n_1^2 & n_1 n_2 & n_1 n_3 \\ n_1 n_2 & n_2^2 & n_2 n_3 \\ n_1 n_3 & n_2 n_3 & n_3^2 \end{bmatrix} = \begin{bmatrix} -n_3^2 & n_1 n_2 & n_1 n_3 \\ n_1 n_2 & -n_3 - n_1^2 & n_2 n_3 \\ n_1 n_3 & n_2 n_3 & -n_2^2 - n_1^2 \end{bmatrix} + \mathbf{I}$$

Which is:

$$\vec{n}\vec{n}^T = [\vec{n}]_\times + \mathbf{I} \tag{D.10}$$

When equation D.9 and equation D.10 are combined the final Rodrigues' formula can be derived:

$$\mathbf{R} = \mathbf{I}\,cos(\alpha) + \left([\vec{n}]_\times^2 + \mathbf{I}\right)(1 - cos(\alpha)) + [\vec{n}]_\times\, sin(\alpha)$$

$$\mathbf{R} = \mathbf{I}\,cos(\alpha) + [\vec{n}]_\times^2 + \mathbf{I} - [\vec{n}]_\times^2\, cos(\alpha) - \mathbf{I}\,cos(\alpha) + [\vec{n}]_\times\, sin(\alpha)$$

$$\mathbf{R} = \mathbf{I} + [\vec{n}]_\times^2 - [\vec{n}]_\times^2\, cos(\alpha) + [\vec{n}]_\times\, sin(\alpha)$$

And finally the Rodrigues' formula is obtained:

$$\mathbf{R} = \mathbf{I} + [\vec{n}]_\times\, sin(\alpha) + [\vec{n}]_\times^2\,(1 - cos(\alpha)) \tag{D.11}$$

E

Experiment results

E.1. Experiment 1: Configuration 1, Procedure 1: limit check

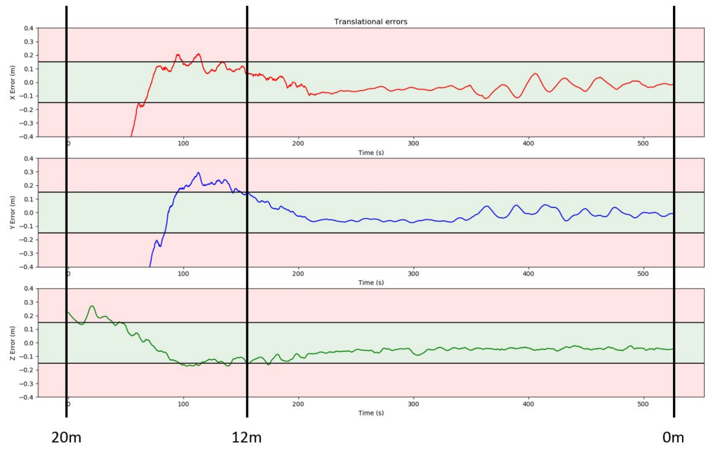

Figure E.1: Topside moving 20m astern towards jacket. Accurate within 0-12 meters

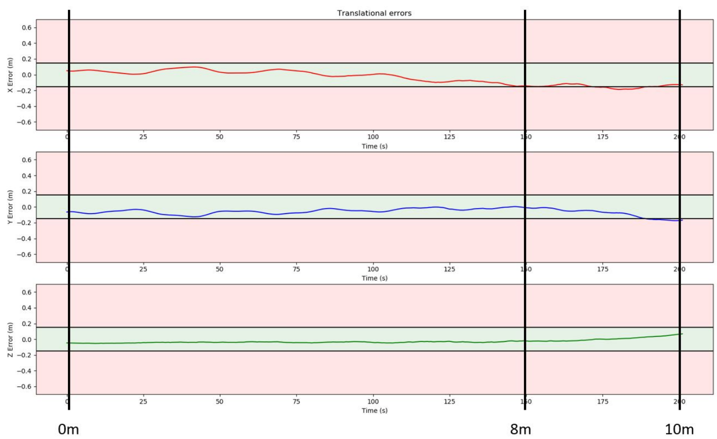

Figure E.2: Topside moving 10 meters to port side. Accurate within 0-8 meters.

E.2. Experiment 1: Configuration 1, Procedure 1

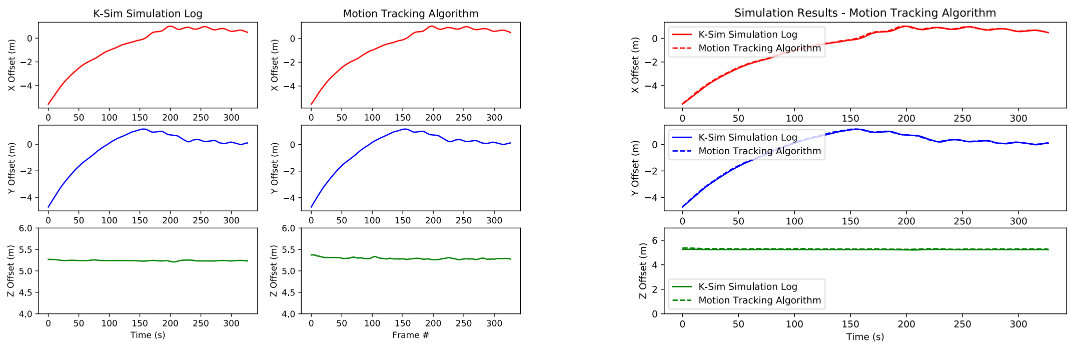

(a) Individual X-, Y-, and Z-Translations from the K-Sim Simulation Log and Motion Tracking Algorithm

(b) Combined X-, Y-, and Z-Translations from the K-Sim Simulation Log and Motion Tracking Algorithm

Figure E.3: X-, Y-, and Z-Translations

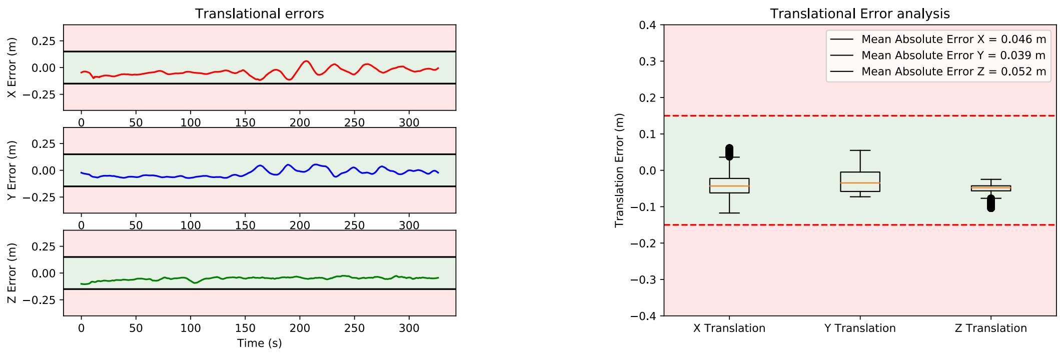

(a) Total error in X-, Y, and Z-Translations over time. Green area indicates 0.15m acceptable error margin.

(b) Distribution of X-, Y, and Z-Translations and Mean Absolute Error

Figure E.4: Error Analysis

E.3. Experiment 1: Configuration 1, Procedure 2

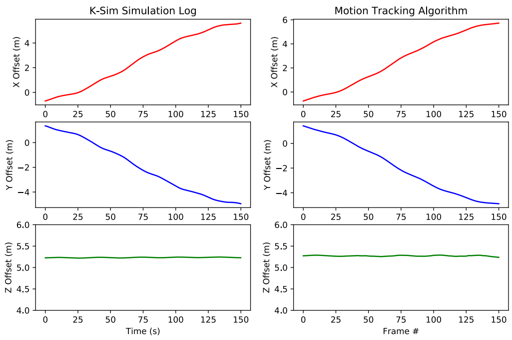

(a) Individual X-, Y-, and Z-Translations from the K-Sim Simulation Log and Motion Tracking Algorithm

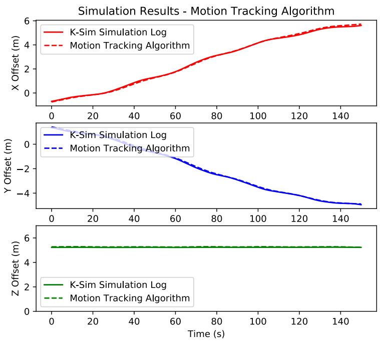

(b) Combined X-, Y-, and Z-Translations from the K-Sim Simulation Log and Motion Tracking Algorithm

Figure E.5: X-, Y-, and Z-Translations

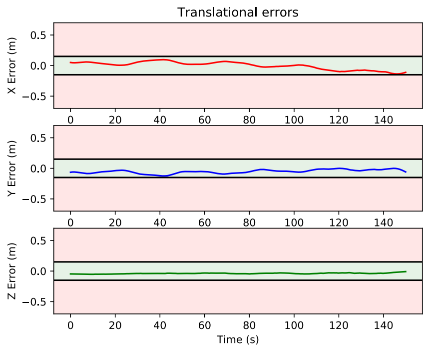

(a) Total error in X-, Y, and Z-Translations over time. Green area indicates 0.15m acceptable error margin.

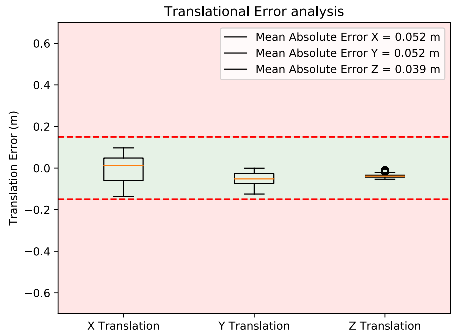

(b) Distribution of X-, Y, and Z-Translations and Mean Absolute Error

Figure E.6: Error Analysis

E.4. Experiment 1: Configuration 1, Procedure 3

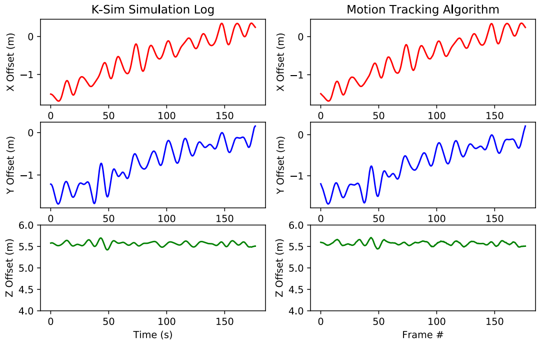

(a) Individual X-, Y-, and Z-Translations from the K-Sim Simulation Log and Motion Tracking Algorithm

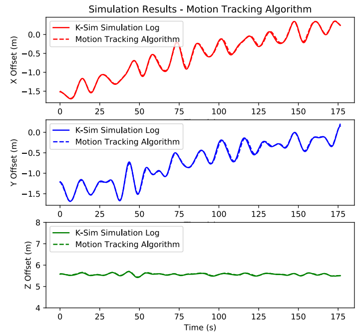

(b) Combined X-, Y-, and Z-Translations from the K-Sim Simulation Log and Motion Tracking Algorithm

Figure E.7: X-, Y-, and Z-Translations

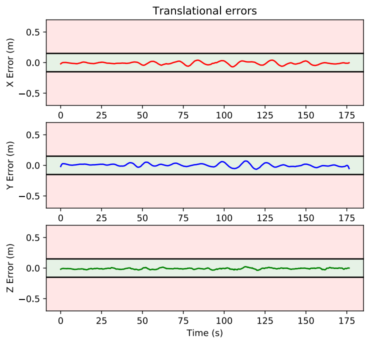

(a) Total error in X-, Y, and Z-Translations over time. Green area indicates 0.15m acceptable error margin.

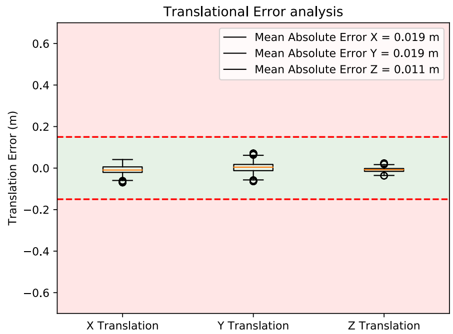

(b) Distribution of X-, Y, and Z-Translations and Mean Absolute Error

Figure E.8: Error Analysis

E.5. Experiment 1: Configuration 1, Procedure 4

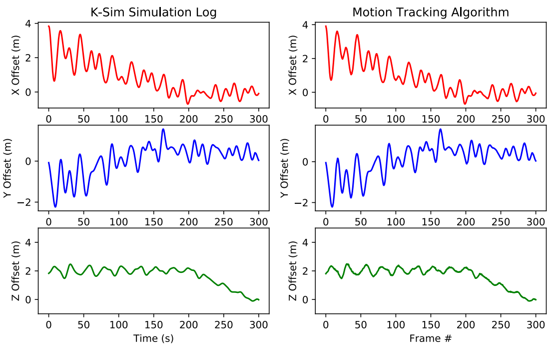

(a) Individual X-, Y-, and Z-Translations from the K-Sim Simulation Log and Motion Tracking Algorithm

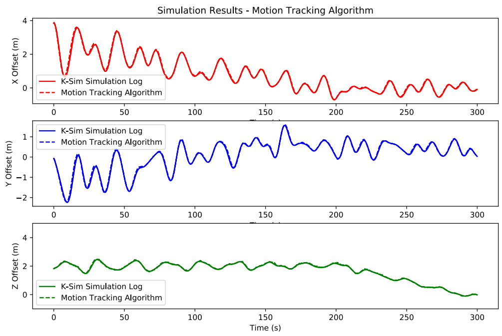

(b) Combined X-, Y-, and Z-Translations from the K-Sim Simulation Log and Motion Tracking Algorithm

Figure E.9: X-, Y-, and Z-Translations

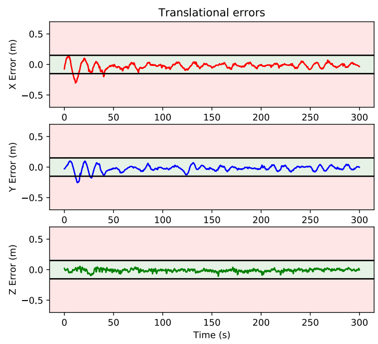

(a) Total error in X-, Y, and Z-Translations over time. Green area indicates 0.15m acceptable error margin.

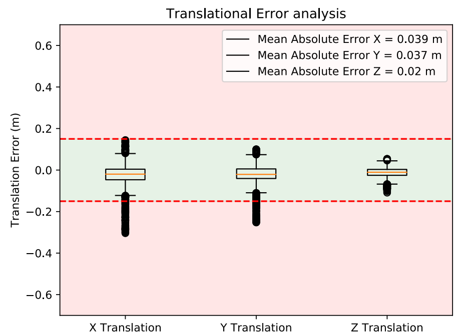

(b) Distribution of X-, Y, and Z-Translations and Mean Absolute Error

Figure E.10: Error Analysis

E.6. Experiment 1: Configuration 2, Procedure 5

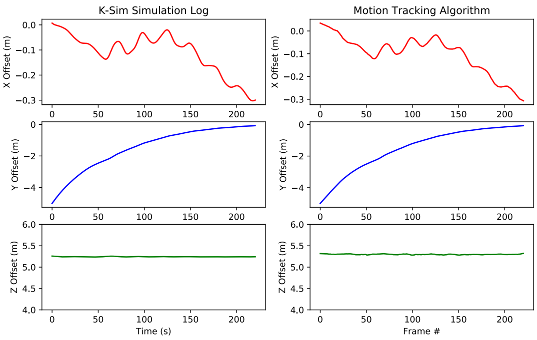

(a) Individual X-, Y-, and Z-Translations from the K-Sim Simulation Log and Motion Tracking Algorithm

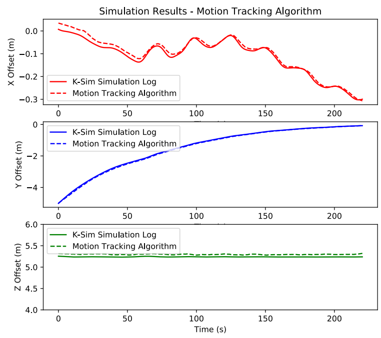

(b) Combined X-, Y-, and Z-Translations from the K-Sim Simulation Log and Motion Tracking Algorithm

Figure E.11: X-, Y-, and Z-Translations

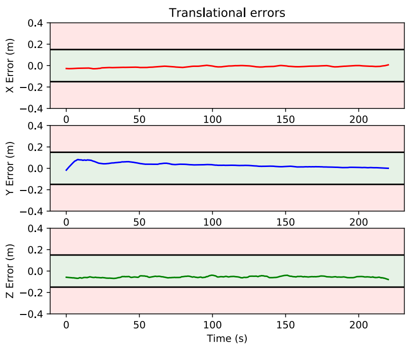

(a) Total error in X-, Y, and Z-Translations over time. Green area indicates 0.15m acceptable error margin.

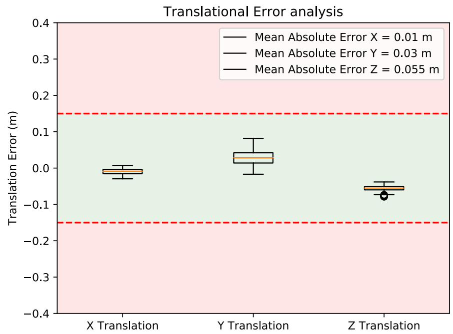

(b) Distribution of X-, Y, and Z-Translations and Mean Absolute Error

Figure E.12: Error Analysis

E.7. Experiment 1: Configuration 2, Procedure 6

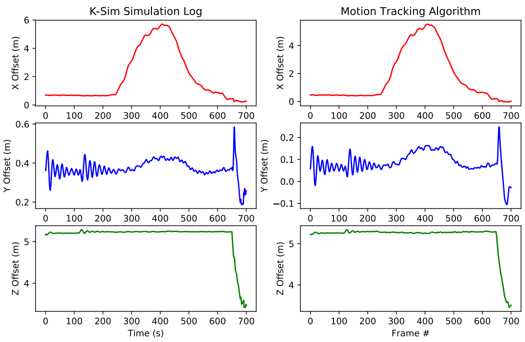

(a) Individual X-, Y-, and Z-Translations from the K-Sim Simulation Log and Motion Tracking Algorithm

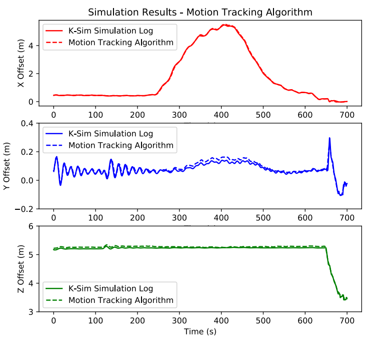

(b) Combined X-, Y-, and Z-Translations from the K-Sim Simulation Log and Motion Tracking Algorithm

Figure E.13: X-, Y-, and Z-Translations

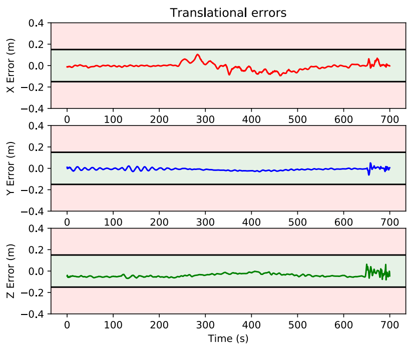

(a) Total error in X-, Y, and Z-Translations over time. Green area indicates 0.15m acceptable error margin.

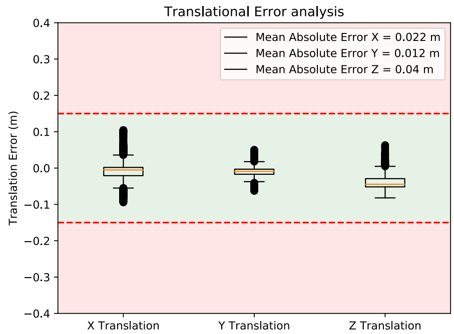

(b) Distribution of X-, Y, and Z-Translations and Mean Absolute Error

Figure E.14: Error Analysis

E.8. Experiment 1: Configuration 2, Procedure 7

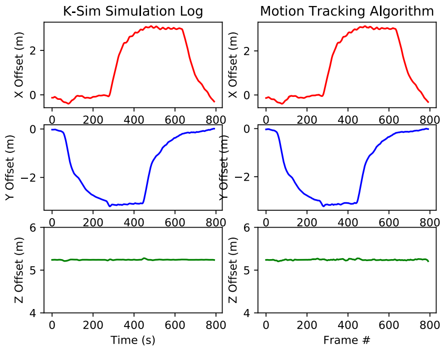

(a) Individual X-, Y-, and Z-Translations from the K-Sim Simulation Log and Motion Tracking Algorithm

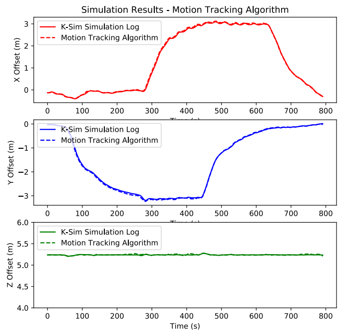

(b) Combined X-, Y-, and Z-Translations from the K-Sim Simulation Log and Motion Tracking Algorithm

Figure E.15: X-, Y-, and Z-Translations

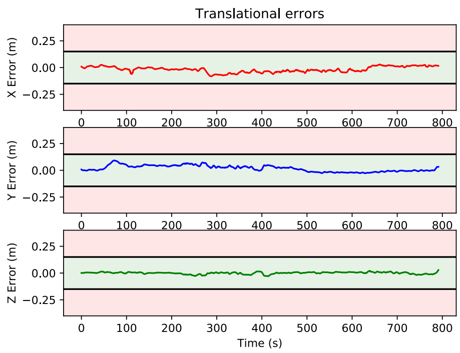

(a) Total error in X-, Y, and Z-Translations over time. Green area indicates 0.15m acceptable error margin.

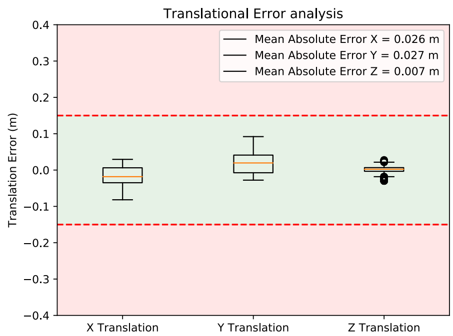

(b) Distribution of X-, Y, and Z-Translations and Mean Absolute Error

Figure E.16: Error Analysis

F

Visual object tracking: a multidisciplinary system

In this research visual object tracking of markers was used to determine the relative position between a topside and a jacket. However, there are a lot of other possibilities to use this technique.

F.1. Free-decay test of a jacket scale model

In addition to the virtual test in the HSC, the motion tracking algorithm was also tested in a physical experiment. This was initially not planned in the study. For an experiment that was part of a larger study within HMC, a method was still being sought to register the movement of a moving object. The aim of this experiment was to determine the damping of a scaled-down jacket frame. A model jacket was hung in the HMC expedition room for this purpose. This model was then provided with a foam-printed ArUco marker. A second ArUco marker was positioned next to it in the same plane. The total setup can be seen in Figure F.1. A web cam was then positioned in such a way that both markers were clearly visible. The web cam was connected to a laptop via a USB cable. The laptop was equipped with the Motion Tracking Algorithm in python. The algorithm was able to determine the distance between the two markers (see Figure F.2). The model jacket was given a 15 cm offset in each test. As a result, the model ended up in a pendulum movement and slowly decayed.

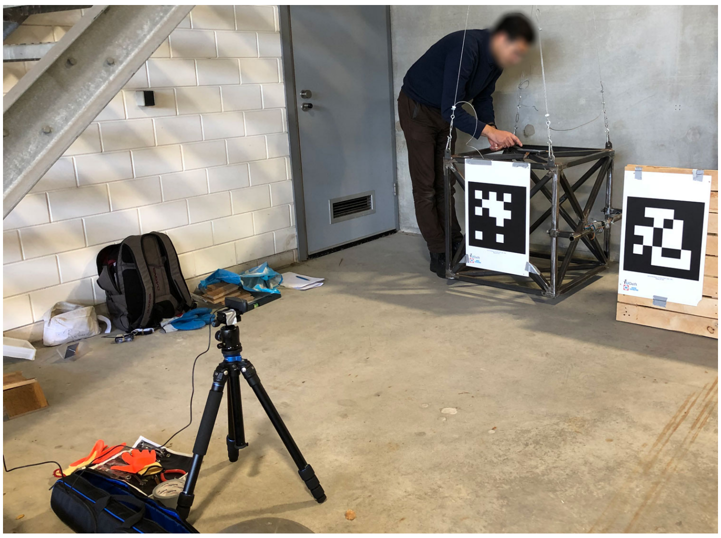

Figure F.1: Experiment setup: tripod with Logitech C920 HD Pro, ArUco markers 0.38x0.38m

Several experiments have been carried out. Herein, the length of the wires and the distance between the suspension points are varied. In addition to allowing the model to move freely, sometimes

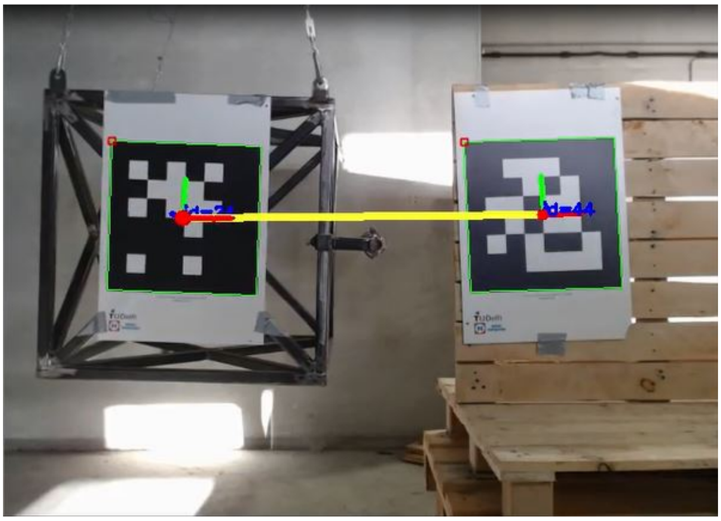

Figure F.2: Screenshot from Motion Tracking Algorithm. Red line represents historical track.

a bumper has been used to measure the effect of impact. All the results can be found in table F.1. All those involved were very satisfied with the results of the motion tracking algorithm. It was seen as a very reliable, cheap and simple method of measuring. The possibility of seeing in real-time what is measured was also mentioned as an advantage. A second measurement method that had been used was the built-in accelerometer of a smartphone. The intention was to use this data as verification. In the end, this data was unfortunately not usable.

Test NR	**Time**	**Width between suspension points [m]**	**Wire length [m]**	**Remarks**	**T [s]**	**Energy**	**Log decr**
						blin [-]	blin [-]
8	12:11	0.575	1.530	Standard decay test	2.7670	0.106%	0.106%
9	13:26	0.575	1.530	Standard decay test	2.7643	0.128%	0.128%
12	13:39	0.575	1.530	2 impacts and guides pulled away	2.7661	0.110%	0.112%
13	14:06	0.575	1.930	Standard decay test	3.0247	0.110%	0.110%
14	14:27	1.085	1.930	Standard decay test	3.0359	0.107%	0.109%
15	14:34	1.085	1.930	Standard decay test	3.0361	0.106%	0.106%
18	14:48	1.085	1.930	1 impact and guides pulled away	3.0367	0.093%	0.093%
19	15:24	1.085	1.540	Standard decay test	2.7642	0.098%	0.098%
20	15:31	1.085	1.540	Standard decay test	2.7648	0.108%	0.106%

Table F.1: Decay test results

F.2. Crane suspended jacket transport

There are various reasons why motion monitoring can be problematic offshore. Determining the z coordinate is difficult due to tides, vessel ballast and waves, and the rolling or pitching motion of a vessel can lead to large angular movements. Furthermore, since the offshore location may be remote, satellite positioning may be less accurate or reliable than at onshore locations. Another situation where motion tracking can be used is during a free hanging transport of a jacket. In such transport a jacket is unrestrained. Normally, a jacket is restrained to increase SSCV stability, reduce horizontal motions of the jacket to the SSCV and reduce horizontal transport loads at lift points. A free hanging transport results in a significant cost saving because there is no need for a financial investment in restraint modifications. It will also have a positive impact on the schedule as a 24 hours restraint outfitting is not required anymore. However, this kind of transport has never been done before by HMC. A concern during this transport are the motions of the jacket relative to the SSCV. Calculations show that this will not be problematic. There is a wish to monitor the motions of the jacket to verify this. To enable this, trackable markers can be placed on the jacket. This marker can be tracked by a fixed camera on the stern of the SSCV or by a fixed camera in the crane boom (or both) (see Fig. F.3).

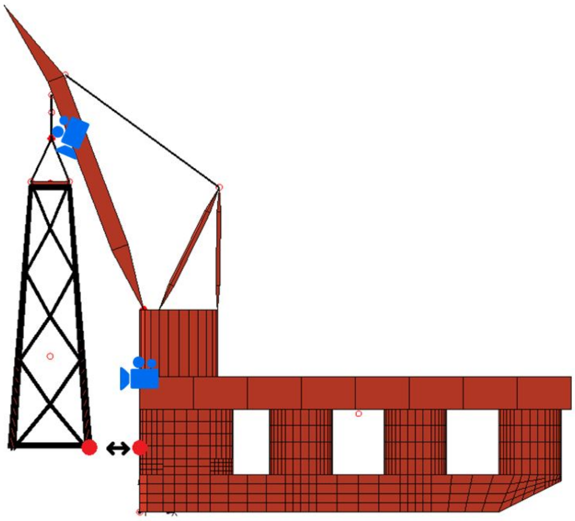

Figure F.3: Jacket monitoring

This will result in the relative motions between the marker reference frame and the camera reference frame. All of the markers required to provide a determination of position may be unique markers. Their positions relative to the structure must be determined by surveying techniques. This is also necessary for the imaging device. If the position and orientation of the marker and imaging device relative to their reference frame is known, the horizontal motions of the jacket towards the SSCV can be monitored.